State-insensitive dynamic polarizabilities of the polar molecules NaK and RbCs in optical lattices

Von der Fakultät für Mathematik und Physik
der Gottfried Wilhelm Leibniz Universität Hannover
zur Erlangung des akademischen Grades

Doktor der Naturwissenschaften
– Dr. rer. nat. –

genehmigte Dissertation von

M. Sc. Wuying She

January, 2020

Referentin/Referent:	Prof.Dr.Silke Ospelkaus
Korreferentin/Korreferent:	Prof.Dr.Milutin Kovacev
	Prof.Dr.Kai Bongs (Universität von Birmingham, UK)
Tag der Promotion:	19.08.2019

Acknowledgement

I would like to express my special appreciation to my supervisor Professor Dr. Silke Ospelkaus for encouraging my research with her patience, motivation and insightful comments. She provided me the opportunity to work here in Germany and has been always supportive to me since the day when I came here. Thanks to Professor Dr. Eberhard Tiemann and Dr. Horst Knöckel who helped me a lot at the beginning of my study. I would also like to thank my colleague, Dr. Mirco Siercke, who has spent time exploring and discussing this topic together with me. His guidance helped me throughout the investigation and the writing of this thesis. There is also sincere gratitude that I would like to express to every group member, Torsten Hartmann, Erik Schwanke, Julia Gerschmann... ..., who made my stay here a wonderful journey in my life.

A special thanks to my husband for all the sacrifices and the huge support during the difficult time I encountered. Thanks to my lovely son, you have been always my power resource, and allow me to have the chance to grow up together with you.

Last but not the least, I would like to thank my families in China for all the spiritually support throughout the years.

Contents

Abstract

In this thesis, we determine the formalism of the dynamic polarizability of diatomic molecules. This approach is then applied to investigate the effect of a DC field on the dynamic polarizability of a few rotational states of RbCs and NaK molecules at a wavelength of 1064 nm. We demonstrate the dependence of the dynamic polarizability on the DC field strength and find that at a certain DC field strength, two lowest rotational states of the molecules have identical dynamic polarizabilities. This magic field strength is verified to be independent of the light polarization. Besides this, we also investigate the angle dependence of the polarizabilities when the light is linearly polarized as a function of the relative angle with respect to the DC field. There exists a magic angle which is independent of the DC field strength. This state-insensitive polarizabilities finding can provide great advantages to the development of experiments where polar molecules trapped in optical lattices are ideal tools for quantum computing and simulations.

Keywords: dynamic polarizability, heteronuclear molecules, DC field strength dependence, magic field strength, magic angle.

Chapter 1

Introduction

When a neutral atom is placed in an oscillating electric field, the positive charges and negative charges experience electrostatic forces in opposite directions. This leads to an induced dipole moment, which can interact with the driving electric field. The resulting two important physical quantities are: an optical dipole potential and a scattering rate. Both of them can be characterized by the polarizability α which describes the response ability of the atom to the light field. The optical dipole potential can be characterized by the real part of the dynamic polarizability $\mathrm{Re}[\alpha]$, and the scattering rate can be characterized by the imaginary part of the dynamic polarizability $\mathrm{Im}[\alpha]$. Making use of the real part of the dynamic polarizability, an atom can be trapped into a region of a red-detuned light field [1] where the electric field has the highest intensity.

Generally, the polarizabilities of two atomic states can differ from each other, therefore they can be trapped with different dipole potentials. This will lead to unfavorable consequence to the experiments with atom system. For example, in the context of an atomic clock in an optical dipole trap where we consider the transition frequency between two atomic states as a time base. A problem is generated since the two atomic states with different polarizabilities will be shifted by different amount of energies, therefore changing the transition frequency. One can circumvent this problem by finding appropriate trapping wavelength [2–7], so that the transition frequency is unperturbed by the laser light, while still benefiting from the trapping environment. Such trapping wavelength is also referred as magic wavelength.

Nowadays, there are various investigations about finding magic conditions for molecules in ultracold experiments. The advantage of the molecules is that they have non-zero dipole moment in the molecular frame. In the laboratory frame, they are zero since the molecules are not aligned. In order to take advantage of the dipole moment in experiments, they need to be non-

zero in the laboratory frame. We can generate this by applying a DC electric field, which has the effect of mixing rotational states [8], thereby aligning the molecules. A long-range dipole-dipole interactions [9] can happen between the molecules. Putting molecular systems with such interactions in optical lattices [10, 11] can offer new opportunities for the development of quantum simulations and quantum optics [12–15]. These applications require a prerequisite that there is sufficient coherence time of the interactions. We can fulfill this by finding certain values of the DC field strength or certain laser polarizations, so that the energies of the mixed rotational states are shifted by the same amount. Similar work has been done in an investigation which found a magic electric field strength and a magic angle for the polarizabilities of rotational states of the molecules KRb and RbCs at a light wavelength of 1090 nm [16]. Magic conditions have also been investigated in other contexts. For example, in the precision measurements with the nonpolar molecules Sr_2 [17, 18], there exists a magic frequency for the vibrational transitions. A magic frequency is also found of a microwave field which induces identical AC Stark shift of the internal levels of the molecules KRb and RbCs [19].

In this thesis, we aim to find ways to realize identical dynamic polarizabilities of the two lowest rotational states of diatomic RbCs and NaK molecules at a wavelength of 1064 nm, which is the most common wavelength used for optical lattices or tweezers. As one of the approaches, the dependence of the dynamic polarizability on the strength value of the external static field is investigated. In addition to that, we also investigate the dynamic polarizability as a function of the relative angle between the DC field and the linearly polarized light.

This thesis is arranged as follows:

In **chapter 2**, we discuss the interaction between an atom and an oscillating field, which results in a dipole potential and a scattering rate. They are proportional to the real part and imaginary part of the polarizability respectively. In order to derive an expression of the polarizability, we use the Lorentz model which is a system consisting of an electron which is elastically bound to a nucleus with an eigenfrequency ω_0 (this eigenfrequency is corresponding to the atomic transition frequency). At the end of the chapter, we go beyond the toy model and obtain the formalism of the polarizability using perturbation theory.

Chapter 3 concentrates on the discussion of the more complex systems: diatomic molecules. The Born-Oppenheimer approximation simplifies the description of a molecule by considering the nuclei as stationary while we are describing the electronic motions. Therefore, the wavefunctions of the diatomic molecule are separated into a electronic component and a nuclear

component. At the end, we derive an expression of the dynamic polarizability of diatomic molecules by the second order energy corrections.

In **chapter 4**, we investigate the optical dynamic polarizabilities of the rotational states with $J = 0$ and $J = 1$ of RbCs and NaK as a function of the laser frequency in the near infrared region.

Chapter 5 discusses the dynamic polarizability when we introduce an external DC field to mix the rotational states, and trap the molecules with a light wavelength of 1064 nm. Since the field strength determines the mixing constants, this motivates us to investigate the dependence of the polarizabilities on the static field strength. A magic field strength is found where the polarizabilities of two mixed rotational states can match. Moreover, we investigate the polarizability as a function of the angle between the laser polarization and the static field direction. There exists also a magic angle.

chapter 6 extends the magic condition in the last chapter to optical lattices with different configurations. We start with the introduction of the simplest 1D optical lattice. Especially, we visualize and compare the dipole potentials of the two mixed rotational states $J = 0, M = 0$ and $J = 1, M = 0$ of NaK in a 1D optical lattice when the DC electric field is smaller than, equal to or larger than the magic field strength. Furthermore, we demonstrate higher dimensional optical lattices different geometries.

Chapter 2

Electric dipole polarizability

There are a lot of mechanisms with which light and atoms can interact. A fairly general way of describing these interactions is given by the polarizability α, which is a property of the atom characterizing its response to the light. The real part of the polarizability $\mathrm{Re}[\alpha]$ characterizes the dipole potential resulting from the interaction between the light-induced dipole moment and the driving field. The imaginary part of the polarizability $\mathrm{Im}[\alpha]$ characterizes the scattering rate, which is induced by the absorption of the light field by the atom. Polarizability is also an important quantity in other various areas of physics and chemistry. For example, it is been used to investigate and explain the collision phenomena [20] between neutral particles.

In general, it is not easy to derive an expression of the atomic polarizability. However, taking a good model will be helpful for us to understand. The toy model we use here is a damping "Lorentz model" [21], where an electron is connected to a nucleus with an eigenfrequency ω_0. The system is in a driving field which has a frequency ω. The polarizability can be obtained when we solve the equation of motion. With this expression, we are able to write the dipole potential and the scattering rate in terms of the polarizability.

Although the "Lorentz model" provides us general formalism for the two mechanisms, a real atom is not as simple as a harmonic oscillator. Fortunately, we can treat the effect of a far-detuned laser light on a two-level atom by perturbation theory [22]. The corresponding polarizability of a state can be derived by evaluating the energy corrections.

A real atom is not a two-level system, it has complex multi-levels. In general, different atomic levels have different polarizabilities, therefore, the dipole potential depends on the specific sub-level of the atom [23, 24]. Under certain conditions, we can ensure that the potentials seen by the two specific levels are identical. This state insensitive investigation can provide great advantages to the precision spectroscopy with atoms [25, 26] and also other

related applications.

2.1 Optical dipole trap

In this section, we introduce the interaction between the oscillator and the radiation field and then characterize the resulting mechanisms with the polarizability.

We use a complex notation for the field,

$$\vec{E}(\vec{r},t) = \hat{e}E(\vec{r})e^{-i\omega t} + c.c. \tag{2.1}$$

where $\hat{e}$ is a unit vector denoting the polarization of light field. ω is the frequency of the field.

This light field induces an electric dipole moment by

$$\vec{d}(\vec{r},t) = \hat{e}d(\vec{r})e^{-i\omega t} + c.c. \tag{2.2}$$

The component $d(\vec{r})$ of the induced dipole moment can be described by a complex polarizability α with

$$d(\vec{r}) = \alpha(\omega)E(\vec{r}) \tag{2.3}$$

where the polarizability is dependent on the light frequency.

We write the potential as a result of the interaction between the induced dipole moment $\vec{d}$ and $\vec{E}$ by [27]

$$V_{\text{dipole}}(\vec{r}) = -\frac{1}{2}\langle\vec{d}\vec{E}\rangle = -\frac{1}{2\epsilon_0 c}\,\text{Re}[\alpha(\omega)]I(\vec{r}) \tag{2.4}$$

where the light intensity $I(\vec{r})$ is expressed by $I(\vec{r}) = 2\epsilon_0 c|E(\vec{r})|^2$. c is the speed of light, and ϵ_0 is the dielectric constant.

A corresponding dipole force is induced due to the gradient of the dipole potential and it is given by

$$\vec{F}_{\text{dipole}}(\vec{r}) = -\nabla V_{\text{dipole}} = \frac{1}{2\epsilon_0 c}\,\text{Re}(\alpha)\nabla I(\vec{r}) \tag{2.5}$$

We still need to discuss another quantity: the atom can also absorb photons from the light field and then reemit them as dipolar radiation. This excitation will heat up the atoms in the trap and therefore limit the performance of the dipole trap.

The absorption of the power from the driving field is given by [28]

$$P_{\text{abs}}(\vec{r}) = \langle \dot{\vec{d}} E \rangle = \frac{\omega}{\epsilon_0 c} \operatorname{Im}(\alpha) I(\vec{r}) \tag{2.6}$$

where the imaginary part of the polarizability characterizes the out-of-phase component of the dipole oscillation.

The corresponding scattering rate is

$$\Gamma_{\text{sc}}(\text{r}) = \frac{P_{\text{abs}}}{\hbar\omega} = \frac{1}{\hbar\epsilon_0 c} \operatorname{Im}(\alpha) I(\vec{r}) \tag{2.7}$$

The two expressions of (2.4) and (2.7) give two important consequences of light-atom interaction: the dipole potential in terms of the real part of the polarizability $\operatorname{Re}(\alpha)$ and light intensity $I(\vec{r})$, and the scattering rate in terms of the imaginary part of the polarizability $\operatorname{Im}(\alpha)$ and light intensity $I(\vec{r})$.

2.2 Polarizability of the Lorentz model

The two mechanisms of dipole potential and scattering rate as functions of the polarizability are crucial if we want to design an optimal optical dipole trap. Therefore, it is necessary for us to derive an expression of the frequency-dependent polarizability $\alpha(\omega)$. Here we take advantage of a Lorentz model. In this classical model, the atom is considered as an electron connecting to a nucleus by a spring of ω_0. The oscillating field has a frequency of ω. See Fig. 2.1.

Now we write the motion equation of the system

$$m\ddot{x} + m\Gamma_\omega \dot{x} + m\omega_0^2 x = -\hat{\varepsilon} e E e^{-i\omega t} \tag{2.8}$$

where Γ_ω is the damping rate.

We solve the Eq. (2.8) and get

$$x = -\hat{\varepsilon} \frac{eE/m}{\omega^2 - \omega_0^2 + i\Gamma_\omega \omega} e^{-i\omega t} \tag{2.9}$$

Therefore, the expression of the polarizability derived by the Lorentz model is

$$\alpha(\omega) = \frac{e^2/m}{\omega_0^2 - \omega^2 - i\Gamma_\omega \omega} \tag{2.10}$$

By taking the real component of the polarizability $\operatorname{Re}[\alpha]$ and the imaginary component of the polarizability $\operatorname{Im}[\alpha]$, we are able to write down the

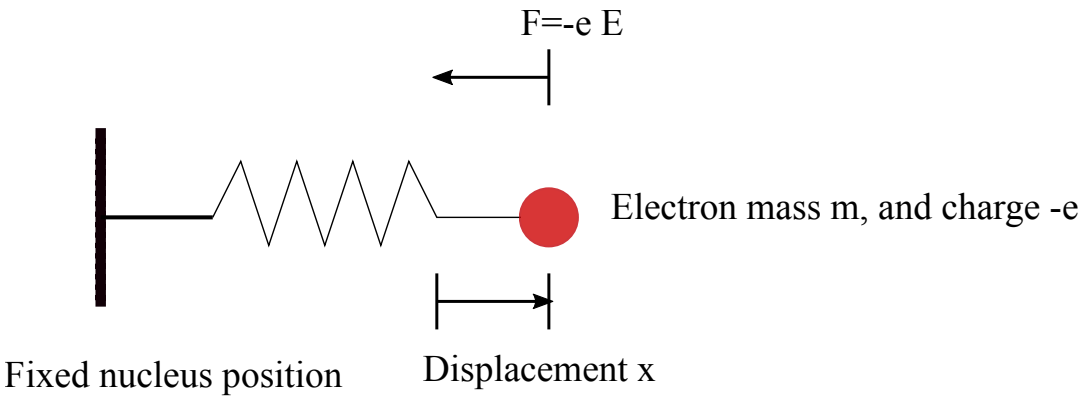

Figure 2.1: The Lorentz atom model. The nucleus mass M is much larger than the electrons' mass m. They are connected with a spring.

dipole potential and the scattering rate in Eq. (2.4) and (2.7)

$$V_{\text{dipole}}(\vec{r}) = -\frac{e^2}{2\epsilon_0 mc}\frac{\omega_0^2 - \omega^2}{(\omega_0^2 - \omega^2)^2 + \Gamma_\omega^2\omega^2} I(\vec{r}) \tag{2.11}$$

$$\Gamma_{\text{sc}}(\vec{r}) = \frac{e^2}{\hbar\epsilon_0 mc}\frac{\Gamma_\omega \omega}{(\omega_0^2 - \omega^2)^2 + \Gamma_\omega^2\omega^2} I(\vec{r}) \tag{2.12}$$

The expressions of the two mechanisms are applicable for any light frequency. From the Eq.(2.11), we get a first clue of an optimal dipole trap: when the laser frequency is tuned to be below the resonance ($\omega - \omega_0 < 0$) (red-detuned), the dipole potential in Eq.(2.11) is negative. This can form a trap for the atoms. The deepest potential locates at the intensity maximum region.

For a case where light frequency is far away from resonances ($|\omega_0 - \omega| \gg \Gamma_\omega$), then

$$V_{\text{dipole}}(\vec{r}) = -\frac{e^2}{4\epsilon_0\omega_0 mc}\left(\frac{1}{\omega_0 - \omega} + \frac{1}{\omega_0 + \omega}\right) I(\vec{r}) \tag{2.13}$$

$$\Gamma_{\text{sc}}(\vec{r}) = \frac{e^2\Gamma_\omega\omega}{4\hbar\epsilon_0 mc\omega_0^2}\left(\frac{1}{\omega_0 - \omega} + \frac{1}{\omega_0 + \omega}\right)^2 I(\vec{r}) \tag{2.14}$$

The second term in the bracket of Eqs.(2.13) and Eqs.(2.14) are contributions from the resonance at negative frequency $\omega = -\omega_0$. If the laser frequency is tuned relative close to the resonance of ω_0 such that $|\omega - \omega_0| \ll \omega_0$,

then the terms with negative frequency are small enough to neglect. This is also known as the "Rotating wave approximation". From this we can derive an important relation between the dipole potential and scattering rate

$$\frac{\Gamma_{\rm sc}}{V_{\rm dipole}} = \frac{\Gamma_\omega}{\hbar\Delta} \tag{2.15}$$

The relation in Eq.(2.15) reveals another important rule for an optimal dipole trap: the detuning Δ can be chosen to be large such that the scattering rate can be suppressed as much as possible. Although the large detuning frequency causes a decrease to the depth of the potential, we can still increase the light intensity $I(\vec{r})$ to compensate this.

A simple optical dipole trap for atoms is constructed by a single red-detuned Gaussian beam which is propagating along z direction (See Fig.2.2). The intensity of a Gaussian beam [29] has its largest value in the center of the beam and then decreases in the radial and axial directions as

$$I(x,y,z) = \frac{2P}{\pi w^2(z)} e^{-2(x^2+y^2)/w^2(z)} \tag{2.16}$$

where P is the total power of the laser beam, and $\omega(z)$ is defined by

$$w(z) = w_0\sqrt{1+\frac{z^2}{z_R^2}} \tag{2.17}$$

where w_0 is the narrowest radius of the Gaussian beam, z is the axial distance to the center of the laser beam. z_R is the Rayleigh range, at this z_R position, the beam waist increases to $\sqrt{2}\omega_0$.

The Gaussian beam has a highest intensity at position $r = 0, z = 0$. The dipole force can attract the atoms to the center of the Gaussian beam for a red-detuned light. When we move the position of the Gaussian Beam, the dipole force can also move the particles correspondingly. This property is also referred as "optical tweezers" [30].

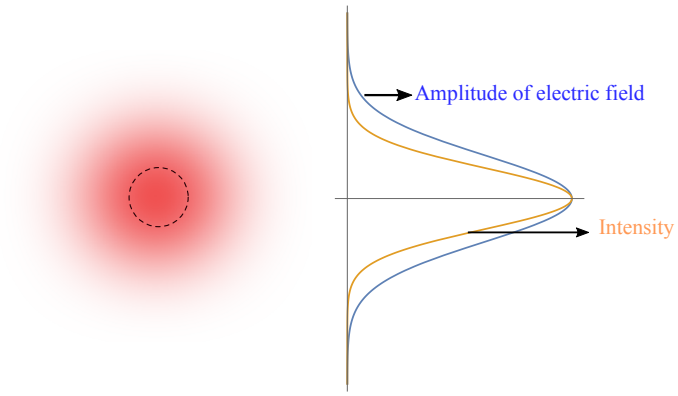

Figure 2.2: The amplitude and intensity profile of a Gaussian beam in the radial direction. Blue curve: the electric field amplitude. Orange curve: the intensity distribution of the beam.

2.3 Polarizability derived by perturbation theory

Although the Lorentz model provides us a classical picture of the interaction between a light field and an atom, especially the sign of detuning and scaling of the dipole potential and the scattering rate. However, real atoms are more complicated than the simple harmonic oscillator. Fortunately, the effect of static and dynamic external field on the atoms is small enough, and we can derive the energy correction of the system by perturbation theory [22]. The corresponding polarizability can be obtained by Eq. (2.4).

In this section, we start with the discussion of static polarizability by time-independent perturbation theory, where the effect of a static electric field is introduced as an interaction Hamiltonian $H' = -dE$. In principle, the dynamic polarizability can be obtained also through time-dependent perturbation theory, just as the treatment for the static polarizability. Instead of this, we treat this problem by doing some transformations to the time-dependent interaction Hamiltonian. We can get a time-independent Hamiltonian-like form which is similar to the Hamiltonian of the DC stark effect. The energy modification and dynamic polarizability can be derived by comparing the two Hamiltonians.

At the end, we state the issue of a state-dependent dipole potential of a multi-level atom.

2.3.1 Corrections to the energies by time-independent perturbation theory

Generally, the various systems in the nature can not be solved exactly for the eigenvalues and eigenfunction. Fortunately, at many times, the interaction with an external field, which we consider as $\hat{H}'$, is only a small perturbation to the original Hamiltonian $\hat{H}_0$ of the system, which means that it only results in a small energy correction compared to the original eigenenergies. This treatment is called perturbation theory, which is a widely used theory in quantum mechanics.

We write this concept as a form

$$H = \hat{H}_0 + \lambda \hat{H}' \tag{2.18}$$

where we split the full Hamiltonian into two parts: the part of unperturbed Hamiltonian $\hat{H}_0$, and the other part $H^{'}$ which describes the perturbation. λ is a small parameter.

The eigenfunctions of $\hat{H}_0$ are

$$\hat{H}_0|\psi_{n\nu}^{(0)}\rangle = E_n^{(0)}|\psi_{n\nu}\rangle, \quad \nu = 1, 2, \cdots, f_n \tag{2.19}$$

$$\langle\psi_{n\nu}^{(0)}|\psi_{m\mu}^{(0)}\rangle = \delta_{nm}\delta_{\nu\mu}, \tag{2.20}$$

where $E_n^{(0)}$ is the eigenenergy and $|\psi_{n\nu}^{(0)}\rangle$ is the corresponding eigenstate. $E_n^{(0)}$ might be non-degenerate ($f_n = 1$), or degenerate ($f_n \geq 2$).

The effect of a DC electric field on atoms is introduced as

$$\hat{H}' = -\vec{d}\cdot\vec{E} \tag{2.21}$$

What's worthwhile to mention is, when we are dealing with some detailed problems, we should choose an appropriate Hamiltonian operator $\hat{H}_0$ and a perturbation $H^{'}$. For some cases, the determination of $\hat{H}_0$ and $\hat{H}'$ is very obvious, for example, the Stark effect here, where we usually take the effect from the external field as the perturbation $H^{'}$ to $\hat{H}_0$. There are still other situations which might be more complex. The determination of $\hat{H}_0$ and $\hat{H}'$ depends always on how to make the calculations of the system more simple.

The Schrödinger equation is

$$\hat{H}|\psi\rangle = E|\psi\rangle \tag{2.22}$$

where E is the eigenenergy of the perturbed system.

The energy and wavefunction can be written in terms of different orders of perturbation as

$$|\psi\rangle = |\psi^{(0)}\rangle + \lambda|\psi^{(1)}\rangle + \lambda^2|\psi^{(2)}\rangle + \cdots , \tag{2.23}$$

$$E = E^{(0)} + \lambda E^{(1)} + \lambda^2 E^{(2)} + \cdots , \tag{2.24}$$

We substitute Eq.(2.23) and Eq.(2.24) into Eq. (2.22), and then compare the same-order terms, we get the eigenfunctions for each order as

$$(\hat{H}_0 - E^{(0)})|\psi^{(0)}\rangle = 0, \tag{2.25a}$$
$$(\hat{H}_0 - E^{(0)})|\psi^{(1)}\rangle = (E^{(1)} - \hat{H}')|\psi^{(0)}\rangle, \tag{2.25b}$$
$$(\hat{H}_0 - E^{(0)})|\psi^{(2)}\rangle = (E^{(1)} - \hat{H}')|\psi^{(1)}\rangle + E^{(2)}|\psi^{(0)}\rangle, \tag{2.25c}$$
$$(\hat{H}_0 - E^{(0)})|\psi^{(3)}\rangle = (E^{(1)} - \hat{H}')|\psi^{(2)}\rangle + E^{(2)}|\psi^{(1)}\rangle + E^{(3)}|\psi^{(0)}\rangle, \tag{2.25d}$$

We multiply the $\langle\psi^{(0)}|$ to both left sides of Eqs.(2.25b), (2.25c), (2.25d), and using the orthogonal conditions, we derive

$$E^{(1)} = \langle\psi^{(0)}|\hat{H}'|\psi^{(0)}\rangle \tag{2.26a}$$
$$E^{(2)} = \langle\psi^{(0)}|\hat{H}'|\psi^{(1)}\rangle \tag{2.26b}$$

We assume that, without the perturbation, the system is non-degenerate ($f_n = 1$) with energy $E_n^{(0)}$,

$$E^{(0)} = E_n^{(0)} \tag{2.27}$$

and the corresponding zero-order eigenstates are

$$|\psi^{(0)}\rangle = |\psi_n^{(0)}\rangle \tag{2.28}$$

To find the first order correction to the eigenstates, we write it as a superposition of non-perturbed states:

$$|\psi^{(1)}\rangle = \sum_n a_n^{(1)}|\psi_n^{(0)}\rangle \tag{2.29}$$

Substituting Eqs.(2.28) and (2.29) to (2.25b) gives,

$$(\hat{H}_0 - E^{(0)})\sum_n a_n^{(1)}|\psi_n^{(0)}\rangle = (E^{(1)} - \hat{H}')|\psi_k^{(0)}\rangle \tag{2.30}$$

Multiplying $\langle\psi_n^{(0)}|$ to both left sides of equation above, and also due to

orthogonality of the eigenstates, we get

$$(E_n^{(0)} - E_k^{(0)})a_n^{(1)} = E^{(1)}\delta_{nk} - H'_{nk} \tag{2.31}$$

where

$$H'_{nk} = \langle\psi_n^{(0)}|\hat{H}'|\psi_k^{(0)}\rangle \tag{2.32}$$

If we set $n = k$, it is the first-order eigenenergy (2.26a), and when $n \neq k$,

$$a_n^{(1)} = \frac{H'_{nk}}{(E_k^{(0)} - E_n^{(0)})} \tag{2.33}$$

Therefore, the energy and wavefunction with the first-order correction are

$$E_n = E_n^{(0)} + \langle\psi_n^{(0)}|\hat{H}'|\psi_n^{(0)}\rangle \tag{2.34a}$$

$$|\psi_n^{(1)}\rangle = \sum_{n\neq k} \frac{H'_{kn}}{(E_k^{(0)} - E_n^{(0)})}|\psi_k^{(0)}\rangle \tag{2.34b}$$

In the context of the atom-light interaction, perturbation theory comes down to calculating the matrix elements of the dipole operator $\hat{\vec{d}}$. For any symmetric or anti-symmetric wavefunction, by letting $\vec{r} = -\vec{r}$, we get that $\langle\psi|\hat{\vec{d}}|\psi\rangle = -\langle\psi|\hat{\vec{d}}|\psi\rangle$. The expectation value of the dipole operator is equal to its negative. In other words, any symmetric or anti-symmetric wavefunction has zero dipole moment. Therefore, the first order correction to the eigenenergy in Eq. (2.34a) is also zero $\langle\psi_n^{(0)}|\hat{H}'|\psi_n^{(0)}\rangle = 0$.

Although the field does not affect the energy of the atomic levels to the first order, there is a correction to the eigenfunction in Eq. (2.34b), which means that the field mixes the states with opposite parity.

The fact that $\hat{H}'_{mn}$ is non-zero only if $|\Psi_n\rangle$ and $|\Psi_m\rangle$ have opposite parities is very insightful. According to the orbital angular momentum $\vec{L}$ [31], the atom orbitals are grouped into S orbitals (L=0), P orbitals (L=1), D orbitals (L=2), etc...and the parity of the orbitals changes alternatively. In other words, every time when L changes by 1, the parity of the orbital changes. S orbitals are symmetric, P-orbitals are anti-symmetric, D orbitals are symmetric again. For first-order, the electric field can couple S orbitals to P orbitals, but not to D orbitals.

It can be easily proved that the expectation value of the dipole moment operator for the new, first order corrected eigenstates $|\psi_n\rangle = |\psi_n^{(0)}\rangle + |\psi_n^{(1)}\rangle$ is not zero. A dipole moment is induced in the atom.

A resulting energy shift comes in as the second order correction to the energy. Substituting Eqs.(2.29) and (2.33) to (2.26b), we get that

$$E_n^{(2)} = \langle \psi_n^{(0)} | \hat{H}' | \psi_k^{(1)} \rangle = \sum_{n \neq k} \frac{H'_{nk} H'_{kn}}{E_k^{(0)} - E_n^{(0)}} \tag{2.35}$$

This second -order energy shift scales with the square of the magnitude of the electric field, which matches the result of dipole potential in Eq. (2.13). This is a consequence of the fact that the energy shift is a second order process: first we need to induce a dipole with a electric field, then we can couple to it.

At the end, the discussion of the convergency of the non-degenerate perturbation theory is necessary. The Eqs.(2.33) and (2.35) show that the convergency requirement to extend the non-degenerate perturbation through orders is

$$\left| \frac{H'_{nk}}{(E_k^{(0)} - E_n^{(0)})} \right| \ll 1 \tag{2.36}$$

which means that the energy difference $E_k^{(0)} - E_n^{(0)}$ has to be large compared with the perturbation Hamiltonian H'_{nk}, in other words, the two energy levels should be separated far enough from each other.

2.3.2 Derivation of the energy shifts of a two-level atom in an AC field

We have introduced the perturbation theory and derived the corrections to the energy and wavefunction when the atoms interact with an DC electric field. It is of significance to investigate the energy shift of the atom due to the AC stark effect since atomic physics work extensively with lasers nowadays. There are many different ways to approach this problem of a two-level atom in a laser field. We will choose a slightly round-about way of doing this.

The electric field of a travelling wave is given by

$$\vec{E} \approx \vec{E}_0 \cos(\vec{k} \cdot \vec{r} - \omega t) \tag{2.37}$$

We make an assumption here: The electric field is spatial independent over the atom. This is due to the reason that the laser wavelength is much larger than the size of the dipole of the atom. Since the magnitude of $\vec{k}$ is inversely related to the wavelength of the incident light, $k = \frac{2\pi}{\lambda}$, therefore

there exists that $\vec{k}\cdot\vec{r} \ll 1$. Then the electric field can be written as

$$\vec{E} \approx \vec{E}_0 \cos(\omega t) \tag{2.38}$$

This approximation is known as the "dipole approximation". The full Hamiltonian then becomes

$$\hat{H} = \begin{pmatrix} E_g & 0 \\ 0 & E_e \end{pmatrix} + \begin{pmatrix} 0 & -\vec{d}\cdot\vec{E}_0\cos(\omega t) \\ -\vec{d}\cdot\vec{E}_0\cos(\omega t) & 0 \end{pmatrix} \tag{2.39}$$

Obviously, this Hamiltonian has a time-dependent part $\cos(\omega t)$. If we try to solve the Schrödinger equation $i\hbar\frac{d\Psi}{dt} = \hat{H}\Psi$ by assuming $\Psi_n(t) = \Psi_n(0)e^{-iE_nt/\hbar}$, we find that

$$\begin{aligned} i\hbar\frac{d\Psi_n(t)}{dt} &= i\hbar\frac{d\Psi_n(0)e^{-iE_nt/\hbar}}{dt} \\ &= i\hbar\Psi_n(0)\frac{d(e^{-iE_nt/\hbar})}{dt} = \Psi_n(0)e^{-iE_nt/\hbar}\left(E_n(t) + t\frac{dE_n(t)}{dt}\right) \end{aligned} \tag{2.40}$$

There energy term is time-dependent in Eq. (2.40). With the following treatment, we are able to get rid of it.

We now decompose the field into its positive- and negative-rotating components

$$\begin{aligned} \vec{E}(t) =& \frac{\vec{E}_0}{2}(e^{-i\omega t} + e^{i\omega t}) \\ =& \vec{E}^{(+)}e^{-i\omega t} + \vec{E}^{(-)}e^{i\omega t} \end{aligned} \tag{2.41}$$

Therefore, the full Hamiltonian can be split into three components

$$\hat{H} = \begin{pmatrix} E_g & 0 \\ 0 & E_e \end{pmatrix} + \begin{pmatrix} 0 & -\frac{\vec{d}\cdot\vec{E}_0}{2}e^{i\omega t} \\ -\frac{\vec{d}\cdot\vec{E}_0}{2}e^{-i\omega t} & 0 \end{pmatrix} + \begin{pmatrix} 0 & -\frac{\vec{d}\cdot\vec{E}_0}{2}e^{-i\omega t} \\ -\frac{\vec{d}\cdot\vec{E}_0}{2}e^{i\omega t} & 0 \end{pmatrix} \tag{2.42}$$

We will at first ignore the last part of the Hamiltonian in Eq. (2.22) to see the effect of only the middle part on the system.

By combining the first two terms of Eq. (2.42), we get

$$\hat{H} = \hbar\begin{pmatrix} \omega_g & \frac{\Omega}{2}e^{i\omega t} \\ \frac{\Omega}{2}e^{-i\omega t} & \omega_e \end{pmatrix} \tag{2.43}$$

where $\Omega = -\frac{\vec{d}\cdot\vec{E}_0}{\hbar}$, $\omega_g = \frac{E_g}{\hbar}$, $\omega_e = \frac{E_e}{\hbar}$.

If we write the wavefunction as

$$|\Psi(t)\rangle \equiv \begin{pmatrix} c_g(t) \\ c_e(t) \end{pmatrix} \tag{2.44}$$

The Schrödinger equation then becomes

$$i \begin{pmatrix} \dot{c_g}(t) \\ \dot{c_e}(t) \end{pmatrix} = \begin{pmatrix} \omega_g & \frac{\Omega}{2} e^{i\omega t} \\ \frac{\Omega}{2} e^{-i\omega t} & \omega_e \end{pmatrix} \begin{pmatrix} c_g(t) \\ c_e(t) \end{pmatrix} \tag{2.45}$$

However, Eq. (2.45) still has a time-dependence in the Hamiltonian, but it is about to change with a small substitution.

We define $\tilde{c_g} = c_g(t)e^{-i\omega t}$ and $\tilde{c_e} = c_e(t)e^{i\omega t}$. The vector $\begin{pmatrix} c_g(t) \\ c_e(t) \end{pmatrix}$ can be written in terms of $\begin{pmatrix} \tilde{c_g}(t) \\ \tilde{c_e}(t) \end{pmatrix}$ by

$$\begin{pmatrix} c_g(t) \\ c_e(t) \end{pmatrix} = \begin{pmatrix} \tilde{c_g}(t)e^{i\omega t/2} \\ \tilde{c_e}(t)e^{-i\omega t/2} \end{pmatrix} \tag{2.46}$$

We also write down the vector $\begin{pmatrix} \dot{c_g}(t) \\ \dot{c_e}(t) \end{pmatrix}$ as a function of $\begin{pmatrix} \tilde{c_g}(t) \\ \tilde{c_e}(t) \end{pmatrix}$ and $\begin{pmatrix} \dot{\tilde{c}}_g(t) \\ \dot{\tilde{c}}_e(t) \end{pmatrix}$,

$$\begin{pmatrix} \dot{c_g}(t) \\ \dot{c_e}(t) \end{pmatrix} = \begin{pmatrix} \dot{\tilde{c}}_g(t)e^{i\omega t/2} + \frac{i\omega}{2}\tilde{c_g}e^{i\omega t/2} \\ \dot{\tilde{c}}_e(t)e^{-i\omega t/2} - \frac{i\omega}{2}\tilde{c_e}e^{-i\omega t/2} \end{pmatrix} \tag{2.47}$$

We substitute Eq. (2.46) and Eq. (2.47) to Eq. (2.45),

$$i \begin{pmatrix} \dot{\tilde{c}}_g(t)e^{i\omega t/2} + \frac{i\omega}{2}\tilde{c_g}e^{i\omega t/2} \\ \dot{\tilde{c}}_e(t)e^{-i\omega t/2} - \frac{i\omega}{2}\tilde{c_e}e^{-i\omega t/2} \end{pmatrix} = \begin{pmatrix} \omega_g & \frac{\Omega}{2} e^{i\omega t} \\ \frac{\Omega}{2} e^{-i\omega t} & \omega_e \end{pmatrix} \begin{pmatrix} \tilde{c_g}(t)e^{i\omega t/2} \\ \tilde{c_e}(t)e^{-i\omega t/2} \end{pmatrix} \tag{2.48}$$

Grouping the time derivatives on one side and the rest on the other side, we get the matrix equation

$$i\begin{pmatrix} e^{i\omega t/2} & 0 \\ 0 & e^{-i\omega t/2} \end{pmatrix}\begin{pmatrix} \dot{\tilde{c}}_g(t) \\ \dot{\tilde{c}}_e(t) \end{pmatrix} = \begin{pmatrix} (\omega_g+\omega/2)e^{i\omega t/2} & \frac{\Omega}{2}e^{i\omega t} \\ \frac{\Omega}{2}e^{-i\omega t} & (\omega_e-\omega/2)e^{-i\omega t/2} \end{pmatrix}\begin{pmatrix} \tilde{c}_g(t) \\ \tilde{c}_e(t) \end{pmatrix} \tag{2.49}$$

We can get rid of $\begin{pmatrix} e^{i\omega t/2} & 0 \\ 0 & e^{-i\omega t/2} \end{pmatrix}$ by multiplying a time derivatives of matrix $\begin{pmatrix} e^{-i\omega t/2} & 0 \\ 0 & e^{i\omega t/2} \end{pmatrix}$ on both sides. We find that

$$i\begin{pmatrix} \dot{\tilde{c}}_g(t) \\ \dot{\tilde{c}}_e(t) \end{pmatrix} = \begin{pmatrix} (\omega_g+\omega/2) & \frac{\Omega}{2} \\ \frac{\Omega}{2} & (\omega_e-\omega/2) \end{pmatrix}\begin{pmatrix} \tilde{c}_g(t) \\ \tilde{c}_e(t) \end{pmatrix} \tag{2.50}$$

We find that Eq. (2.50) is familiar, except that all the $\begin{pmatrix} c_g(t) \\ c_e(t) \end{pmatrix}$ now become to $\begin{pmatrix} \tilde{c}_g(t) \\ \tilde{c}_e(t) \end{pmatrix}$. Most importantly, there is no time dependence left in the matrix and we essentially have an equation of the form $i\hbar\dot{\tilde{\Psi}}(t) = \tilde{H}\tilde{\Psi}(t)$ which is a Schrödinger-like equation with a time-independent Hamiltonian.

Since the overall energy of a state doesn't matter, only the energy difference matters. In other words, we can define that $E_g = 0, E_{\mathrm{e}} = E$ or $E_{\mathrm{e}} = 0, E_{\mathrm{g}} = -E$. The two choices are the same. We can therefore add any constant we want to ω_g as long as we also add the same to ω_e.

We shift the energies by adding the constant $(\omega_e - \omega_g)/2$ to the atomic frequencies. Defining that $\omega_{eg} \equiv \omega_e - \omega_g$ and $\Delta = \omega_{eg} - \omega$, we can write down the matrix form of $\hat{\tilde{H}}$ in terms of ω_{eg} and Ω

$$\hat{\tilde{H}} = \hat{H}_{AC} = \hbar\begin{pmatrix} (\omega-\omega_{eg})/2 & \Omega/2 \\ \Omega/2 & -(\omega-\omega_{eg})/2 \end{pmatrix} = \hbar\begin{pmatrix} -\Delta/2 & \Omega/2 \\ \Omega/2 & \Delta/2 \end{pmatrix} \tag{2.51}$$

The Schrödinger-like equation 2.50 now becomes:

$$i\begin{pmatrix} \dot{\tilde{c}}_g(t) \\ \dot{\tilde{c}}_e(t) \end{pmatrix} = \begin{pmatrix} -\Delta/2 & \Omega/2 \\ \Omega/2 & \Delta/2 \end{pmatrix}\begin{pmatrix} \tilde{c}_g(t) \\ \tilde{c}_e(t) \end{pmatrix} \tag{2.52}$$

With the math and a few approximations, we notice that the Hamiltonian above is essentially the same as the Hamiltonian for a DC field [32]

$$\hat{H}_{DC} = \hbar \begin{pmatrix} -\omega_{eg}/2 & \Omega/2 \\ \Omega/2 & \omega_{eg}/2 \end{pmatrix} \tag{2.53}$$

while

$$\hat{H}_{AC} = \hbar \begin{pmatrix} -\Delta/2 & \Omega/2 \\ \Omega/2 & \Delta/2 \end{pmatrix} \tag{2.54}$$

In other words, all our formulas and reasonings for DC field still apply, with only the difference that the energy difference term $E_\mathrm{e} - E_\mathrm{g}$ in $\hat{H}_{DC}$ is now replaced with the detuning of the laser from the resonance $(E_\mathrm{e} - E_\mathrm{g}) - \hbar\omega$ in $\hat{H}_{AC}$. Therefore, it is reasonable if we replace the energy difference term in the Eqs.(2.35) with a detuning term to obtain the energy correction of the states for the AC field. Here we choose to find the exact eigenenergies.

The time-independent Schrödinger-like equation is written in a matrix form as

$$\hbar \begin{pmatrix} -\Delta/2 & \Omega/2 \\ \Omega/2 & \Delta/2 \end{pmatrix} \begin{pmatrix} \tilde{c_g}(t) \\ \tilde{c_e}(t) \end{pmatrix} = E_n \begin{pmatrix} \tilde{c_g}(t) \\ \tilde{c_e}(t) \end{pmatrix} \tag{2.55}$$

We can get the eigenenergies by

$$\det \begin{pmatrix} -\frac{\hbar\Delta}{2} - E_n & \frac{\hbar\Omega}{2} \\ \frac{\hbar\Omega}{2} & \frac{\hbar\Delta}{2} - E_n \end{pmatrix} = 0 \tag{2.56}$$

and the eigenenergies are $E_n = \pm\frac{\Delta\hbar}{2}\sqrt{1 + \dfrac{\Omega^2}{\Delta^2}}$.

We consider the case $\dfrac{\Omega}{\Delta} \ll 1$, where the interaction is much weaker than the detuning of the laser frequency from the resonance. The energy can be expanded in a Taylor series around $\frac{\Omega}{\Delta} \approx 0$ up to order of $(\frac{\Omega}{\Delta})^2$. For a monochromatic optical field of the form

$$\vec{E}(t) = \frac{\vec{E}_0}{2} e^{-i\omega t} = \vec{E}^{(+)} e^{-i\omega t} \tag{2.57}$$

we get the perturbed energies

$$E'_\mathrm{g} = E_\mathrm{g} - \frac{\hbar\Omega^2}{4\Delta} = E_\mathrm{g} - \frac{|\langle g|\vec{d}\cdot\hat{\epsilon}|e\rangle|^2 |E^{(+)}|^2}{\hbar(\omega_0 - \omega)} \tag{2.58}$$

$$E'_{\mathrm{e}} = E_{\mathrm{e}} + \frac{\hbar\Omega^2}{4\Delta} = E_{\mathrm{e}} + \frac{|\langle g|\vec{d}\cdot\hat{\epsilon}|e\rangle|^2|E^{(+)}|^2}{\hbar(\omega_0-\omega)} \tag{2.59}$$

where we write here $\omega_{eg} = \omega_0$ and $\vec{E}_0 = \hat{\epsilon}E_0$.

They are the eigenenergies of the tilde-system. In principle, we could try to find the energies in the non-tilde system. Fortunately, when $\Omega = 0$, the ground state energy E_g and excited state energy E_e in the tilde system are corresponding to that of the non-tilde system. It is therefore reasonable for us to assign the perturbed energies in Eq. 2.58 and Eq. 2.59 to the non-tilde system.

Until now, we should not forget the fact that we ignored the last part of our Hamiltonian in Eq. (2.42). Now we take it into account. Fortunately, we don't have to go through all the math again, we just realized that if we had thrown out the middle term in (2.42) instead of the last, our calculation would have performed with $\omega \longrightarrow -\omega$. Correspondingly, our Hamiltonian would then be

$$\hat{H}_{AC} = \hbar\begin{pmatrix} -(\omega+\omega_{eg})/2 & \Omega/2 \\ \Omega/2 & (\omega+\omega_{eg})/2 \end{pmatrix} \tag{2.60}$$

The energy shift would then be

$$-\frac{|\langle g|\vec{d}\cdot\hat{\epsilon}|e\rangle|^2|E^{(-)}|^2}{\hbar(\omega_0+\omega)} \quad \text{and} \quad \frac{|\langle g|\vec{d}\cdot\hat{\epsilon}|e\rangle|^2|E^{(-)}|^2}{\hbar(\omega_0+\omega)} \tag{2.61}$$

If $\omega \approx \omega_0$, then $\Delta = \omega_0 - \omega \ll \omega_0 + \omega$, and the energy shifts in Eq. (2.61) are small to be neglected. This is also known as the Rotating Wave Approximation (RWA). That is way we threw out the rotating wave term in Eq. (2.42). If it turns out that $\Delta = \omega_0 - \omega \sim \omega_0 + \omega$, we need to keep them however. In that case, we would simply add the two perturbations together:

$$\Delta E_{\mathrm{g}} = -\frac{|\langle g|\vec{d}\cdot\hat{\epsilon}|e\rangle|^2|E^{(+)}|^2}{\hbar(\omega_0-\omega)} - \frac{|\langle g|\vec{d}\cdot\hat{\epsilon}|e\rangle|^2|E^{(+)}|^2}{\hbar(\omega_0+\omega)} \tag{2.62}$$

and

$$\Delta E_{\mathrm{e}} = \frac{|\langle g|\vec{d}\cdot\hat{\epsilon}|e\rangle|^2|E^{(+)}|^2}{\hbar(\omega_0-\omega)} + \frac{|\langle g|\vec{d}\cdot\hat{\epsilon}|e\rangle|^2|E^{(+)}|^2}{\hbar(\omega_0+\omega)} \tag{2.63}$$

where $|E^{(+)}|^2 = |E^{(-)}|^2$. For a two-level atom in a red-detuned laser light, the energy shift is negative for the ground state and positive for the excited

state. Therefore, the effect of the perturbation is to raise the energy of the excited state and lower the ground state. The behaviors of the two states is demonstrated in Fig 2.3.

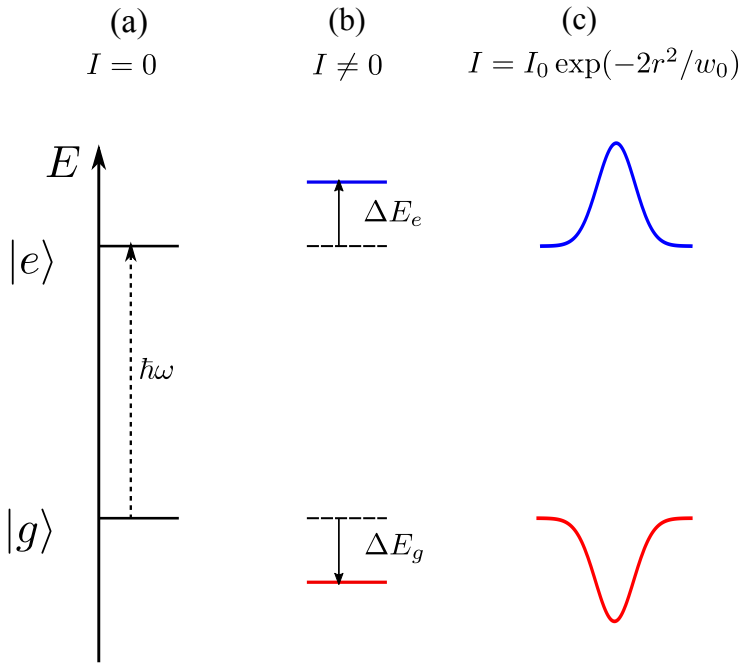

Figure 2.3: Schematic of the energy shift of a two-level atom in a red-detuned light with intensity I. (a) The energy shift is zero when $I = 0$. (b) The ground state energy is shifted down by ΔE_g, and the excited state energy is shifted up by ΔE_e, respectively. (c) The energy shifts of ground state and excited state in a Gaussian beam.

The energy shift increases with the strength of the Ω^2 which is proportional to the intensity of the light. The energy shift also decreases with the detuning of the laser from the resonance .

With the relation between the potential and polarizability in Eq.(2.4), we get the corresponding dynamic polarizability

$$\mathrm{Re}[\alpha(\omega)] = \frac{2\omega_0 |\langle g|\vec{d}\cdot\hat{\epsilon}|e\rangle|^2}{\hbar(\omega_0^2 - \omega^2)} \tag{2.64}$$

2.3.3 Polarizability of a multi-level atom

Until now, we treated the atom as a two-level system, however, real atoms have multiple levels. Therefore, we need to sum over contributions of multiple levels in order to drive a right expression of the polarizability of the state $|i\rangle$

$$\mathrm{Re}[\alpha(\omega)] = \sum_{j\neq i} \frac{2\omega_{ji}|\langle i|\vec{d}\cdot\hat{\epsilon}|j\rangle|^2}{\hbar(\omega_{ji}^2-\omega^2)} \tag{2.65}$$

The matrix element $\langle i|\vec{d}\cdot\hat{\epsilon}|j\rangle$ can be written as a product of a reduced matrix element $||d||$ and a real transition coefficient c_{ij} by the Wigner Eckart theorem [33],

$$\langle i|\vec{d}\cdot\hat{\epsilon}|j\rangle = c_{ij}||d|| \tag{2.66}$$

where $||d||$ depends on the electronic orbital wavefunctions. The transition coefficient c_{ij} refers to the coupling strength between two specific sublevels $|i\rangle$ and $|j\rangle$.

If we consider the angular momentum quantum number of the states $|i\rangle$ and $|j\rangle$ as J_i and J_j, with the corresponding magnetic quantum numbers as m_i and m_j. The coefficient c_{ij} can be written as [29]

$$c_{ij} = \sqrt{(2J_j+1)}\begin{pmatrix} Ji & 1 & J_j \\ -m_i & p & m_j \end{pmatrix} \tag{2.67}$$

where p denotes the polarization of the laser light. $p = 0$ stands for π-polarized light, and $p = \pm 1$ are for circularly-polarized light. The expression above is not zero only when

$$m_i + p = m_j \tag{2.68}$$

Therefore, the specific transition matrix element is then

$$\langle i|\vec{d}\cdot\hat{\epsilon}|j\rangle = \sqrt{(2J_j+1)}\begin{pmatrix} Ji & 1 & J_j \\ -m_i & p & m_j \end{pmatrix}||d|| \tag{2.69}$$

In order to calculate the state-dependent ground-state dipole potential or state-dependent polarizability, we have to sum up the contributions from all transition allowed specific excited states, with linestrengths c_{ij} and detunings Δ_{ij} taken into account.

Although this state-dependent consideration gives modifications to the dipole transitions, making the calculations more complex, it can provide

great advantages to the experiments with the ultracold atoms. An example is the context of an atomic clock in an optical dipole trap [34], where the transition frequency between two atomic states serves as a time base for the atomic clock. However, this transition frequency is changed if the two atomic states have different polarizabilities, thereby experiencing difference energy shifts in the optical dipole trap. This problem can be solved by finding an appropriate light frequency, such that the frequency-dependent polarizabilities of the two atomic states are identical. Consequently, the transition frequency of the clock is unperturbed by the laser light, while the experiment still benefits from the trapping environment. This frequency is also known as magic frequency.

Chapter 3

Polarizable system-diatomic molecules

As we mentioned in the introduction, it is worthwhile to extend the investigation of the dynamic polarizability to diatomic molecules due to their special properties. According to the formalism of the polarizability in the last chapter, the derivation of the molecular polarizability requires a knowledge of the energy difference ω_{ji} between two molecular states $|i\rangle$ and $|j\rangle$ and the operator $|\langle i|\vec{d}\cdot\hat{\epsilon}|j\rangle|$. They are not easy to obtain since molecules possess complex internal structures with more internal degrees of freedom than atoms. Fortunately, we can simplify the description of diatomic molecules with the Born-Oppenheimer approximation [35] which separates the molecular wavefunction into an electronic component and a nuclear component. With this approximation, we are able to derive the molecular energy as contributions from the electrons and nuclei. This separation works also for the transition dipole moment.

3.1 Separation of diatomic molecular wavefunctions with Born-Oppenheimer approximation

Atoms and molecules both contain negatively charged electrons and positively charged nuclei. However, in contrast to atoms which contain only one nucleus, molecules contain two or more positively charged nuclei. Diatomic molecules consist of two positively charged nuclei which are connected by the internuclear axis. The electrons move outside the nuclei, meanwhile, the two nuclei in diatomic molecules can vibrate, changing the internuclear dis-

tance. They can also rotate with respect to each other around an axis. The vibrational motion and rotational motion make the structures of diatomic molecules complex. In total, all the particles which make up the molecules are moving relative to each other. Therefore, it can be very difficult when we try to get the energies of diatomic molecules by solving the Schrödinger equation.

Fortunately, there exist various sophisticated approximations in quantum mechanics. We introduce here the Born-Oppenheimer approximation, which simplifies the motions of diatomic molecules by separating them into a nuclear component and an electronic component. If we write this concept in the math frame, the full Hamiltonian of a diatomic molecule can be written with two components

$$\hat{H} = \hat{H}_{\mathrm{nu}} + \hat{H}_{\mathrm{e}} \tag{3.1}$$

where

$$\hat{H}_{\mathrm{nu}} = -\frac{\hbar^2}{2}\sum_{k=1}^{2}\frac{1}{M_k}\nabla_k^2 \tag{3.2}$$

and

$$\hat{H}_{\mathrm{e}} = -\frac{\hbar^2}{2m_e}\sum_i \nabla_i^2 - \frac{e^2}{4\pi\epsilon_0}\sum_i \frac{Z_1}{r_{1i}} - \frac{e^2}{4\pi\epsilon_0}\sum_i \frac{Z_2}{r_{2i}} + \frac{e^2}{4\pi\epsilon_0}\sum_{ij}\frac{1}{r_{ij}} + \frac{e^2}{4\pi\epsilon_0}\frac{Z_1 Z_2}{R} \tag{3.3}$$

$\hat{H}_{\mathrm{nu}}$ represents the kinetic energies of the nuclei 1 and 2, M_1, M_2 are the mass of the nuclei 1 and 2, ∇_1^2 and ∇_2^2 are the Laplace operator of the nuclear positions. The first term of $\hat{H}_{\mathrm{e}}$ is the electronic kinetic energy, m_e is the mass of an electron, ∇_i^2 is the Laplace operator of the electronic position. The second and third terms are the attractive Coulomb potentials between the nuclei and the electrons, r_{1i} is the distances between nuclei 1 and electrons. r_{2i} is the distances between nuclei 2 and electrons, Z_1 and Z_2 are the atomic number of the nuclei 1 and nuclei 2. The fourth term is the repulsive Coulomb potential between the electrons, r_{ij} is the distance between electrons i and j. The last term of $\hat{H}_{\mathrm{e}}$ is a repulsive term, R is the distance between the two nuclei.

The repulsive term $\frac{e^2}{4\pi\epsilon_0}\frac{Z_1 Z_2}{R}$ in the $\hat{H}_{\mathrm{e}}$ has a dependence on the inter-nuclear distance R. This is based on the fact that: Since the mass of the nuclei M are heavier than the electrons m_e, the electrons in molecules move much faster than the nuclei. We can consider the two motions are largely

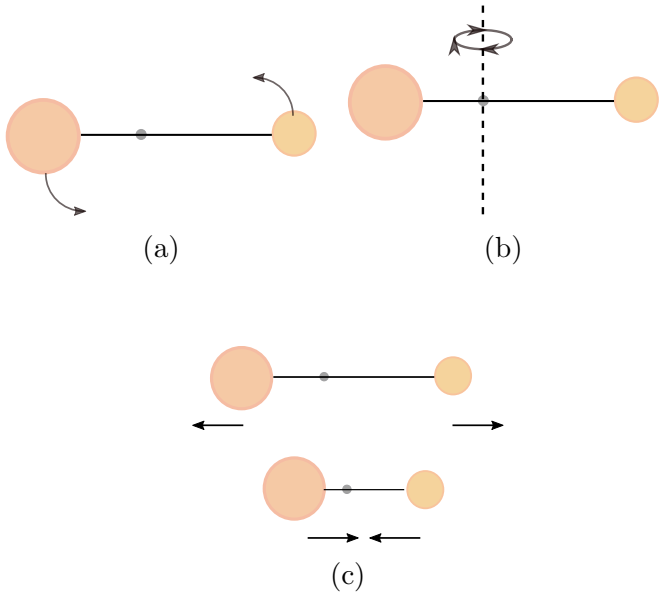

Figure 3.1: The nuclei motion includes: (a) Rotation in the plane of the paper. (b) Rotation out of the plane of the paper. (c) Vibrational motion along the bond between two nucleus.

decoupled. In other words, the nuclei are taken as stationary when we are describing the electronic motions. However, the nuclei can be stationary at different positions. Therefore, the electronic motion depends parametrically on the nuclei coordinate.

Based on this, we can separate the wavefunctions $\psi(\vec{r_i}, \vec{R_k})$ into nuclear part and electronic part.

$$\psi(\vec{r_i}, \vec{R_k}) = \Psi(\vec{R_k})\varphi_{\mathrm{e}}(\vec{r_i}, \vec{R_k}) \tag{3.4}$$

where $\Psi(\vec{R_k})$ is the nuclear wavefunction which depends on the positions $\vec{R_k}$ of the nuclei. $\varphi_{\mathrm{e}}(\vec{r_i}, \vec{R_k})$ is the electronic wavefunction of a clamped molecule at fixed nuclear parameter $\vec{R_k}$. $\vec{r_i}$ is the position of the electrons.

Inserting Eq. (3.4) into the Schrödinger equation of diatomic molecules, we obtain that

$$[\hat{H}_{\mathrm{nu}} + \hat{H}_{\mathrm{e}}]\Psi(\vec{R_k})\varphi_{\mathrm{e}}(\vec{r_i}, \vec{R_k}) = E\Psi(\vec{R_k})\varphi_{\mathrm{e}}(\vec{r_i}, \vec{R_k}) \tag{3.5}$$

where E is the total energy of the molecule.

By expanding all terms in the last equation,

$$\varphi_{\mathrm{e}}(\vec{r_i},\vec{R_k})\hat{H}_{\mathrm{nu}}\Psi(\vec{R_k})+\Psi(\vec{R_k})E_{\mathrm{e}}(\vec{R_k})\varphi_{\mathrm{e}}(\vec{r_i},\vec{R_k})=\Psi(\vec{R_k})\varphi_{\mathrm{e}}(\vec{r_i},\vec{R_k}) \tag{3.6}$$

we derive a Schrödinger-like equation with just the nuclear degrees of freedom.

$$[\hat{H}_{\mathrm{nu}}+E_{\mathrm{e}}(\vec{R_k})]\Psi(\vec{R_k})=E\Psi(\vec{R_k}) \tag{3.7}$$

The energy term $E_{\mathrm{e}}(R_k)$ in Eq. (3.7) depends on the nuclear coordinates. It is obtained by the following process: for a fixed nuclear coordinate R_k, we solve the electronic Schrödinger equation

$$\hat{H}_{\mathrm{e}}(\vec{r_i},\vec{R_k})\varphi_{\mathrm{e}}(\vec{r_i},\vec{R_k})=E_{\mathrm{e}}\varphi_{\mathrm{e}}(\vec{r_i},\vec{R_k}) \tag{3.8}$$

If we keep on repeating the calculations of the energies of E_{e} in Eq. (3.8) at many nuclear coordinates, we can get this $E_e(\vec{R_k})$ which is an electronic energy curve with a parametric dependence on the nuclear position. We usually call this the electronic potential energy curve.

The eigenenergy E of the molecular system can be derived if the electronic potential energy $E_{\mathrm{e}}(\vec{R_k})$ and the nuclear Hamiltonian are known.

3.2 Solving the nuclear Schrödinger equation

In this section, we will try to solve the nuclear Schrödinger equation (3.7) by discussing the kinetic energy term $\hat{H}_{\mathrm{nu}}$.

The Eq. (3.7) can be translated to

$$\left[-\frac{\hbar^2}{2\mu}\nabla^2+E_e(R)\right]\Psi(\vec{R})=E\Psi(\vec{R}) \tag{3.9}$$

This is an equation of a "particle" with reduced mass $\mu=M_AM_B/(M_A+M_B)$ in a potential of $E_e(R)$ which depends only on the internuclear distance R between the two nuclei. However, the nuclear wavefunction $\Psi(\vec{R})$ depends not only on the distance R, but also on the orientation of nuclei in space which we describe with the spherical harmonics $Y(\theta,\phi)$. Therefore, the nuclear wavefunction $\Psi(\vec{R})$ can be written as

$$\Psi(\vec{R})=\chi(R)Y(\theta,\phi) \tag{3.10}$$

If we insert the 3.10 and write out the Laplace operator ∇^2 into Eq. (3.9),

it becomes as

$$\Big[-\frac{\hbar^2}{2\mu}\Big(\frac{1}{R^2}\frac{\partial}{\partial R}\Big[R^2\frac{\partial}{\partial R}\Big] - \frac{\hat{J}^2}{\hbar^2 R^2}\Big) + E_e(R)\Big]\chi(R)Y(\theta,\phi) = E\chi(R)Y(\theta,\phi) \tag{3.11}$$

where J is the operator of the rotational angular momentum

Analogous to the treatment of the hydrogen atom, we can get equations for the radial part and the angular part,

$$\hat{J}^2 Y(\theta,\phi) = J(J+1)\hbar^2 Y(\theta,\phi) \tag{3.12}$$

$$\Big[-\frac{\hbar^2}{2\mu}\frac{1}{R^2}\frac{d}{dR}\Big(R^2\frac{d}{dR}\Big) - \frac{J(J+1)\hbar^2}{2\mu R^2} + E_e(R)\Big]\chi(R) = E\chi(R) \tag{3.13}$$

where J is the quantum number of the rotational angular momentum. The angular dependent term $\dfrac{J(J+1)\hbar^2}{2\mu R^2}$ in Eq. (3.13) is also referred as a rotational energy

$$E_{\text{rot}} = \frac{\hbar^2}{2\mu R^2}J(J+1) \tag{3.14}$$

The energy interval between two rotational levels J and $J+1$ is

$$\Delta E_{\text{rot}} = E_{\text{rot}}(J+1) - E_{\text{rot}}(J) = \frac{(J+1)\hbar^2}{2\mu R^2} \tag{3.15}$$

which is not equidistant, however, it increases linearly the with the rotational quantum number J.

Around the bottom of the potential R_e, the potential energy $E_e(R)$ in Eq. (3.13) can be well approximated by a parabolic potential

$$E_e(R) \approx E_e(R_e) + \frac{1}{2}kx^2 \tag{3.16}$$

where $x = R - R_e$ and $k = \left.\dfrac{d^2E_e(R)}{dR^2}\right|_{R=R_e}$.

By putting Eq. (3.16) into the nuclear radial Schrödinger equation (3.13) and define a vibrational wavefunction $\Psi_\upsilon = \chi(R)R$, it becomes as

$$\Big[-\frac{\hbar^2}{2\mu}\frac{\partial}{\partial x^2} + \frac{1}{2}kx^2\Big]\Psi_\upsilon = E_\upsilon\Psi_\upsilon \tag{3.17}$$

where

$$E_\upsilon = E - \frac{\hbar^2}{2\mu R^2} J(J+1) - E_e(R_e) \tag{3.18}$$

This is the Schrödinger equation for the 1D quantum harmonic oscillator. In a harmonic approximation of the potential energy, the vibrational energy is

$$E_\upsilon = (\upsilon + \frac{1}{2})\hbar\sqrt{\frac{k}{\mu}} \tag{3.19}$$

υ is the vibrational quantum number.

The total energy E is thus

$$\begin{aligned} E = E_{e\upsilon J} &= E_e(R_e) + E_\upsilon + E_{\text{rot}} \\ &= E_e(R_e) + (\upsilon + \frac{1}{2})\hbar\sqrt{\frac{k}{\mu}} + \frac{\hbar^2}{2\mu R^2} J(J+1) \end{aligned} \tag{3.20}$$

Now we have finished the process of finding the total energy of diatomic molecules with a few approximations, however, we should be aware that the parabolic potential is only a good approximation in the vicinity of the potential minimum at $R = R_e$. When $|R - R_e|$ gets larger, this harmonic potential approximation breaks down. A typical potential curve behaves like this: when the two atoms in the molecules are very far from each other, the potential energy curve will flatten out, showing a dissociation limit, where the molecule is no longer bound, but two separate atoms instead. When R is getting smaller, the potential energy is going down below the dissociation limit. The curve keeps going down until the two atoms reach an equilibrium distance value R_e. The energy arises when R is smaller than R_e. If $R \ll R_e$, the internuclear repulsion gets so large that the potential is large and positive. A common-used function which is used to describe this behavior is the Morse potential [36] $E_e(R) = D_e[1 - e^{-a(R-R_e)}]^2$ is plotted in Fig 3.2, where D_e is the difference between dissociation energy and energy at equilibrium position. There are also many excited states which are not bound, and their potential energy curves decay with the internuclear distance exponentially.

The corresponding expression of the vibrational energy levels with the Morse potential can be derived by the potential into the Eqs. (3.13). In such cases, the intervals between adjacent levels are no longer equidistant, the separations decrease with increasing vibrational quantum number υ. This agrees well with experimental observations.

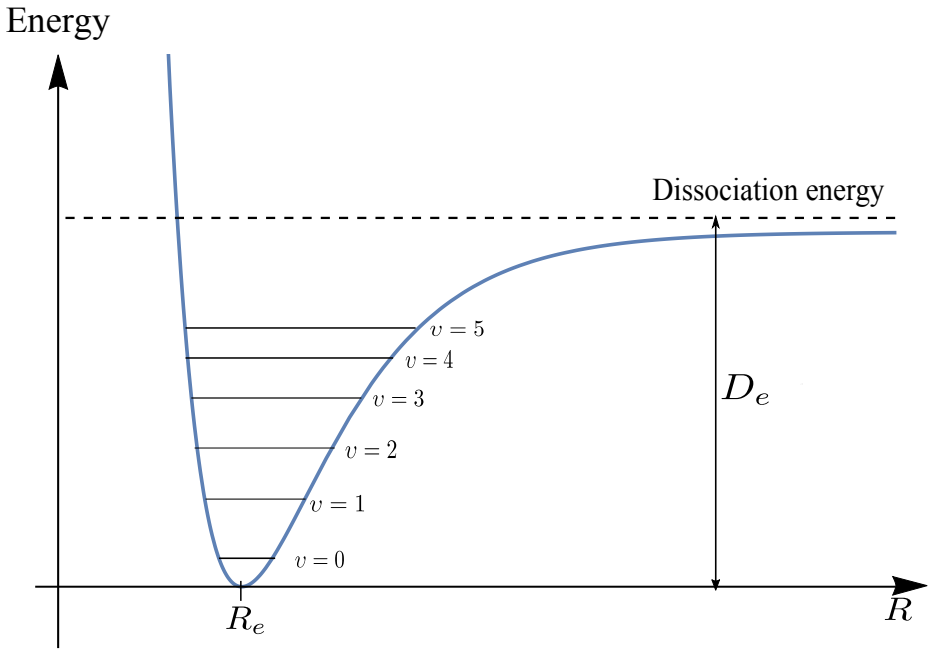

Figure 3.2: A sketch of a Morse potential [36] for a bound electronic state of a diatomic molecule. The energy curve flattens out at very large internuclear distance where the molecule is no longer bound. It is two separate atoms instead. As the two atoms move towards each other, the potential energy decreases. The energy reaches a minimum value at an internuclear distance R_e. D_e is the dissociation energy. The vibrational energy difference between two adjacent vibrational levels decreases, which is different from that of a harmonic potential.

3.3 Determination of the analytical potential energy functions

Although Morse potential describe the anharmonicity part of the potential, it is a simple function which is defined only with three parameters, therefore, it is not used often in modern spectroscopy. Nowadays, there is considerable amount of work which has developed sophisticated potentials of diatomic molecules. Among them, there are theoretical approaches, e.g. *ab initio* methods [37, 38], however, the derivation of potential energy with spectroscopic data from the experimental measurements can provide more accuracy than the theoretical approaches. In this section, we will introduce several common used examples.

The first one is the parameter-fit/Rydberg-Klein-Rees(RKR) method [39] (demonstrated in Fig. 3.3) which decides the diatomic potential by calculating the turning point of the potential. It is been known that the energy levels of diatomic molecules can be described with the [40] expressions

$$G(\upsilon) = \omega_e(\upsilon + \frac{1}{2}) - \omega_e x_e(\upsilon + \frac{1}{2})^2 + \omega_e y_e(\upsilon + \frac{1}{2})^3 + \cdots \tag{3.21}$$

$$F_\upsilon(J) = B_\upsilon J(J+1) - D_\upsilon[J(J+1)]^2 + H_\upsilon[J(J+1)]^3 + \cdots \tag{3.22}$$

$$B_\upsilon = B_e - \alpha_e(\upsilon + \frac{1}{2}) + \gamma_e(\upsilon + \frac{1}{2})^2 + \cdots \tag{3.23}$$

$$D_\upsilon = D_e + \beta_e(\upsilon + \frac{1}{2}) + \cdots \tag{3.24}$$

In the next step, the parameters G_υ, B_υ, D_υ, H_υ in the expressions are obtained by fitting the experimental data with an empirical fitting procedure [41]. With the two parameters G_υ and B_υ, a RKR potential can be produced by an inversion procedure [42]. Doing one round of this procedure might not ensure the consistency. This is due to the reason that: by using the program "Level" [43], the RKR potential can reversely generate parameters of D_υ, H_υ, etc., which might not consistent with those from the empirical fitting procedure. We therefore have to do iterative procedure. It is done as follows: We keep the D_υ, H_υ generated from the program "Level" and then operate another fit from the experimental data to get the improved parameters G_υ and B_υ. With these two improved G_υ and B_υ, a RKR potential is again produced. Repeat this iterative procedure several times until the self consistency test is done.

This parameter-fit/RKR method has some limitations, e.g. it lacks information to extrapolate the point wise potential to a region beyond the experimental data.

Regarding the limitations, there are approaches which directly define analytical potential function for wide range of internuclear distance R and fit the experimental data with the potential function directly. The determination procedure is demonstrated in Fig. 3.4:

Step 1: At first, parametrized potential functions are chosen for diatomic molecules of interest.

Step 2: Inserting the potential to the radial Schrödinger equation 3.13

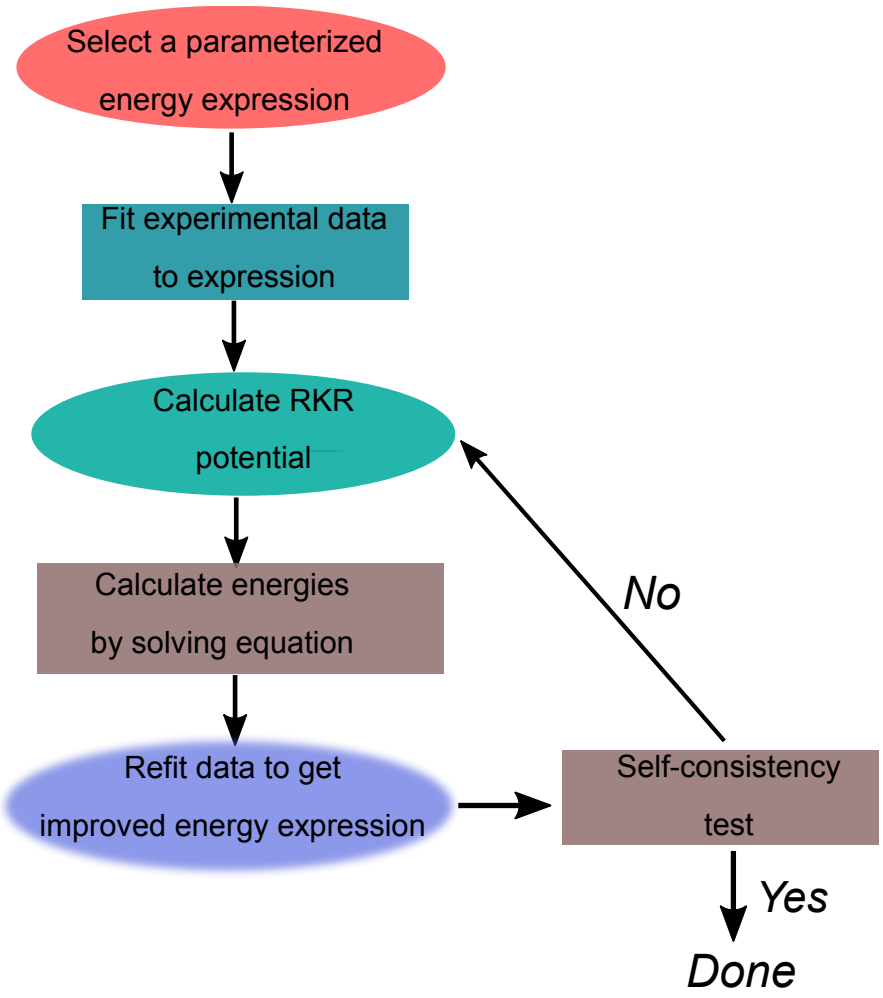

Figure 3.3: Outline of the iterative constrained-parameter fitting procedure. Fitting the experimental data to an empirical energy expression is done by the program [41]. Then a point-wise potential can be decided by RKR inversion procedure [42]. The energies are derived by solving the Schrödinger equation with the program "Level" [43].

and solving it by the program "Level" [43], we obtain the eigenvalues of the molecules.

Step3: Now compare the calculated transition frequencies with the experimental frequency data.

Step 4: Adjusting the parameters of the analytical potential function if they are not consistent with each other.

In recent years, there are a number of groups which developed successful analytical potential functions for various diatomic molecules. Here we introduce two which we use to describe the potentials of the molecules of interest in this thesis.

(i) The "Morse/Lennard-Jones" potential function V(r) was proposed by R. J. Le. Roy and P. G. Hajigeorgiou in [45]. For example, this potential function was adopted in a paper [46] to decide the potential of the state $D^1\Pi$ of NaK molecules. The expression of the analytical potential is

$$V_{\mathrm{MLJ}}(R) = \mathscr{D}_e\left[1 - \frac{(R_e)^6}{R^6} e^{-\phi_{\mathrm{MLJ}}(R) y_p(R)}\right]^2 \tag{3.25}$$

where R is the internuclear distance, R_e is the equilibrium distance and $\mathscr{D}_e$ is the vertical potential difference between the dissociation limit and equilibrium distance.

$\phi_{\mathrm{MLJ}}(R)$ and $y_p(R)$ are functions which are defined as

$$\phi_{\mathrm{MLJ}}(R) = [1 - y_p(R)] \sum_{i=0}^{N_S(\mathrm{or}N_L)} \phi_i y_p(R)^i + y_p(R)\phi_\infty \tag{3.26}$$

$$y_p(R) = \frac{R^p - R_e^p}{R^p + R_e^p} \tag{3.27}$$

where p, ϕ_i, ϕ_∞ are parameters. For short-range of the potential ($R < R_e$), $\phi_{\mathrm{MLJ}}(R)$ sums from $i = 0$ to N_S. For long-range of the potential ($R > R_e$), $\phi_{\mathrm{MLJ}}(R)$ sums from N_S to N_L. In the paper [46], $p = 2$, $N_s = 2$ and $N_L = 8$. The parameters of ϕ_i are chosen with optimized values.

(ii) Another analytical potential curve is introduced by Tiemann and coworkers [47,48] where a complete potential energy curve is divided into three parts, a repulsive short range part $U_{SR}(R)$, an inner well $U(R)$ which includes the equilibrium position R_e and a long range part $U_{LR}(R)$.

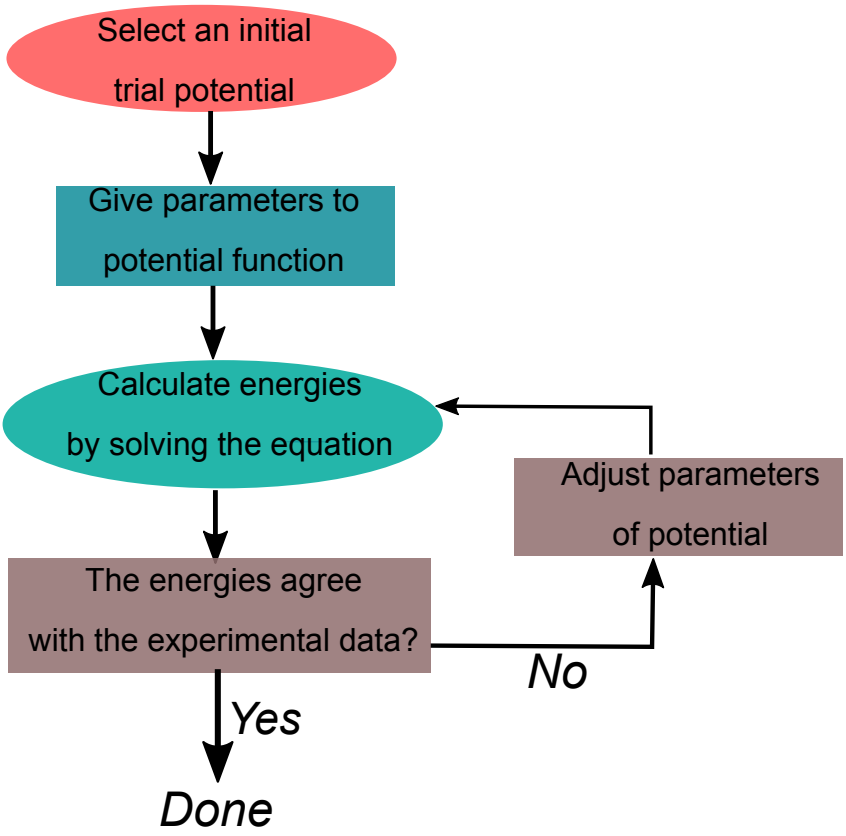

Figure 3.4: Schematic of the direct fitting potential procedure which fits the observed experimental data to a compact analytical potential function by a least-square fitting method [44].

The expressions for the three ranges are given respectively as

$$U_{\mathrm{SR}}(R) = A + \frac{B}{R^q} \qquad \text{for} \quad R < R_i \tag{3.28}$$

$$U(R) = \sum_{k=0}^{n} a_k x^k \qquad \text{for} \quad R_i \leq R \leq R_o \tag{3.29}$$

$$\text{with} \qquad x = \frac{R - R_m}{R + bR_m} \tag{3.30}$$

and

$$U_{\mathrm{LR}}(R) = -\frac{C^6}{R^6} - \frac{C^8}{R^8} - \frac{C^{10}}{R^{10}} \pm E_{\mathrm{ex}} \qquad \text{for} \quad R > R_o \tag{3.31}$$

where R_i and R_o are turning points which separate the R into short range, inner well and long range. R_m is chosen to be close to the equilibrium distance R_e. A and B are parameters for the short-range potential, they are set together with q so that the short range potential connects smoothly with the inner well potential at the position R_i. C_6, C_8 and C_{10} are coefficients in the inverse power series for the long range potential and E_{ex} is the exchange term with expression of

$$E_{\mathrm{ex}} = A_{\mathrm{ex}} R^{\gamma} e^{-\beta R} \tag{3.32}$$

For deeply bound levels, the parameters C_6, C_8 and C_{10} don't make significant contributions, and they are set only to extend the potential curves smoothly in the long range part to the dissociation limit.

Besides a variety of potential functions, the potential can be expanded generally as

$$E_e(R) = \frac{1}{n!} \left(\frac{\partial^n E_e(R)}{\partial R^n} \right)_{R_e} (R - R_e)^n \tag{3.33}$$

It is not easy to solve the Schrödinger equation for this general potential expansion. Fortunately, Dunham [49] generated an expression for the vibrational-rotational energies

$$E_{\nu J} = \sum Y_{ij} \left(\nu + \frac{1}{2} \right)^i [J(J+1)]^j \tag{3.34}$$

where Y_{ij} are the Dunham parameters. They are carefully chosen such that the energy expression can fit with the experimental values.

The Dunham energy expression of the vibrational-rotational energy levels corresponds to the Herzberg energy level expressions in Eq. (3.21) to (3.24). The parameters in the two expressions are corresponding to each other by $Y_{01} = B_e$, $Y_{10} = \omega_e$, $Y_{11} = -\alpha_e$, and so forth.

3.4 Hund's cases

In atoms, the electronic spin S and the electronic orbital angular momentum L couple with each other with an form of $AL \cdot S$, where A is the spin-orbit coupling constant. For molecules, besides the spin-orbit coupling, there is also an electrostatic force resulting from the two nuclei, which are connected along the internuclear axis. Due to this electrostatic force, L can then couple to the internuclear axis electrostatically, giving a projection Λ, S can couple to L through spin-orbit coupling. Moreover, the rotation of the molecule N which is absent in atoms, also produces a field which interacts with the momentum of the electrons. However, the effect of the nuclear spin is neglected here. The total angular momentum for a diatomic molecule is written as

$$J = L + N + S \tag{3.35}$$

In the absence of an external electric field, the total angular momentum conserves with the eigenvalues of $J(J+1)\hbar^2$ for operator J^2 and $M\hbar$ for the operator J_Z, Z is the quantized axis in a space-fixed coordinate system (Labeled with X, Y and Z).

In order to describe the relative strength of the electrostatic, spin-orbit and rotation coupling, Hund identified five cases [50, 51]. We introduce here mainly from Case (a) to Case (d) which is demonstrated in Figure 3.5.

Hund's case (a): The electrostatic interaction of the nuclei is much larger than the spin-orbit interaction. Since nuclei in diatomic molecules are connected by the internuclear axis z, therefore the electrostatic interaction has an axial symmetry. The electronic orbital angular momentum precesses about this internuclear axis, giving a projection of $\pm\Lambda\hbar$. The spin-orbit coupling in this case is larger than the interaction with the rotation. The electronic spin possesses also a projection of $\Sigma\hbar$ to the internuclear axis, where $\Sigma = -S, -S+1, \cdots, S-1, S$. The total projection is $\Omega = \Lambda + \Sigma$. For a given value of Λ, there are $2S+1$ fine-structure levels. For example, for an electronic state $^3\Pi$, which has quantum numbers of $\Lambda = 1$ and $S = 1$, then $\Sigma = -1, 0, 1$, therefore $\Omega = 0, 1, 2$. The multiple fine structures are written as $^3\Pi_0$, $^3\Pi_1$, $^3\Pi_2$.

Then, the rotational angular momentum N couples with the electronic angular momentum and we have the total angular momentum $J = \Omega + N$.

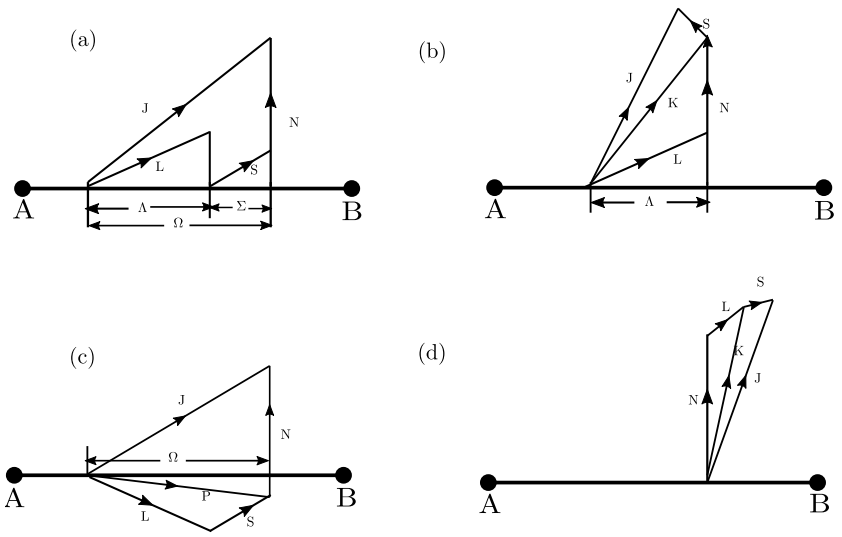

Figure 3.5: Hund's coupling cases

For each fine structure $^3\Pi_0$, $^3\Pi_1$, $^3\Pi_2$, there are multiple rotational levels.

In Hund's case (b), the spin-orbit coupling is weak when $\Lambda \neq 0$, or zero when $\Lambda = 0$. In the situation of $\Lambda \neq 0$, although L precesses about the internuclear axis, giving a projection with quantum number Λ, it does not couple to the electronic spin. However, it couples to the rotation N to get a K, and then K couples with S to form a total angular momentum J.

For diatomic molecules with light atoms, the electrostatic coupling is stronger than spin-orbit coupling, hence Hund's case (a) and (b) are good approximations. However, the spin-orbit coupling will get stronger than the electrostatic interaction when the number of electrons in molecules is getting larger, Hund's case (a) and (b) are not useful approximations. We therefore introduce Hund's case (c) for molecules consisting of heavy atoms.

In Hund's case (c), the spin angular momentum couples to the orbit angular momentum strongly, therefore the quantum numbers of Λ and Σ are not good quantum numbers any more. Spin and orbit form a vector P which will precess about the internuclear axis. We denote the projection to the axis as $\Omega\hbar$, the total angular momentum is then $J = \Omega + N$. Since N is perpendicular to the internuclear axis, the projection of the total angular momentum to the z axis is also Ω. The rotational energy expression is therefore the same as Hund's case (a).

In Hund's case (d), the electrostatic effect is relative weaker compared with the rotational coupling, therefore, L couples to N to form K which then interacts to S to form a total angular momentum J.

Hund's cases are ideal cases, molecules can undergo transformation be-

tween different cases. For example, in Hund's case (a), S couples with the internuclear axis for low J, however, for high J levels, S can decouple with the axis, but couple with K instead.

3.5 Transition dipole moment of the diatomic molecules

Although we have introduced the way of obtaining the diatomic energy levels, the derivation of the polarizability in Eq. (2.65) also requires the knowledge of the interaction operator $\vec{d}\cdot\hat{\epsilon}$ between two molecular states. This will be discussed with more details in this section.

At first, the dipole operator of diatomic molecules can be written as two components: the electronic dipole operator and the nuclear dipole operator $\vec{d}=\vec{d}_{\rm e}+\vec{d}_{\rm nu}$. If we recall the Born-Oppenheimer approximation and describe two molecular states $|i\rangle$ and $|j\rangle$ by Eq. (3.4), the transition dipole moment between these two state can be written as

$$\vec{d}_{ij}=\iint \Psi_i^*\varphi_i^*(\vec{d}_{\rm e}+\vec{d}_{\rm nu})\Psi_j\varphi_j d\tau_{\rm e}d\tau_{\rm nu} \tag{3.36}$$

where $\tau_{\rm e}$ refers to the coordinates in the electronic wavefunction ($\vec{r}$ and $\vec{R}$). $\tau_{\rm e}$ are the coordinates to describe the nuclear wavefunction (R, θ and ϕ).

The Eq. (3.36) can be expanded as two terms

$$\vec{d}_{ij}=\int \Psi_i^*\left[\int \varphi_i^*\vec{d}_{\rm e}\varphi_j d\tau_{\rm e}\right]\Psi_j d\tau_{\rm nu}+\int \Psi_i^*\vec{d}_{\rm nu}\left[\int \varphi_i^*\varphi_j d\tau_{\rm e}\right]\Psi_j d\tau_{\rm nu} \tag{3.37}$$

We can discuss Eq. (3.37) for two different transition cases:

Transition case (a): The dipole transition happens in the same electronic state, but in different vibrational-rotational states. Due to the symmetry property of the dipole moment, the first term of Eq. (3.37) is zero,

$$\int \Psi_i^*\left[\int \varphi_i^*\vec{d}_{\rm e}\varphi_j d\tau_{\rm e}\right]\Psi_j d\tau_{\rm nu}=0 \tag{3.38}$$

Therefore, the transition dipole moment d_{ij} becomes as

$$\begin{aligned}\vec{d}_{ij} &= \int \Psi_i^* \vec{d}_{\rm nu} \left[\int \varphi_i^* \varphi_j d\tau_{\rm e} \right] \Psi_j d\tau_{\rm nu} \\ &= \int \Psi_i^* \vec{d}_{\rm nu} \Psi_j d\tau_{\rm nu}\end{aligned} \tag{3.39}$$

The dipole transition in this case $\int \Psi_i^* \vec{d}_{\rm nu} \Psi_j d\tau_{\rm nu}$ can happen as a pure rotational transition between the same vibrational state, or between different vibrational states.

It is worthwhile to mention that the homonuclear diatomic molecules have no vibrational-rotational spectra in the same electronic state because $Z_1 = Z_2$ and $M_1 = M_2$, therefore $\vec{R}_2 = -\vec{R}_2$. This makes $\vec{d}_{\rm nu} = e(Z_A \vec{R}_1 + Z_B \vec{R}_2) = 0$.

Transition case (b) : The dipole transition occurs between two different electronic states. Since different electronic eigenstates are orthogonal to each other, therefore the second term of Eq. (3.37) is zero,

$$\int \Psi_i^* \vec{d}_{\rm nu} \left[\int \varphi_i^* \varphi_j d\tau_{\rm e} \right] \Psi_j d\tau_{\rm nu} = 0 \tag{3.40}$$

The transition dipole moment d_{ij} in Eq. (3.37) becomes as

$$\begin{aligned}\vec{d}_{ij} &= \int \Psi_i^* \left[\int \varphi_i^* \vec{d}_{\rm e} \varphi_j d\tau_{\rm e} \right] \Psi_j d\tau_{\rm nu} \\ &= \int \Psi_i^* \vec{d}_{ij}^{\,e} \Psi_j d\tau_{\rm nu}\end{aligned} \tag{3.41}$$

where the electronic transition dipole moment $\vec{d}_{ij}^{\,e}$ is a parametric function of the internuclear distance R. Because of the electronic contribution, the electronic transition dipole moment can be along the internuclear axis, or perpendicular to the internuclear axis.

The function $\vec{d}_{ij}^{\,e}$ can be expanded about the equilibrium distance R_e as

$$\vec{d}_{ij}^{\,e}(R) = \vec{d}_{ij}^{\,e}(R_e) + (R - R_e) \frac{d}{dR} \vec{d}_{ij}^{\,e}(R) \Big|_{R=R_e} + \cdots \tag{3.42}$$

Actually, $\vec{d}_{ij}^{\,e}(R)$ changes slowly against the internuclear distance, we can make a rough approximation by taking the first term of Eq. (3.42)

$$\vec{d}_{ij}^{\,e}(R) \approx \vec{d}_{ij}^{\,e}(R_e) \tag{3.43}$$

Therefore the matrix element in Eq. (3.41) becomes that

$$\vec{d}_{ij} = \vec{d}^{e}_{ij}(R_e) \int \Psi_i^*(R)\Psi_j(R)dR \tag{3.44}$$

If the interaction between the vibration and rotation is neglected, and we only consider the vibrational part of the nuclear wavefunction $\Psi(R)$ in Eq. (3.44), we introduce here the Franck-Condon factor [52, 53]

$$FCF(\upsilon_i, \upsilon j) = \left| \int \Psi^*_{\upsilon_i}(R)\Psi_{\upsilon_j}(R)dR \right|^2 \tag{3.45}$$

The Franck-Condon factor describes the probability of the vibrational transition between two different electronic states. If the two vibrational wavefunctions overlap more, the vibrational transition is more likely to happen. It is approximated that the coordinates of the nuclei are not changed during the electronic transition. Therefore, this transition is also referred as vertical transition.

The formalism of the dynamic polarizability requires not only the knowledge of the transition dipole moment, but also the matrix dipole moment of the operator $\vec{d}\cdot\hat{\epsilon}$. There exists a problem that the molecular dipole moment $\vec{d}$ is defined in the molecule-fixed system (labeled with x, y and z), and the light field $\hat{\epsilon}$ is defined in the space-fixed system (labeled with X, Y and Z). In order to make a dot product of them, we need to make a transformation of the dipole moment from the molecule-fixed system to the space-fixed system. This transformation is accomplished by the rotation matrices [50, 54].

We now write $\vec{d}\cdot\hat{\epsilon}$ with the tensor form

$$T^1_p(\hat{\epsilon}) \sum_{q=-1}^{1} \mathscr{D}^{1\ *}_{pq} T^1_q(\vec{d}) \tag{3.46}$$

where p indicates the polarization of light, $\mathscr{D}^{1\ *}_{pq}$ is the rotational matrix which rotates the dipole moment from the molecular-fixed system to the space-fixed system. $T^1_q(\vec{d}) = \vec{d}_q$ denotes the electronic dipole moment in the molecular frame. $T^1_0(\vec{d}) = \vec{d}_0 = \vec{d}_z$ which is along the internuclear axis z. $T^1_{\pm1}(\vec{d}) = \vec{d}_{\pm1} = \mp\frac{1}{\sqrt{2}}(\vec{d}_x \pm i\vec{d}_y)$ are perpendicular to the z axis.

Putting Eq. (3.46) into $\langle i|\vec{d}\cdot\hat{\epsilon}|j\rangle$, we obtain that

$$\langle i|\vec{d}\cdot\hat{\epsilon}|j\rangle = \sum_{q=-1}^{1} \left\langle \upsilon_i|\vec{d}_q(e_i, e_j)|\upsilon_j \right\rangle \left\langle J_i, \Omega_i, M_i|\mathscr{D}^{1\ *}_{pq}|J_j, \Omega_j, M_j \right\rangle \tag{3.47}$$

where the rotational wavefunction is included in the nuclear wavefunction.

$\left\langle \upsilon_i|d_q(e_i,e_j)|\upsilon_j\right\rangle = \int \Psi^*_{\upsilon_i}(R)\left[\int \varphi_i^*(r,R)d_q\varphi_j(r,R)d\tau_e\right]\Psi_{\upsilon_j}(R)d\tau_{\rm nu}$. e denotes the electronic state and υ denotes vibrational function $\Psi_\upsilon(R)$. . It is assumed here that the vibrational wavefunction is independent of the rotational part here. J, Ω and M are the quantum numbers of the total angular momentum and its projection to the internuclear axis and the space-fixed quantization axis respectively.

The eigenfunction with $|J,\Omega,M\rangle$ in Eq. (3.47) can be written as rotational matrices

$$|J,\Omega,M\rangle = \sqrt{\frac{(2J+1)}{8\pi^2}}\mathscr{D}^{J}_{M\Omega}{}^{*} \tag{3.48}$$

Therefore, the last term of Eq. (3.47) $\left\langle J_i,\Omega_i,M_i|\mathscr{D}^1_{pq}{}^*|J_j,\Omega_j,M_j\right\rangle$ is an integral of three rotational matrices. We can evaluate it by angular momentum algebra [55]

$$\begin{aligned}\left\langle J_i,\Omega_i,M_i|\mathscr{D}^1_{0q}{}^*|J_j,\Omega_j,M_j\right\rangle &= [(2J_i+1)(2J_j+1)]^{1/2}\\ &\times\begin{pmatrix} J_i & 1 & J_j\\ -M_i & p & M_j\end{pmatrix}\begin{pmatrix} J_i & 1 & J_j\\ -\Omega_i & q & \Omega_j\end{pmatrix}\end{aligned} \tag{3.49}$$

With the expression in Eq. (3.49), Eq. (3.47) can be written as

$$\begin{aligned}\langle i|\vec{d}\cdot\hat{\epsilon}|j\rangle &= \sum_{q=-1}^{1}\left\langle \upsilon_i|\vec{d}_q(e_i,e_j)|\upsilon_j\right\rangle[(2J_i+1)(2J_j+1)]^{1/2}\\ &\times\begin{pmatrix} J_i & 1 & J_j\\ -M_i & p & M_j\end{pmatrix}\begin{pmatrix} J_i & 1 & J_j\\ -\Omega_i & q & \Omega_j\end{pmatrix}\end{aligned} \tag{3.50}$$

Finally, we can reach a general formalism of the polarizability for the diatomic molecular state $|i\rangle$ as

$$\begin{aligned}{\rm Re}[\alpha(\omega)] = &\sum_{e_j\upsilon_jJ_jM_j\Omega_j}\frac{2\omega_{e_i\upsilon_iJ_iM_i\Omega_i,e_j\upsilon_jJ_jM_j\Omega_j}}{\hbar(\omega^2_{e_i\upsilon_iJ_iM_i\Omega_i,e_j\upsilon_jJ_jM_j\Omega_j}-\omega^2)}\\ &\times\sum_{q=-1}^{1}\left|\left\langle \upsilon_i|\vec{d}_q(e_i,e_j)|\upsilon_j\right\rangle\right|^2(2J_i+1)(2J_j+1)\\ &\times\left[\begin{pmatrix} J_i & 1 & J_j\\ -M_i & p & M_j\end{pmatrix}\begin{pmatrix} J_i & 1 & J_j\\ -\Omega_i & q & \Omega_j\end{pmatrix}\right]^2\end{aligned} \tag{3.51}$$

where $\omega_{e_i v_i J_i M_i \Omega_i, e_j v_j J_j M_j \Omega_j} = \omega_{e_i v_i J_i M_i \Omega_i} - \omega_{e_j v_j J_j M_j \Omega_j}$ is the rovibrational energy difference between the state $|i\rangle$ and the state $|j\rangle$. The 3-j symbol is nonzero when $q = \Omega_i - \Omega_j$.

Chapter 4

Optical dynamic polarizability of the diatomic molecules RbCs and NaK

As we stated the significance of the magic wavelength for atoms, a magic wavelength is also expected to be found for diatomic molecules, such that two molecular states have identical polarizabilities. Motivated by this, in this chapter, we will take advantage of the theoretical approach in the last chapter and discuss the dynamic polarizabilities of the rotational states in the ground state $X^1\Sigma^+$ of the NaK and RbCs molecules at a light polarization along Z axis. This chapter is arranged as follows: first, the formalism of the dynamic polarizability is reorganized for the ground state $X^1\Sigma^+$. In other words, we need to figure out which excited levels should be taken into account in the summation of Eq.(3.51). Second, we demonstrate the potential curves of the ground state $X^1\Sigma^+$ and the excited states, as well as the transition dipole moments. Third, we use the program "Level" [43] to obtain the rovibrational energy and matrix element of transition dipole moment. An output example is demonstrated between the ground state $X^1\Sigma^+$ and the excited state $A^1\Sigma^+$ of NaK. At the end, we demonstrate the dynamic dipole polarizabilities of the two lowest rotational states of RbCs and NaK as a function of the laser frequency in a near infrared region when the light polarization is along Z axis.

4.1 Dynamic polarizability formalism of the ground state $X^1\Sigma^+$

According to the discussion in the last chapter, we will identify the transition dipole moment between the state $X^1\Sigma^+$ and the excited states with $q = 0$ and $q = \pm 1$ cases.

In the case of the $q = 0$ electronic transition, Eq. (3.50) reduces to

$$\begin{aligned}\langle i|\vec{d}\cdot\hat{\epsilon}|j\rangle = &\left\langle \upsilon_i|\vec{d}_0(\Omega_i,\Omega_j)|\upsilon_j\right\rangle [(2J_i+1)(2J_j+1)]^{1/2} \\ &\times \begin{pmatrix} J_i & 1 & J_j \\ -M_i & p & M_j \end{pmatrix}\begin{pmatrix} J_i & 1 & J_j \\ -\Omega_i & 0 & \Omega_j \end{pmatrix}\end{aligned} \tag{4.1}$$

Here $p = 0$ for polarization along Z axis. Since $\Omega_i = 0$, therefore $\Omega_j = 0$, and $\vec{d}_0(\Omega_i, \Omega_j)$ is the electronic transition dipole moment from Σ state to Σ state $\vec{d}_0(\Sigma, \Sigma)$. The $\Sigma - \Sigma$ transition is also referred as parallel transition. The 3-j symbol in Eq. (4.1) is nonzero when $M_i = M_j$.

In the case of the $q = \pm 1$ electronic transition,

$$\begin{aligned}\langle i|\vec{d}\cdot\hat{\epsilon}|j\rangle = &\left\langle \upsilon_i|\vec{d}_{\pm1}(\Omega_i,\Omega_j)|\upsilon_j\right\rangle [(2J_i+1)(2J_j+1)]^{1/2} \\ &\times \begin{pmatrix} J_i & 1 & J_j \\ -M_i & p & M_j \end{pmatrix}\begin{pmatrix} J_i & 1 & J_j \\ -\Omega_i & \pm1 & \Omega_j \end{pmatrix}\end{aligned} \tag{4.2}$$

Here $p = 0$. We know that $\Omega_i = 0$ and $\Omega_j = \mp 1$. $\vec{d}_{\pm1}(\Omega_i, \Omega_j)(q = \pm 1)$ is the electronic transition dipole moment from the Σ state to the Π state $\vec{d}_{\pm1}(\Sigma, \Pi)$. The $\Sigma - \Pi$ transition is also referred as perpendicular transition. The 3-j symbol in Eq. (4.2) is nonzero when $M_i = M_j$.

With the two expressions in Eq. (4.1) and Eq. (4.2), the diatomic polar-

izability of the ground state $X^1\Sigma^+$ can be specified as

$$\begin{aligned}\mathrm{Re}[\alpha(\omega)] = &\sum_{e_j v_j J_j M_j \Omega_j \in \Sigma} \frac{2\omega_{e_i v_i J_i M_i \Omega_i, e_j v_j J_j M_j \Omega_j}}{\hbar(\omega^2_{e_i v_i J_i M_i \Omega_i, e_j v_j J_j M_j \Omega_j} - \omega^2)} |\left\langle v_i|\vec{d}_0(\Sigma,\Sigma)|v_j\right\rangle|^2 \\ &\times (2J_i+1)(2J_j+1)\left[\begin{pmatrix} J_i & 1 & J_j \\ -M_i & 0 & M_j \end{pmatrix}\begin{pmatrix} J_i & 1 & J_j \\ 0 & 0 & 0 \end{pmatrix}\right]^2 \\ &+ \sum_{e_j v_j J_j M_j \Omega_j \in \Pi} \frac{2\omega_{e_i v_i J_i M_i \Omega_i, e_j v_j J_j M_j \Omega_j}}{\hbar(\omega^2_{e_i v_i J_i M_i \Omega_i, e_j v_j J_j M_j \Omega_j} - \omega^2)} |\left\langle v_i|\vec{d}_{\pm 1}(\Sigma,\Pi)|v_j\right\rangle|^2 \\ &\times (2J_i+1)(2J_j+1)\left[\begin{pmatrix} J_i & 1 & J_j \\ -M_i & 0 & M_j \end{pmatrix}\begin{pmatrix} J_i & 1 & J_j \\ 0 & \pm 1 & \mp 1 \end{pmatrix}\right]^2\end{aligned} \tag{4.3}$$

4.2 Molecular potential energy function and transition dipole moment data of RbCs and NaK

In principle, we should consider all singlet Σ and Π excited states ($A^1\Sigma^+$, $B^1\Pi$, $C^1\Sigma$, $D^1\Pi$, ...). However, only a few excited states can make noticeable contributions to the sum in Eq. (3.51). The main contributions are from the transition to the excited states $A^1\Sigma^+$ and $B^1\Pi$, since these two excited states have similar potential curves as the ground state $X^1\Sigma^+$ and their equilibrium position are close with that of the state $X^1\Sigma^+$. Higher excited states don't make remarkable contributions to the polarizability since the electronic transition dipole moment from the ground state towards them are much weaker. Furthermore, the polarizability scales in inverse proportion to the difference of the square of energies $\omega_{ji}^2 - \omega^2$, therefore, excited states with higher energies contribute even less to the polarizability. Due to these reasons, it is reasonable for us to consider only a few excited states, while the validity is still ensured.

In the table 4.1, we list the potentials and transition dipole moments of the RbCs and NaK molecules. The data are derived from experimental measurements as well as theoretical results. For example, an analytical potential expression of the ground state $X^1\Sigma^+$ of NaK is taken from the work by E.Tiemann's group [59], where the analytical potential function is split into a repulsive short range part $U_{\mathrm{SR}}(R)$, an inner well $U(R)$ which contains the equilibrium position and a long range part $U_{\mathrm{LR}}(R)$. The parameters of the analytical potential function from the work of [59] are given in table 4.2.

Table 4.1: We list in this table the potential energy curves of the ground state as well as some excited states of RbCs and NaK. Some of them are derived by ab inito calculations, and some are derived from experimental data. In addition, the spin-orbit coupling is also considered in some potentials, although it is less important for lighter molecules.

Molecule	Experimental ground state $X^1\Sigma^+$	ab initio excited potential energy	Experimental excited states	S-O coupling	PDMs TDMs
RbCs	[56]	$2^1\Sigma^+, 1^3\Pi$ $2^3\Sigma^+, 1^1\Pi$ [57]	$2^1\Sigma^+, 1^3\Pi$ [58]	$(2^1\Sigma^+/1^3\Pi)$ $(2^3\Sigma^+/1^1\Pi)$	[57]
NaK	[59]	$(4,5)^1\Sigma^+$ $(2-4)^1\Pi$ [57]	$A^1\Sigma^+, b^3\Pi$ [60] $B^1\Pi$ [61],$C^1\Sigma$ [62] $D^1\Pi, d^3\Pi$ [46]	$(A^1\Sigma^+/b^3\Pi)$ $(D^1\Pi/d^3\Pi)$	[63]

The reference paper [63] gives non-zero transition dipole moments between the singlet state and triplet states, which does not agree with the general transition rules. This is due to the spin-orbit coupling (SO) [64–66] The singlet excited states can couple with triplet excited states, resulting a non-zero transition dipole moment from the ground state $X^1\Sigma^+$ to the triplet electronic states. For example, in the paper [63] where the coupling between the singlet state $A^1\Sigma^+$ and the triplet state $b^3\Pi$ of NaK are introduced.

We plot the potential curves of the ground state and several electronic higher states of RbCs in Fig. 4.2. The transition dipole moments of RbCs are given in Fig. 4.3. The potentials of NaK is demonstrated in Fig. 4.4 for NaK. The permanent dipole moment of the ground state $X^1\Sigma^+$ of NaK, as well as its transition dipole moments towards excited states are given in Fig. 4.1.

Table 4.2: Here we cite the potential energy function of the ground state $X^1\Sigma^+$ of NaK from [59]. The potential is given with respect to the common asymptote $3s$+$4s$.

For $R < R_i = 2.53\mathring{A}$	
A	–0.44525554× 10^4 cm^{-1}
B	+ 0.107112840 × 10^6 $cm^{-1}\mathring{A}^4$
q	8.3980
For $2.53\mathring{A} = R_i \leq R \leq R_o = 11.3\mathring{A}$	
b	-0.4
R_m	3.49901422 $\mathring{A}$
a_0	–5273.6205 cm^{-1}
a_1	–0.1254 cm^{-1}
a_2	0.14536158 × 10^5 cm^{-1}
a_3	0.11484948 × 10^5 cm^{-1}
a_4	–0.3902171 × 10^3 cm^{-1}
a_5	–0.16931635 × 10^5 cm^{-1}
a_6	–0.374520762 × 10^5 cm^{-1}
a_7	0.106906160 × 10^6 cm^{-1}
a_8	0.5495867136 × 10^6 cm^{-1}
a_9	–0.2164021160× 10^7 cm^{-1}
a_{10}	–0.10160808788 × 10^8 cm^{-1}
a_{11}	0.22144308806× 10^8 cm^{-1}
a_{12}	0.10995928468 × 10^9 cm^{-1}
a_{13}	–0.15497420539× 10^9 cm^{-1}
a_{14}	–0.782460886034 × 10^9 cm^{-1}
a_{15}	0.764737283856 × 10^9 cm^{-1}
a_{16}	0.3818679376129 × 10^{10} cm^{-1}
a_{17}	–0.270560881733 × 10^{10} cm^{-1}
a_{18}	–0.1307771478369× 10^{11} cm^{-1}
a_{19}	0.6931241396136 × 10^{10} cm^{-1}
a_{20}	0.3179698977691 × 10^{11} cm^{-1}
a_{21}	–0.1275832531699 × 10^{11} cm^{-1}
a_{22}	–0.5474439830834 × 10^{11} cm^{-1}
a_{23}	0.1640384471424 × 10^{11} cm^{-1}
a_{24}	0.6534858404306 × 10^{11} cm^{-1}
a_{25}	–0.139350481085 × 10^{11} cm^{-1}
a_{26}	–0.5148927815627 × 10^{11} cm^{-1}
a_{27}	0.700666554236 × 10^{10} cm^{-1}
a_{28}	0.240949154116 × 10^{11} cm^{-1}
For $R > R_o 11.3\mathring{A}$	
C_6	0.1179302 × 10^8 $cm^{-1}\mathring{A}^6$
C_8	0.3023023× 10^9 $cm^{-1}\mathring{A}^8$
C_{10}	0.9843378 × 10^{10} $cm^{-1}\mathring{A}^{10}$
A_{ex}	0.1627150× 10^4 $cm^{-1}\mathring{A}^{-\gamma}$
γ	5.25669
β	2.11445 ×$^{-1}\mathring{A}^{-1}$

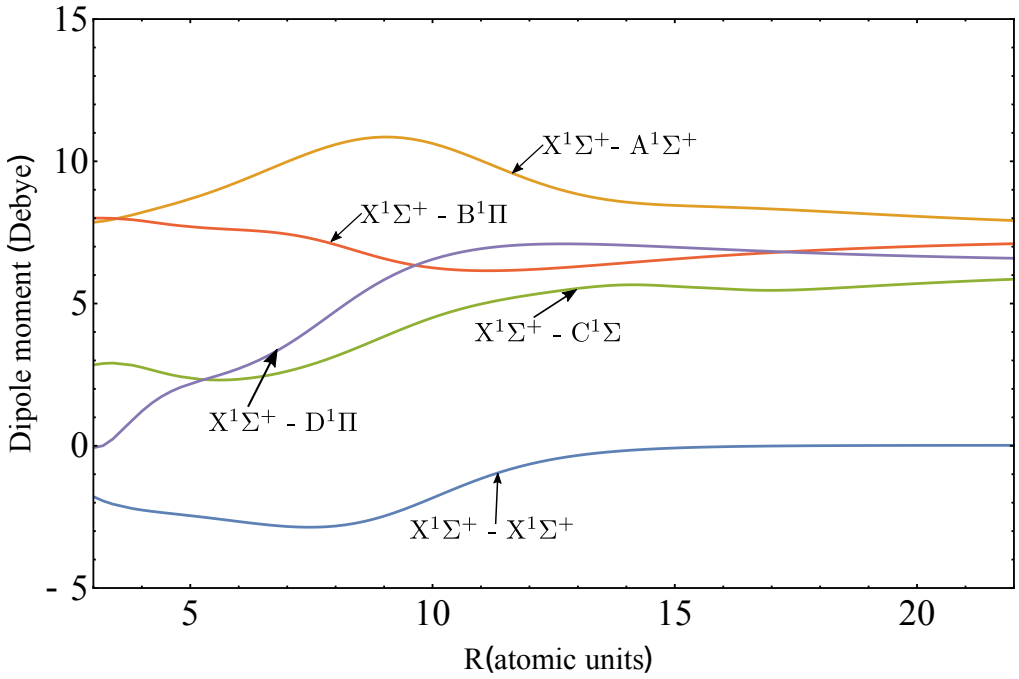

Figure 4.1: The permanent dipole moment of the ground state $X^1\Sigma^+$ (blue curve) and the transition dipole moments to other excited states of NaK. All the dipole moment data are taken from [63].

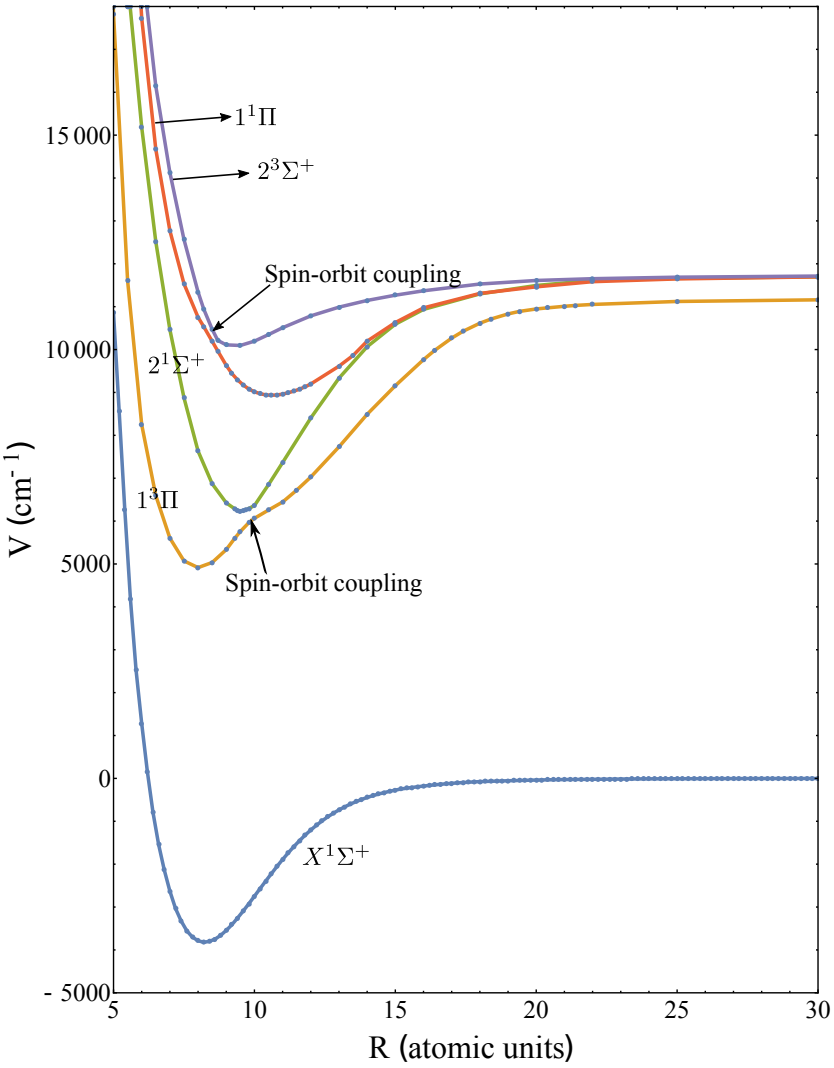

Figure 4.2: We take the potentials of the ground singlet state $X^1\Sigma^+$ and other electronic excited of RbCs from the paper [57](The excited states of $2^1\Sigma^+, 1^3\Pi, 2^3\Sigma^+, 1^1\Pi$ are corresponding to the convention of $A^1\Sigma^+, a^3\Pi, b^3\Sigma^+, B^1\Pi$). The points in the plot are the pointwise data obtained by the ab initio calculations.

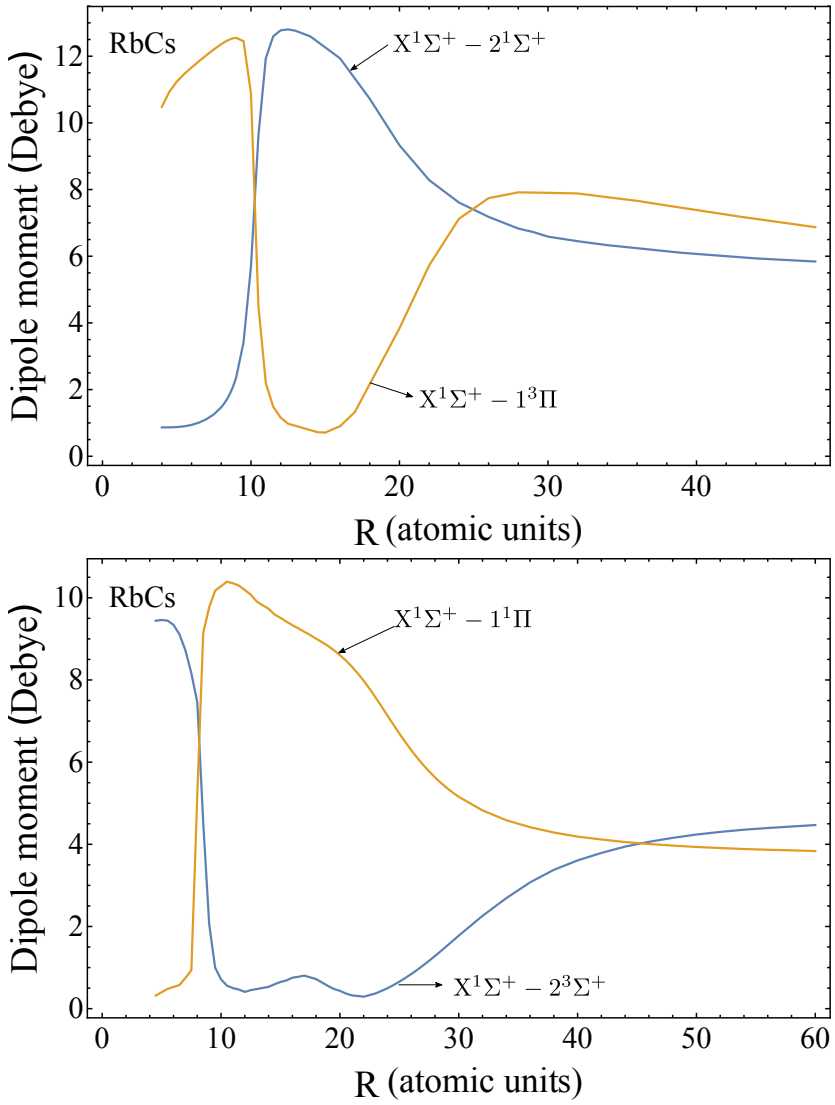

Figure 4.3: Pointwise transition dipole moments (TDMs) of RbCs from the ground state $X^1\Sigma^+$ to excited states as a function of internuclear separation R are from [57]. At short-range internuclear separation, the dipole moments depend stronger on R than the long-range. The dipole moment curves change suddenly near $10a_0$ of the top panel and $8.2a_0$ of the bottom panel, which means that there are avoided crossings between two potentials due to the spin-orbit coupling.

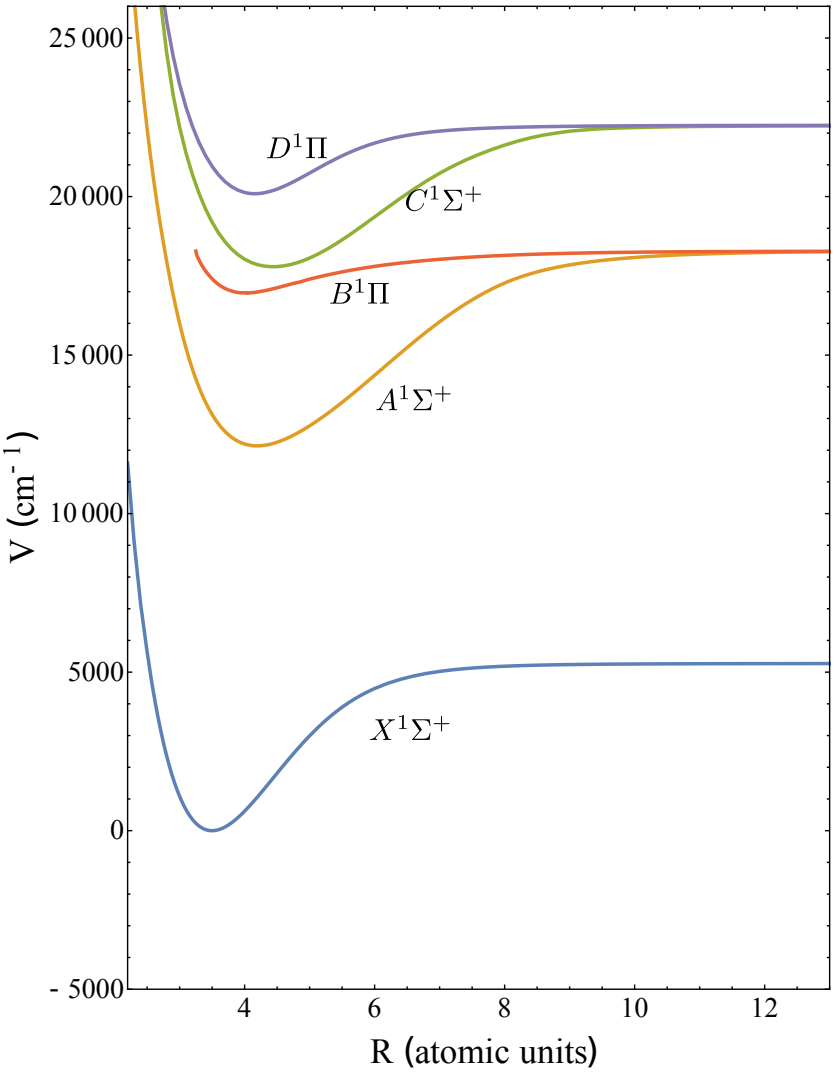

Figure 4.4: The analytical potential of the ground singlet state $X^1\Sigma^+$ and other electronic excited states of NaK as a function of the internuclear distance R. The references where we cite the potentials are listed in the table 4.1.

4.3 Derivation of the rovibrational energies for RbCs and NaK

Now we will insert the potential energy information introduced in the last section into the radial Schrödinger equation (3.13) and solve the equation by taking advantage of the program "Level" [43]. In the program, the potential can be given either by potential functions or by pointwise potential data. In the former case, in order to characterize the potential function, a series of parameters which defines the potential function are assigned to the READ statements. In the latter case where potential is given by read-in pointwise data, an interpolation has to be operated to generate a data array which is sufficient for the numerical integral in Eq.(3.13). Besides the derivation of the rovibrational energy, the program also provides other calculations, e.g., it can evaluate expectation values or the matrix element between two rovibrational levels.

In this thesis, we use the program and calculate energy difference and dipole moment for several transitions. The table down below is an output example. The transition is between the ground state $X^1\Sigma^+$ and the excited state $A^1\Sigma^+$ of NaK. υ', J' and υ'', J'' in the program stand for the upper and lower states. E' and E'' label the energy. A(Einstein) in the table denotes Einstein coefficient [67]. $\langle \upsilon' J' | M | \upsilon'' J'' \rangle$ is the matrix element of the transition dipole moment. The R here is not the internuclear distance. It is the R branch of the rotational transitions. The D in the table is the notation of the exponential of 10.

```
=====================================================================

dJ(J") v'  v"   E'     E"-E'      A(Einstein)  F-C Factor  <v'J'|M|v"J">
 ----- ------  -----  ---------  -----------  -----------  -----------
 R(0)  0 - 0   61.86  12115.8682  6.18719D+02  3.24364D-05  5.76866D-02,
 R(0)  1 - 0   61.86  12196.5782  5.35357D+03  2.76966D-04 -1.68006D-01,
 R(0)  2 - 0   61.86  12276.7813  2.40211D+04  1.22664D-03  3.52395D-01,
 R(0)  10 - 0  61.86  12902.2563  1.84052D+06  8.52669D-02  2.86306D+00,
 R(0)  11 - 0  61.86  12978.6345  1.99859D+06  9.15374D-02 -2.95718D+00,
 R(0)  12 - 0  61.86  13054.6480  2.04549D+06  9.26331D-02  2.96558D+00,
 R(0)  13 - 0  61.86  13130.3050  1.98561D+06  8.89237D-02 -2.89664D+00,
 R(0)  14 - 0  61.86  13205.6126  1.83788D+06  8.14053D-02  2.76300D+00,
 R(0)  15 - 0  61.86  13280.5772  1.62939D+06  7.13884D-02 -2.57957D+00,
 R(0)  16 - 0  61.86  13355.2043  1.38900D+06  6.02040D-02  2.36175D+00,
 R(0)  17 - 0  61.86  13429.4986  1.14237D+06  4.89896D-02 -2.12409D+00,
 R(0)  18 - 0  61.86  13503.4640  9.09112D+05  3.85779D-02  1.87932D+00,
```

```
R(0)  19 - 0  61.86  13577.1039  7.01873D+05  2.94750D-02 -1.63787D+00,
R(0)  20 - 0  61.86  13650.4211  5.26899D+05  2.19000D-02  1.40768D+00,
R(0)  21 - 0  61.86  13723.4176  3.85399D+05  1.58561D-02 -1.19432D+00,
R(0)  22 - 0  61.86  13796.0950  2.75172D+05  1.12074D-02  1.00122D+00,
R(0)  23 - 0  61.86  13868.4544  1.92099D+05  7.74613D-03 -8.30004D-01,
R(0)  24 - 0  61.86  13940.4963  1.31317D+05  5.24304D-03  6.80930D-01,
R(0)  25 - 0  61.86  14012.2209  8.80192D+04  3.48007D-03 -5.53207D-01,
R(0)  26 - 0  61.86  14083.6280  5.79203D+04  2.26795D-03  4.45352D-01,
R(0)  27 - 0  61.86  14154.7169  3.74603D+04  1.45281D-03 -3.55462D-01,
R(0)  28 - 0  61.86  14225.4865  2.38369D+04  9.15721D-04  2.81438D-01,
R(0)  29 - 0  61.86  14295.9357  1.49376D+04  5.68476D-04 -2.21147D-01,
R(0)  30 - 0  61.86  14366.0627  9.22670D+03  3.47886D-04  1.72535D-01,
R(0)  31 - 0  61.86  14435.8655  5.62219D+03  2.10035D-04 -1.33705D-01,
R(0)  32 - 0  61.86  14505.3420  3.38213D+03  1.25201D-04  1.02959D-01,
R(0)  33 - 0  61.86  14574.4897  2.01005D+03  7.37374D-05 -7.88085D-02,
R(0)  34 - 0  61.86  14643.3059  1.18099D+03  4.29360D-05  5.99824D-02,
R(0)  35 - 0  61.86  14711.7875  6.86396D+02  2.47330D-05 -4.54097D-02,
R(0)  36 - 0  61.86  14779.9315  3.94865D+02  1.41029D-05  3.42039D-02,
R(0)  37 - 0  61.86  14847.7343  2.24960D+02  7.96449D-06 -2.56403D-02,
R(0)  38 - 0  61.86  14915.1923  1.26992D+02  4.45717D-06  1.91339D-02,
R(0)  39 - 0  61.86  14982.3019  7.10678D+01  2.47307D-06 -1.42177D-02,
R(0)  40 - 0  61.86  15049.0588  3.94467D+01  1.36115D-06  1.05221D-02,
R(0)  41 - 0  61.86  15115.4590  2.17265D+01  7.43492D-07 -7.75751D-03,
R(0)  42 - 0  61.86  15181.4979  1.18796D+01  4.03222D-07  5.69886D-03,
R(0)  43 - 0  61.86  15247.1711  6.45088D+00  2.17215D-07 -4.17239D-03,
R(0)  44 - 0  61.86  15312.4738  3.48017D+00  1.16271D-07  3.04503D-03,
R(0)  45 - 0  61.86  15377.4009  1.86586D+00  6.18610D-08 -2.21551D-03,
R(0)  46 - 0  61.86  15441.9474  9.94410D-01  3.27215D-08  1.60727D-03,
R(0)  47 - 0  61.86  15506.1078  5.26948D-01  1.72112D-08 -1.16276D-03,
R(0)  48 - 0  61.86  15569.8767  2.77723D-01  9.00425D-09  8.38953D-04,
R(0)  49 - 0  61.86  15633.2484  1.45642D-01  4.68697D-09 -6.03850D-04,
R(0)  50 - 0  61.86  15696.2168  7.60492D-02  2.42879D-09  4.33725D-04,
R(0)  51 - 0  61.86  15758.7759  3.95818D-02  1.25410D-09 -3.11045D-04,
R(0)  52 - 0  61.86  15820.9192  2.05648D-02  6.46077D-10  2.22882D-04,
```

4.4 Dynamic polarizabilities of ultracold polar molecules NaK and RbCs

The Fig. 4.5 down below shows the dynamic polarizability as a function of laser frequency in the near infrared domain when the light polarization is along the Z direction. The four states shown in the figure are υ=0, J=0, $M = 0$, and υ=0, J=1, M=0, $\pm$1 of the $X^1\Sigma^+$ ground state. The laser light range we choose is in a region from 9000 cm^{-1} to 10000 cm^{-1}, where an often-used wavelength 1064 nm (or wavenumber of 9398cm^{-1}) for optical latttice or optical tweezer is included. One atomic unit of polarizability is 1.648 777 2731$\times$ $10^{-41}C^2$ m^2/J.

It is obvious that the polarizability curves of four states as a function of the laser frequency do not cross in this near-infrared region. In other words, with only the influence of a near-infrared trapping laser field, we can not find a "magic frequency" where the polarizabilities of two rotational states of RbCs and NaK are identical. Unfortunately, this result does not provide magic conditions to the experiments where the molecules are trapped in optical lattices.

In the next chapter, another approach is introduced to find the magic conditions where we apply a static electric field to align the molecules and trap the molecules with a wavelength of 1064 nm.

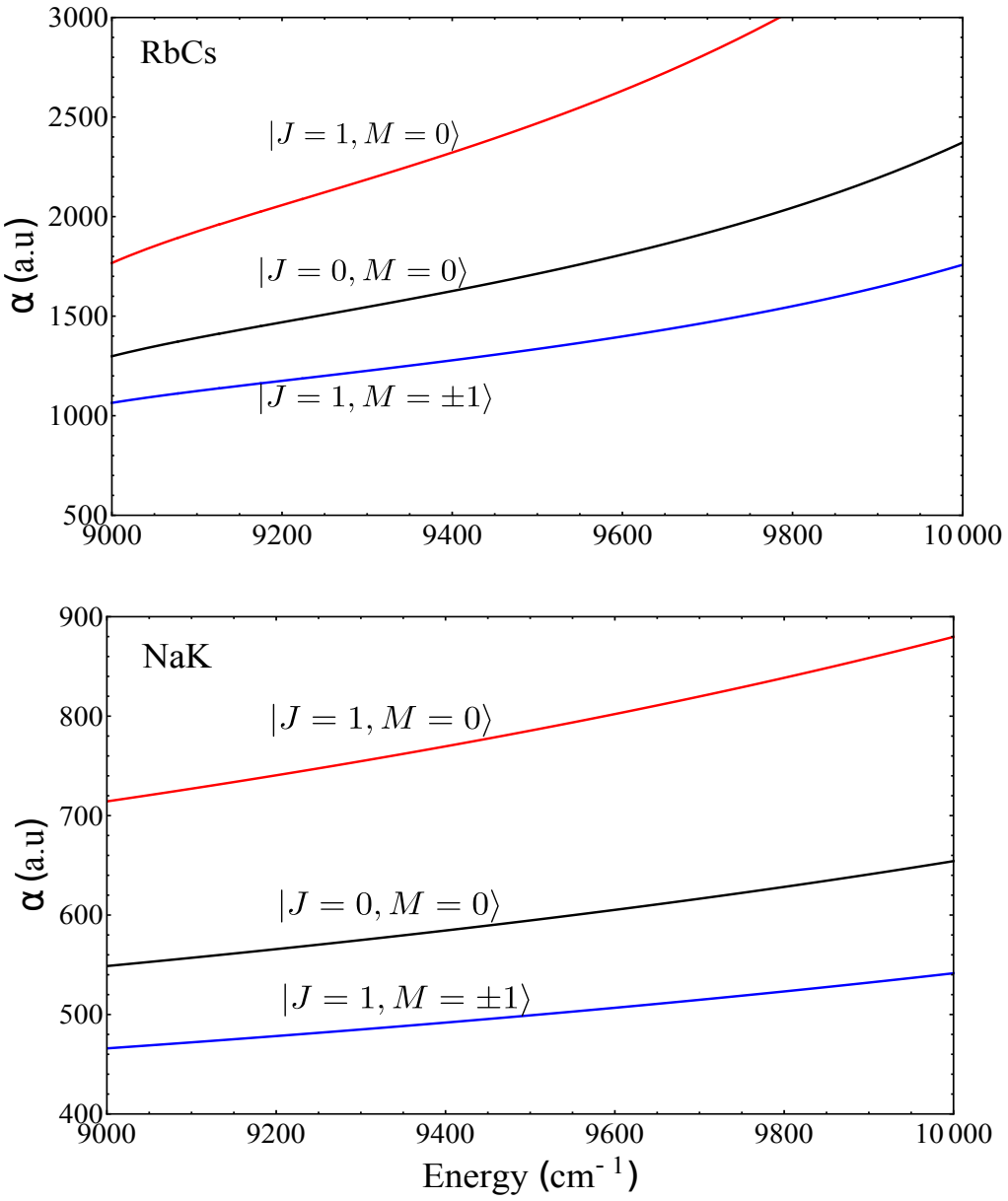

Figure 4.5: We calculate the real part of the dynamic polarizability of the rotational states $J = 0$ and $J = 1$ of RbCs (top panel) and NaK (bottom panel) as a function of laser frequency in the near-infrared region. The polarizability curves of different rotational states do not cross. In other words, we can not find a "magic frequency" in the near infrared region.

Chapter 5

Magic field strength and magic angle for rotational states of RbCs and NaK

The inducement of the dipole moment in the lab frame by mixing the rotational states with a DC electric field is of great significance to the experiments. The corresponding mixing strength depends on the electric field value. This motivates us to investigate the polarizability of the mixed rotational states in the ground state $X^1\Sigma^+$ as a function of the DC electric field strength. In this thesis, we present this dependence of a few low rotational states of RbCs and NaK when the trapping light has a specified wavelength at 1064 nm, which is different from the last chapter where the wavelength is a variable. A magic field strength value is expected, where the polarizabilities of two mixed rotational states match. In addition, we verify that this magic field strength is independent of the light polarization by discussing the dynamic polarizability at different laser polarizations.

Similar work has been done in a publication [16] where the dependence of the mixed rotational states of RbCs was discussed when the linearly polarized light has a different wavelength at 1090 nm.

Besides that, we also investigate the polarizability when the light is linearly polarized as a function of the relative angle with respect to the DC field. This angle dependence is discussed when the field strength ε is set with several discrete values. Similar to the magic field strength, a magic angle is also expected between two mixed rotational states.

5.1 Mixing rotational states with a DC field

First we discuss the mixing of the rotational states in the ground state $X^1\Sigma^+$ by an external DC electric field $\vec{\varepsilon}$ which is aligned along the space-fixed Z direction ($\vec{\varepsilon} = \varepsilon\hat{Z}$). The full Hamiltonian of a diatomic system in an electric field is given by

$$H = H_0 - \vec{d}\cdot\vec{\varepsilon} \tag{5.1}$$

The Hamiltonian H_0 has an eigenenergy expression of

$$E(\upsilon, J) = G_\upsilon + B_\upsilon J(J+1) \tag{5.2}$$

where G_υ is the vibrational energy and B_υ is the rotational constant of the vibrational level υ. We consider here only the lowest order of the rotational energy.

The matrix element of the DC stark shift between two rovibrational states $|\upsilon_i J_i M_i \Omega_i\rangle$ and $|\upsilon_j J_j M_j \Omega_j\rangle$ in the ground state can be written as

$$\begin{aligned}\langle \upsilon_i J_i M_i \Omega_i| - \vec{d}\cdot\vec{\varepsilon}|\upsilon_j J_j M_j \Omega_j\rangle = &-\sqrt{(2J_i+1)(2J_j+1)} \times \langle \upsilon_i|d|\upsilon_j\rangle \times \varepsilon \\ &\times \begin{pmatrix} J_i & 1 & J_j \\ -M_i & 0 & M_j \end{pmatrix} \times \begin{pmatrix} J_i & 1 & J_j \\ -\Omega_i & q & \Omega_j \end{pmatrix}\end{aligned} \tag{5.3}$$

where $q = \Omega_i = \Omega_j = 0$, since the transition occurs in the same electronic state $X^1\Sigma^+$. $\langle \upsilon_i|d|\upsilon_j\rangle = \int_0^\infty dR \Psi^*_{\upsilon_i}(R) d(R) \Psi_{\upsilon_j}(R)$ where $d(R)$ is the permanent electric dipole moment of the ground state $X^1\Sigma^+$. Ψ_υ is the vibrational wavefunction. The two 3-j symbols are non-zero when $M_i = M_j$ and $J_i + J_j + 1$ is even. We are able to make the assumption here that the coupling between different vibrational states is neglected here.

By diagonalizing the full Hamiltonian matrix, we can obtain the resulting new rotational states $|\upsilon\tilde{J}M\rangle$. It is can be expressed as a superposition of the original rotational states by $|\upsilon\tilde{J}M\rangle = \sum_J U^{\upsilon M}_{\tilde{J},J} |\upsilon J M\rangle$. $U^{\upsilon M}_{\tilde{J},J}$ is the corresponding coupling constant of the rotational states $|\upsilon J M\rangle$.

For example, the new rotational state of $|\tilde{J} = 0, M = 0\rangle$ can be written as

$$\begin{aligned}&|\upsilon, \tilde{J} = 0, M = 0\rangle \\ =&U^{\upsilon M}_{\tilde{J}=0,J=0} |\upsilon, J = 0, M = 0\rangle + U^{\upsilon M}_{\tilde{J}=0,J=1} |\upsilon, J = 1, M = 0\rangle \\ +&U^{\upsilon M}_{\tilde{J}=0,J=2} |\upsilon, J = 2, M = 0\rangle + \cdots .\end{aligned} \tag{5.4}$$

For zero static electric field strength value, the mixing constant $U^{\upsilon M}_{\tilde{J}=0,J=0}$

of the state $|\upsilon, J=0, M=0\rangle$ is equal to 1, and other constants are zero. The DC field that we use here is up to a strength of 15 kV/cm. At this strength value, we can treat that the state $|\tilde{J}=0, M=0\rangle$ is a mixture of rotational states which are truncated at $J=10$.

The fact that the mixing constants $U^{\upsilon M}_{\tilde{J},J}$ depend on ε motivates us to explore the dynamic polarizability of the state $|\upsilon \tilde{J} M\rangle$ as a function of the field strength. In this thesis, we are interested at the two lowest rotational states with $\tilde{J}=0$ and $\tilde{J}=1$ in the first vibrational state of the electronic ground state $X^1\Sigma^+$.

5.2 Dynamic polarizabilities of non-degenerate states

Now we will reorganize the polarizability formula in order to write it in terms of the mixing constant $U^{\upsilon M}_{\tilde{J},J}$ and the original rotational states $|\upsilon J M\rangle$ [1]

$$\begin{aligned}
\mathrm{Re}[\alpha(\omega)] = & \sum_{e_j \upsilon_j J_j M_j \Omega_j} \frac{2\omega_{e_j \upsilon_j J_j M_j \Omega_j}}{(\omega_{e_j \upsilon_j J_j M_j \Omega_j} - \omega_{\upsilon \tilde{J} M})^2 - \omega^2} \\
& \times \langle \upsilon \tilde{J} M | \vec{d} \cdot \hat{\epsilon} | e_j \upsilon_j J_j M_j \Omega_j \rangle \langle e_j \upsilon_j J_j M_j \Omega_j | \vec{d} \cdot \hat{\epsilon}^* | \upsilon \tilde{J} M \rangle \\
= & \sum_{J_1, J_2} U^{\upsilon M}_{\tilde{J},J_1} U^{\upsilon M}_{\tilde{J},J_2} \times \sum_{e_j \upsilon_j J_j M_j \Omega_j} \frac{2\omega_{e_j \upsilon_j J_j M_j \Omega_j}}{(\omega_{e_j \upsilon_j J_j M_j \Omega_j} - \omega_{\upsilon \tilde{J} M})^2 - \omega^2} \\
& \times \langle \upsilon J_1 M | \vec{d} \cdot \hat{\epsilon} | e_j \upsilon_j J_j M_j \Omega_j \rangle \langle e_j \upsilon_j J_j M_j \Omega_j | \vec{d} \cdot \hat{\epsilon}^* | \upsilon J_2 M \rangle
\end{aligned} \tag{5.5}$$

where J_1 can be different from J_2.

As the way discussed in Eq. (3.51), the polarizability can be further written as

$$\begin{aligned}
\mathrm{Re}[\alpha(\omega)] = & \sum_{\Omega_j} \alpha^{\Omega_j}(\omega) \sum_{J_1, J_2} U^{\upsilon M}_{\tilde{J},J_1} U^{\upsilon M}_{\tilde{J},J_2} \\
& \times \sum_{J_j, M_j} [(2J_1+1)(2J_j+1)]^{1/2} \begin{pmatrix} J_1 & 1 & J_j \\ -M & p & M_j \end{pmatrix} \begin{pmatrix} J_1 & 1 & J_j \\ 0 & q & \Omega_j \end{pmatrix} \\
& \times [(2J_2+1)(2J_j+1)]^{1/2} \begin{pmatrix} J_j & 1 & J_2 \\ -M_j & -p & M \end{pmatrix} \begin{pmatrix} J_j & 1 & J_2 \\ -\Omega_j & -q & 0 \end{pmatrix},
\end{aligned} \tag{5.6}$$

where

$$\alpha^{\Omega_j}(\omega) \approx \sum_{e_j v_j} \langle v|d_\mu|e_j v_j \Omega_j\rangle\langle e_j v_j \Omega_j|d_\nu|v\rangle \times \frac{2\omega_{e_j v_j}}{(\omega_{e_j v_j} - \omega_v)^2 - \omega^2} \tag{5.7}$$

When $q = 0$, $\Omega_j = 0$, the transition is corresponding to the $\Sigma - \Sigma$ transition. When $q = \pm 1$, $\Omega_j = \mp 1$, the transition is corresponding to the $\Sigma - \Pi$ transition. Here we make the approximation that $\langle v|d|e_j v_j \Omega_j\rangle$ and $\omega_{e_j v_j} - \omega_v$ in Eq. (5.7) depend nearly only on the electronic and vibrational levels.

5.2.1 Light polarized along the Z axis

Fig. 5.1 gives the dynamic polarizabilities of the four mixed rotational levels $|\tilde{J} = 0, M = 0\rangle$, $|\tilde{J} = 1, M = 0\rangle$ and $|\tilde{J} = 1, M = \pm 1\rangle$ of RbCs and NaK as a function of the electric field from 0 to 15 kV/cm. Here the laser field here is polarized along the external DC electric field ($\hat{\epsilon}$=$\hat{Z}$).

We see that the polarizability curves of the states $|\tilde{J} = 0, M = 0\rangle$ and $|\tilde{J} = 1, M = 0\rangle$ cross at a strength of 5.2 kV/cm for NaK and 2 kV/cm for RbCs.

The magic field strength value of RbCs molecules is smaller for NaK molecules, this can be explained by the perturbation theory of the rotating molecules in external electric field. In the perturbative assumption, the dipole interaction due to the DC Stark shift is considered much smaller than the rigid rotor energy level splitting

$$d\varepsilon \ll B_v \tag{5.8}$$

According to Eq.(2.33), the first order correction to the rotational wavefunction has a dependence on $d\varepsilon/B_v$. In other words, it depends on the relative strength between the DC Stark effect Hamiltonian and the rotational energy splitting. As a consequence, the magic field strength scales with B_v/d. This can be verified in the following table where we list out the dipole moment and rotational constant for RbCs and NaK compare their magic field strengths.

Molecules	$B_v(\text{cm}^{-1})$	d(Debye)	$\frac{B_v}{d}(\text{cm}^{-1}/\text{Debye})$	Magic field(kV/cm)
RbCs	0.0166	1.3	0.0127	2
NaK	0.095	2.76	0.0333	5.2

The scale of the magic electric field strengths between RbCs and NaK molecules is $2/5.2 \approx 0.384$. It agrees well with the scale of the B_v/d of these two molecules, which is $0.0127/0.0333 \approx 0.382$. Therefore, if the permanent dipole moment and the rotational constant of other diatomic molecules are known, the magic field strength can be predicted without repeating the calculation discussed above.

Moreover, the polarizabilities of the states $|\tilde{J} = 1, M = -1\rangle$ and $|\tilde{J} = 1, M = 1\rangle$ remain degenerate and they cross with the state $\tilde{J} = 1, M = 0$ around 12 kV/cm for NaK and 4.7 kV/cm for RbCs.

5.2.2 Circularly-polarized light

We now extend the investigation of the dependence of the dynamic polarizability on the field strength to the case when ultracold molecules are trapped with circularly-polarized light. A good example is the 2D hexagonal optical lattice discussed in the paper [68], where the polarizations at the potential minima are changing from $\sigma+$ to $\sigma-$ alternately.

We illustrate the dynamic polarizability dependence in this case in Fig. 5.2. The magic field strength of the states $|\tilde{J} = 0, M = 0\rangle$ and $|\tilde{J} = 1, M = 0\rangle$ is 2 kV/cm for RbCs and 5.2 kV/cm for NaK, which remain the same as that when the light is polarized along Z. Moreover, we can verify that whether the light polarization is $\sigma+$ or $\sigma-$ does not change the polarizability of a state.

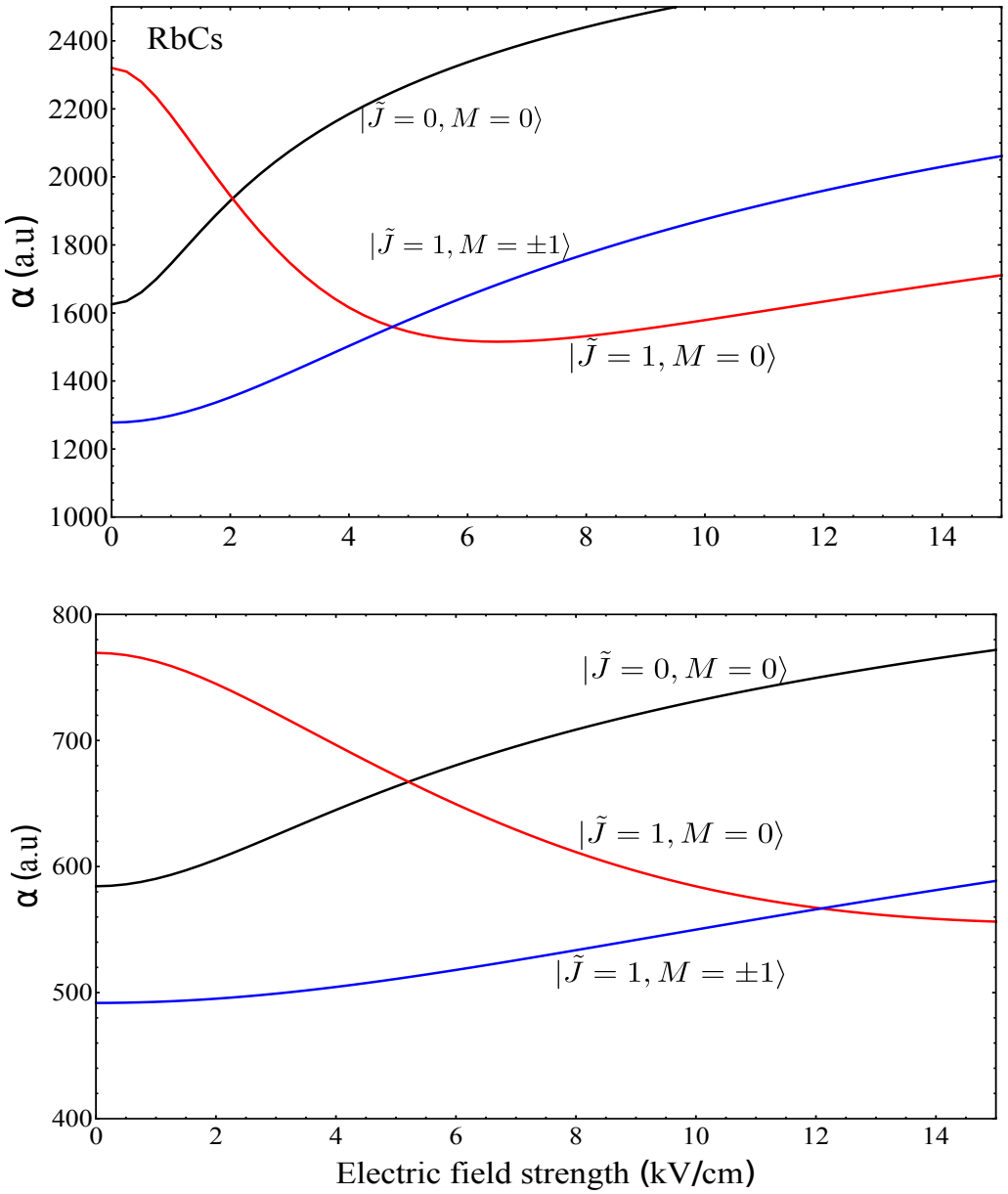

Figure 5.1: We demonstrate the dependence of the dynamic polarizabilities of the mixed rotational states $\tilde{J} = 0$ and $\tilde{J} = 1$ on the DC electric field strength at a wavelength 1064 nm. The laser is polarized along $Z(\hat{\epsilon}=\hat{Z})$. The polarizabilities of the states $|\tilde{J} = 0, M = 0\rangle$ and $|\tilde{J} = 1, M = 0\rangle$ meet at a strength 5.2 kV/cm for NaK and 2kV/cm for RbCs. Besides, there is another crossing point between the states $|\tilde{J} = 1, M = 0\rangle$ and $|\tilde{J} = 1, M = \pm1\rangle$ which occurs at 12 kV/cm for NaK and 4.7 kV/cm for RbCs.

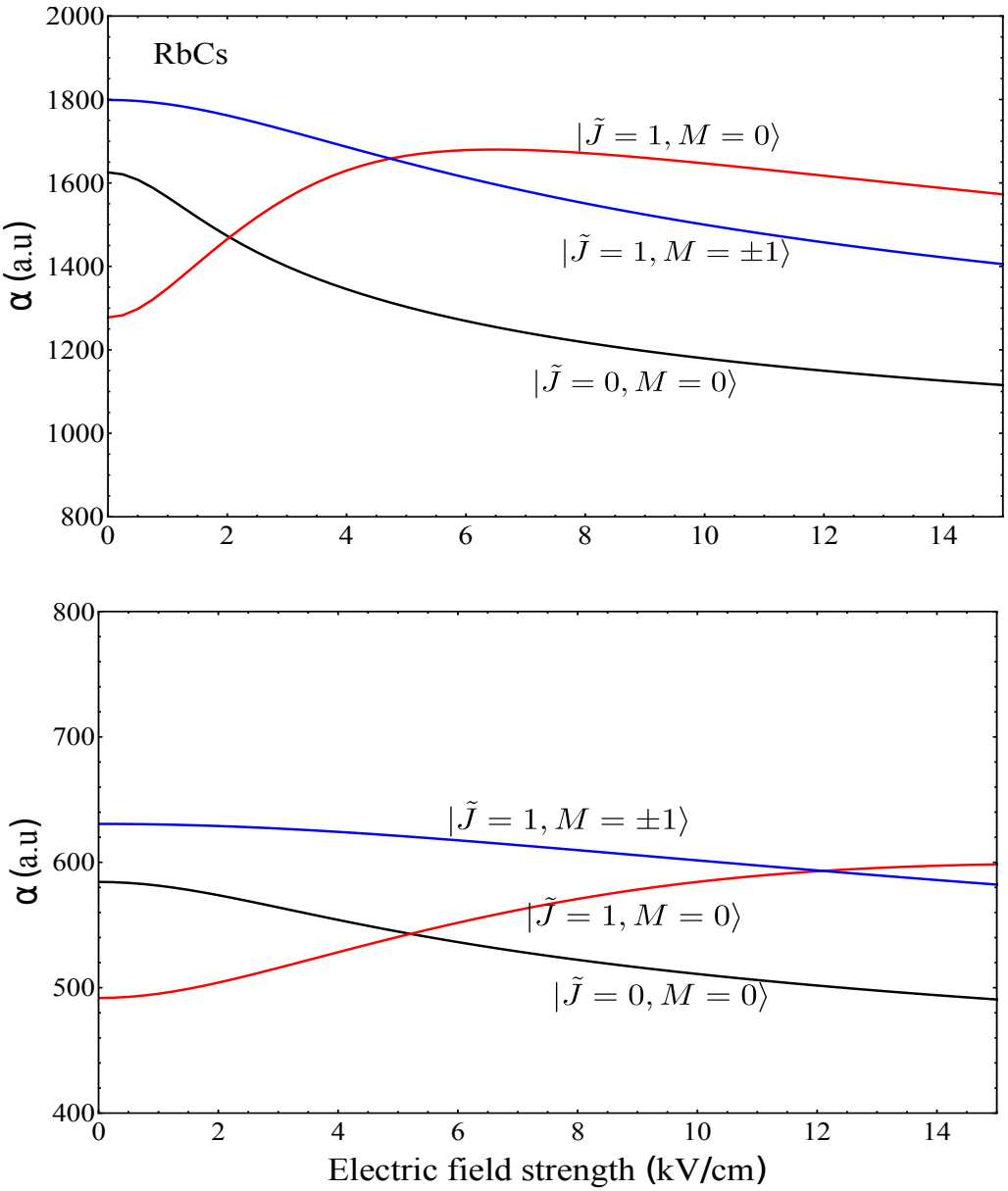

Figure 5.2: We present the dynamic polarizabilities of the rotational states of RbCs (top panel) and NaK (bottom panel) when they are trapped with circularly-polarized ($\sigma+$ or $\sigma-$) light. Actually, whether light is $\sigma+$ or $\sigma-$ doesn't change the polarizability of a state. Moreover, the magic field strength between the states $|\tilde{J}=0, M=0\rangle$ and $|\tilde{J}=1, M=0\rangle$ is 2kV/cm for RbCs and 5.2kV/cm for NaK, which are the same as that when the light is polarized along Z.

5.3 Dynamic polarizabilities of degenerate states with M >0

We now investigate the dynamic polarizability when the light is polarized along X or Y directions. In this case, the dynamic polarizability of the degenerate rotational states $|\upsilon\tilde{J}, M\rangle$ and $|\upsilon\tilde{J}, -M\rangle$ with $M > 0$ are derived by degenerate perturbation theory [69]. The corresponding right eigenstates are the combination of the degenerate states $|\upsilon\tilde{J}M, \pm\rangle = (|\upsilon\tilde{J}, M\rangle \pm |\upsilon\tilde{J}, -M\rangle)/\sqrt{2}$.

The dynamic polarizabilities for the new eigenstates are then

$$\begin{aligned}\mathrm{Re}[\alpha^{\upsilon\tilde{J}M,\pm}(\omega)] = &\sum_{e_j\upsilon_j J_j M_j\Omega_j} \frac{2\omega_{e_j\upsilon_j J_j M_j\Omega_j}}{(\omega_{e_j\upsilon_j J_j M_j\Omega_j} - \omega_{\upsilon\tilde{J}M})^2 - \omega^2} \\ &\times \langle \upsilon\tilde{J}M, \pm|\vec{d}\cdot\hat{\epsilon}|e_j\upsilon_j J_j M_j\Omega_j\rangle\langle e_j\upsilon_j J_j M_j\Omega_j|\vec{d}\cdot\hat{\epsilon}^*|\upsilon\tilde{J}M, \pm\rangle \\ = &\sum_{J_1,J_2} U^{\upsilon M}_{\tilde{J},J_1} U^{\upsilon M}_{\tilde{J},J_2} \times \sum_{e_j\upsilon_j J_j M_j\Omega_j} \frac{2\omega_{e_j\upsilon_j J_j M_j\Omega_j}}{(\omega_{e_j\upsilon_j J_j M_j\Omega_j} - \omega_{\upsilon\tilde{J}M})^2 - \omega^2} \\ &\times \langle \upsilon J_1 M, \pm|\vec{d}\cdot\hat{\epsilon}|e_j\upsilon_j J_j M_j\Omega_j\rangle\langle e_j\upsilon_j J_j M_j\Omega_j|\vec{d}\cdot\hat{\epsilon}^*|\upsilon J_2 M, \pm\rangle \end{aligned} \tag{5.9}$$

where $|\upsilon J_1 M, \pm\rangle = \{|\upsilon J_1, M\rangle \pm |\upsilon J_1, -M\rangle\}/\sqrt{2}$ and $|\upsilon J_2, M\pm\rangle = \{|\upsilon J_2, M\rangle \pm |\upsilon J_2, -M\rangle\}/\sqrt{2}$.

Expanding all terms, Eq. (5.9) becomes

$$\begin{aligned}\mathrm{Re}[\alpha^{\upsilon\tilde{J}M,\pm}(\omega)] = &\frac{1}{2}\sum_{J_1,J_2} U^{\upsilon M}_{\tilde{J},J_1} U^{\upsilon M}_{\tilde{J},J_2} \times \sum_{e_j\upsilon_j J_j M_j\Omega_j} \frac{2\omega_{e_j\upsilon_j J_j M_j\Omega_j}}{(\omega_{e_j\upsilon_j J_j M_j\Omega_j} - \omega_{\upsilon\tilde{J}M,\pm})^2 - \omega^2} \\ &\times \Big\{ \langle \upsilon J_1, M|\vec{d}\cdot\hat{\epsilon}|e_j\upsilon_j J_j M_j\Omega_j\rangle\langle e_j\upsilon_j J_j M_j\Omega_j|\vec{d}\cdot\hat{\epsilon}^*|\upsilon J_2, M\rangle \\ &\pm \langle \upsilon J_1, M|\vec{d}\cdot\hat{\epsilon}|e_j\upsilon_j J_j M_j\Omega_j\rangle\langle e_j\upsilon_j J_j M_j\Omega_j|\vec{d}\cdot\hat{\epsilon}^*|\upsilon J_2, -M\rangle \\ &\pm \langle \upsilon J_1, -M|\vec{d}\cdot\hat{\epsilon}|e_j\upsilon_j J_j M_j\Omega_j\rangle\langle e_j\upsilon_j J_j M_j\Omega_j|\vec{d}\cdot\hat{\epsilon}^*|\upsilon J_2, M\rangle \\ &+ \langle \upsilon J_1, -M, |\vec{d}\cdot\hat{\epsilon}|e_j\upsilon_j J_j M_j\Omega_j\rangle\langle e_j\upsilon_j J_j M_j\Omega_j|\vec{d}\cdot\hat{\epsilon}^*|\upsilon J_2, -M\rangle \Big\} \end{aligned} \tag{5.10}$$

where the transition dipole moments and the energy terms in Eq.(5.10) can be calculated in the same way as Eq. (5.6) and (5.7).

5.3.1 Light polarized along the X axis

We demonstrate in Fig.5.3 the dependence of the dynamic polarizability on the field strength when the polarization of the light field is perpendicular to the external electric field direction and along X axis ($\hat{\epsilon}$=$\hat{X}$).

We see that in the static field strength range from 0 to 15 kV/cm, the polarizability curves cross only at one point which occurs between the states $|\tilde{J}=0, M=0\rangle$ and $|\tilde{J}=1, M=0\rangle$. It is interesting to find out that the "magic field strength" value is the same as the case when diatomic molecules are trapped with parallelly polarized light ($\hat{\epsilon}$=$\hat{Z}$).

For the states $|\tilde{J}=1, M=1\rangle + |\tilde{J}=1, M=-1\rangle$ and $|\tilde{J}=1, M=1\rangle - |\tilde{J}=1, M=-1\rangle$, however, their dynamic polarizabilities are not degenerate any more.

5.3.2 Light polarized along the Y axis

Fig.5.4 gives the the dynamic polarizabilities of the mixed rotational states when the light is polarized along Y axis ($\hat{\epsilon}$=$\hat{Y}$).

By comparing the Fig.5.3 and Fig.5.4, we see that the dynamic polarizabilities of the states $|\tilde{J}=0, M=0\rangle$ and $|\tilde{J}=1, M=0\rangle$ do not change no matter the laser polarization is along the X axis or Y axis and the magic field strength for these two mixed rotational states remains at 2 kV/cm for RbCs and 5.2 kV/cm for NaK. Actually, according to the discussions with several polarizations, we can verify that the magic field strength remains the same for any polarizations.

The states $|\tilde{J}=1, M=1\rangle + |\tilde{J}=1, M=-1\rangle$ and $|\tilde{J}=1, M=1\rangle - |\tilde{J}=1, M=-1\rangle$ switch their polarizabilities if the light polarization direction changes from X axis to Y axis. This is quite understandable due to the form of X-polarization and Y-polarization.

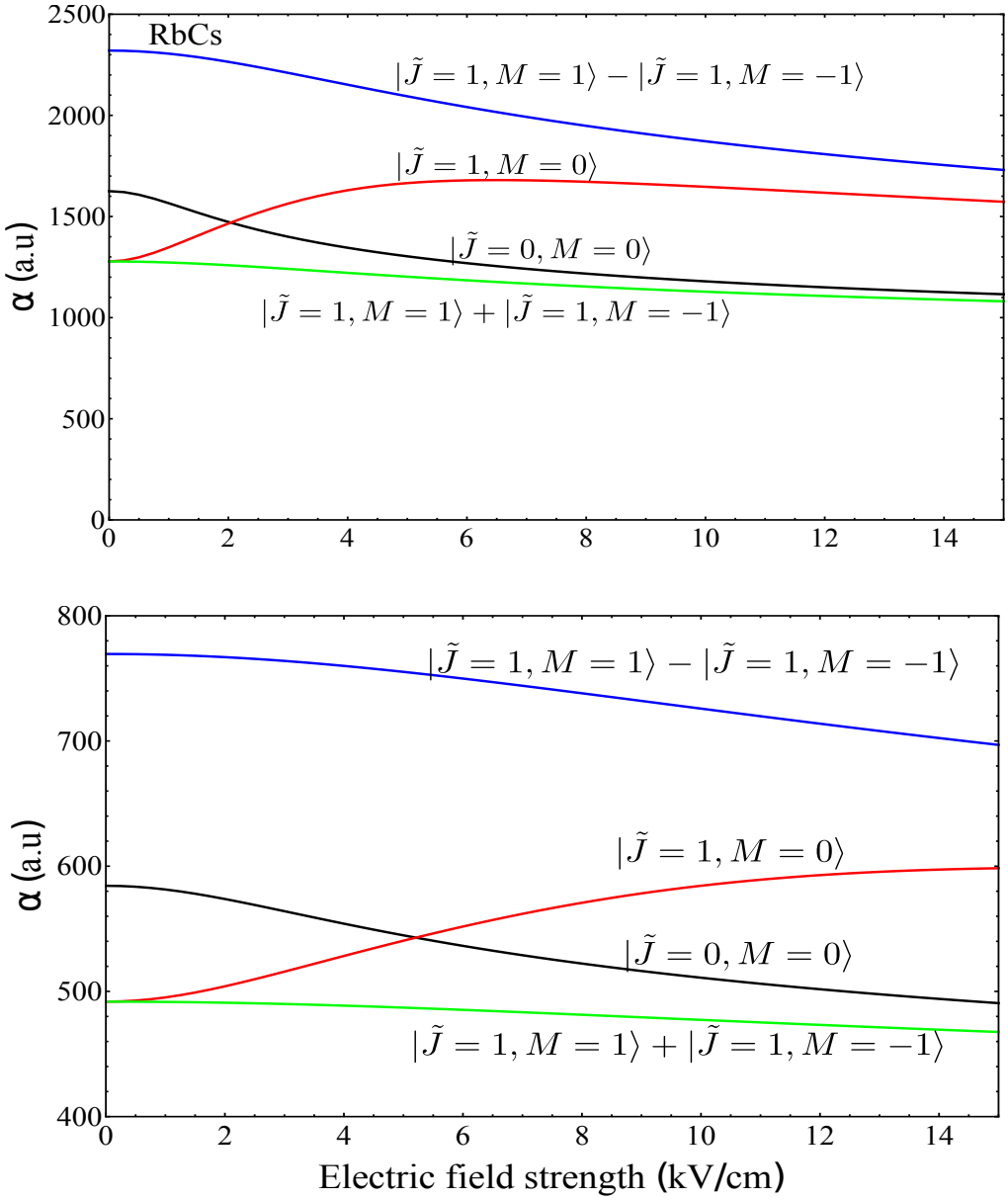

Figure 5.3: We calculate the dynamic polarizabilities of a few mixed rotational states of RbCs and NaK when the molecules are trapped with X-polarized trapping light ($\hat{\epsilon}$=$\hat{X}$). The polarizability curves cross only at one field strength between the states $|\tilde{J}=0,M=0\rangle$ and $|\tilde{J}=1,M=0\rangle$. This magic field strength is the same as that when the light is polarized along the Z axis. However, in contrast to Fig.5.1, the polarizability degeneracy of the states $|\upsilon\tilde{J}M,\pm\rangle = (|\upsilon\tilde{J},M\rangle \pm |\upsilon\tilde{J},-M\rangle)$ is lifted.

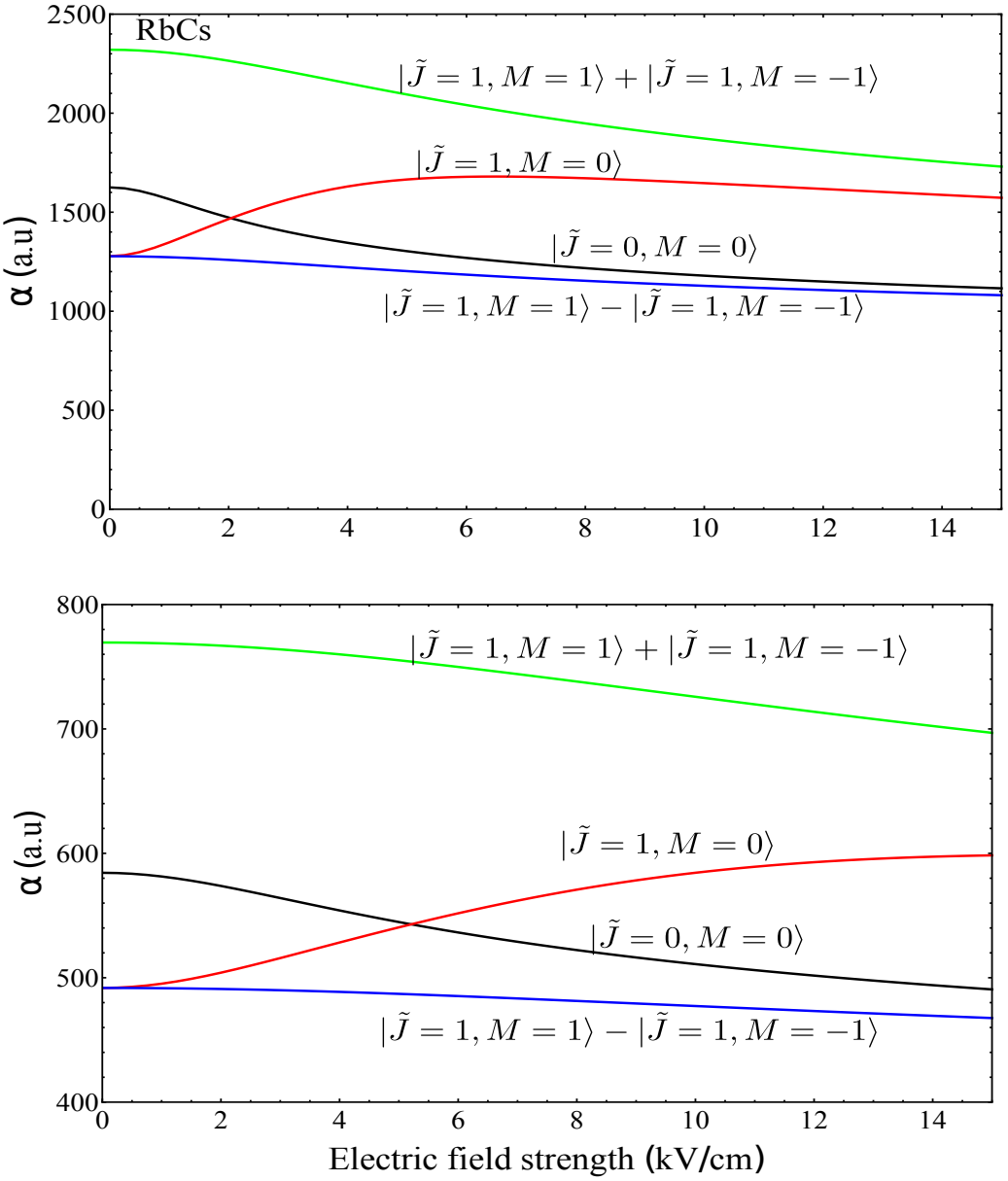

Figure 5.4: We calculate the dynamic polarizabilities of the mixed rotational states with $\tilde{J}=0$ and $\tilde{J}=1$ of RbCs and NaK when the light polarization is along the Y axis ($\hat{\epsilon}$=$\hat{Y}$). We find out that the polarizabilities of the states $|\tilde{J}=0,M=0\rangle$ and $|\tilde{J}=1,M=0\rangle$ remain the same no matter if the laser polarization is along Z, X or Y directions. However, the states $|\tilde{J}=1,M=1\rangle+|\tilde{J}=1,M=-1\rangle$ and $|\tilde{J}=1,M=1\rangle-|\tilde{J}=1,M=-1\rangle$ switch their polarizabilities if the polarization direction changes from X axis to Y axis.

5.3.3 Elliptically-polarized light

We have introduced the polarizabilities of the mixed rotational states when the light polarization is either circular or linear. Here we introduce another case where the polarization is elliptical and formed by

$$\hat{\epsilon} = a\hat{X} + ib\hat{Y} \tag{5.11}$$

where $a^2 + b^2 = 1$.

In Fig. 5.5, we present the dependence of an example with

$$a = \sqrt{\frac{1}{3}}, \quad b = \sqrt{\frac{2}{3}} \tag{5.12}$$

The polarizability curves of the states $|\tilde{J} = 0, M = 0\rangle$ and $|\tilde{J} = 1, M = 0\rangle$ in an elliptical polarization case remain the same as the situations with the circular polarization and perpendicular polarization. Moreover, the magic field strength in Fig. 5.5 confirms again that the strength value is independent of the polarization of the light.

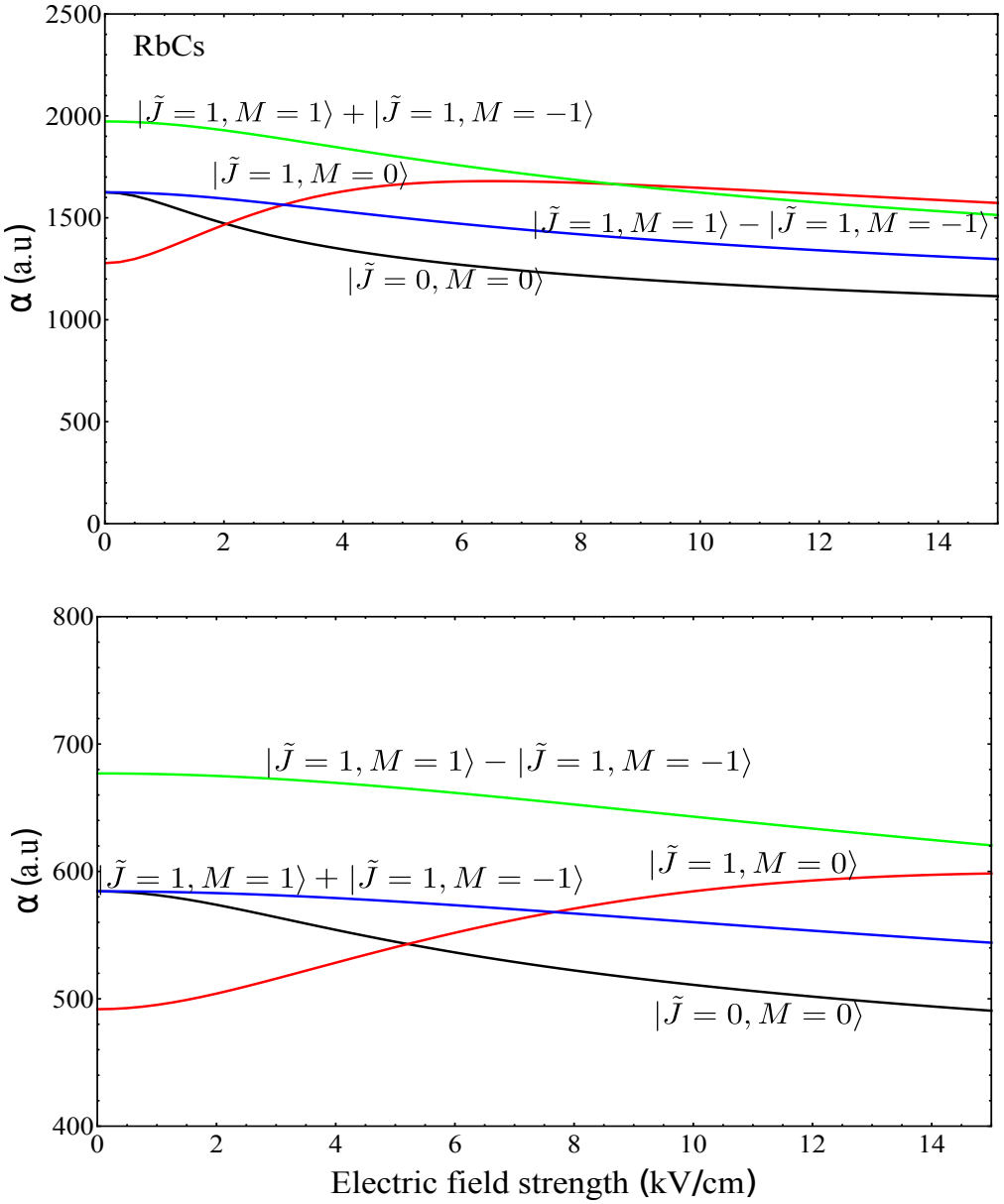

Figure 5.5: We demonstrate here the dynamic polarizabilities of the rotational states with $\tilde{J}=0$ and $\tilde{J}=1$ of RbCs and NaK when the light is elliptically-polarized with $\vec{\epsilon}=\sqrt{1/3}\hat{X}+i\sqrt{2/3}\hat{Y}$. The polarizability curves of the states $|\tilde{J}=0,M=0\rangle$ and $|\tilde{J}=1,M=0\rangle$ cross at an electric field strength value of 5.2 kV/cm. Actually, the magic field strength value of the two rotational states $|\tilde{J}=0,M=0\rangle$ and $|\tilde{J}=1,M=0\rangle$ remains the same, regardless of the polarization of the light.

5.4 Dynamic polarizability as a function of the relative orientation

We are also interested in the dynamic polarizability property when the light with a wavelength of 1064 nm is polarized in the $X - Z$ plane

$$\hat{\epsilon} = \cos\theta\hat{Z} + \sin\theta\hat{X}. \tag{5.13}$$

where θ is the angle between the light polarization and the DC electric field.

The angle dependence of the dynamic polarizability is demonstrated in Fig. 5.6 for RbCs and Fig. 5.7 for NaK. Each curve in the figures is calculated when the external DC electric field has a specified value, which ranges from 0.25 kV/cm to 2.5 kV/cm in steps of 0.75 kV/cm. The top rows of Fig. 5.6 and Fig. 5.7 give the dynamic polarizabilities of the states $|\tilde{J} = 0, M = 0\rangle$ and $|\tilde{J} = 1, M = 0\rangle$. The bottoms rows of Fig. 5.6 and Fig. 5.7 demonstrate the dynamic polarizabilities of the states $\tilde{J} = 1, (|+1\rangle + |-1\rangle)/\sqrt{2}$ and $\tilde{J} = 1, (|+1\rangle - |-1\rangle)/\sqrt{2}$.

We found that there exists a magic angle θ_0 with $\cos^2\theta_0 = 1/3$ where the polarizabilities of the rotational states $|\tilde{J} = 0, M = 0\rangle$ and $|\tilde{J} = 1, M = 0\rangle$ are identical. Especially, this magic angle value stays the same, when the DC electric field has different values. This property can be explained by the fact that the polarizability is a rank-two tensor operator. A more explicit derivation and explanation can be found in [70].

No magic angle exists for the states $\tilde{J} = 1, (|+1\rangle + |-1\rangle)/\sqrt{2}$ and $\tilde{J} = 1, (|+1\rangle - |-1\rangle)/\sqrt{2}$ of both molecules RbCs and NaK.

Besides that, we find that for small and near-zero DC field strength value, the angle dependence of the $|\tilde{J} = 1, M = 0\rangle$ is larger than that of the state $|\tilde{J} = 0, M = 0\rangle$. This is due to the fact that: at zero DC field, the polarizability of the state $|\tilde{J} = 0, M = 0\rangle$ at 1064 nm is a scalar and independent of the polarization direction. At small DC field ε, the dependence of the state $|\tilde{J} = 0, M = 0\rangle$ extends the behavior at zero DC field and changes slowly with the angle. When ε gets larger, the dependence curves of the two states start to get closer to each other. When the field ε reaches the value of magic field strength, the polarizability curves of the two states overlap. If ε is larger than this magic field value, the curves of the two states start to cross over each other.

The knowledge of the "magic angle" is helpful if we try to build a state-insensitive 3D optical lattice with three orthogonal retroreflected laser beams.The

polarization directions $\hat{\epsilon}_a$, $\hat{\epsilon}_b$, $\hat{\epsilon}_c$ can be arranged such that

$$|\hat{\epsilon}_a \cdot \hat{Z}|^2 = |\hat{\epsilon}_b \cdot \hat{Z}|^2 = |\hat{\epsilon}_c \cdot \hat{Z}|^2 = \frac{1}{3}. \tag{5.14}$$

The frequencies of lasers are chosen to be slightly different from each other, such that the interference term between the lasers can average to zero over the time.

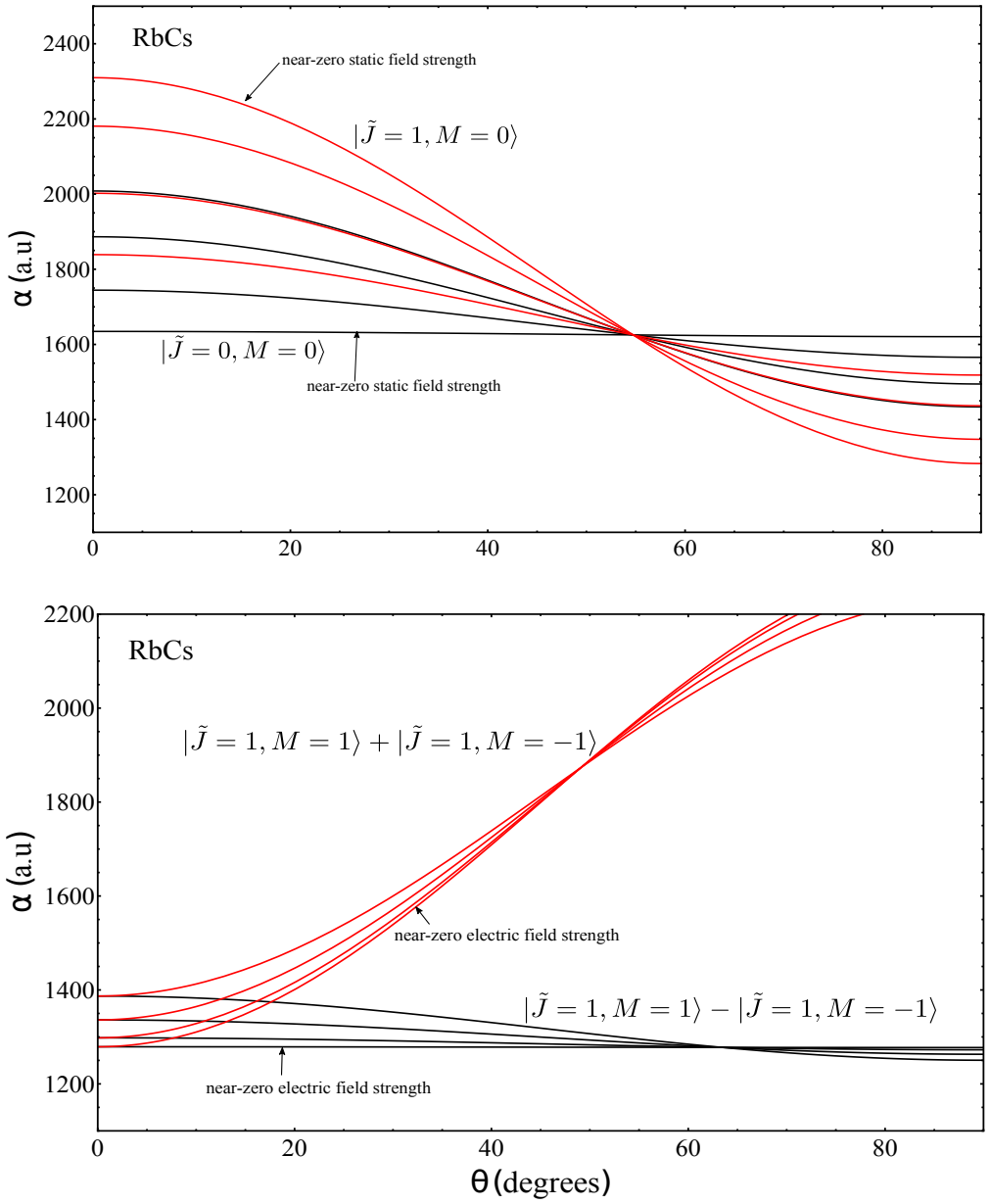

Figure 5.6: We demonstrate here the dynamic polarizability of the rotational states of RbCs as a function of the angle θ when the laser field with a wavelength 1064 nm is polarized as $\hat{\epsilon} = \cos\theta\hat{Z} + \sin\theta\hat{X}$. Each curve is evaluated under a certain DC field strength value, which ranges from 0.25 to 2.5 kV/cm in steps of 0.75 kV/cm. At the angle θ_0 with $\cos^2\theta_0 = 1/3$, the polarizabilities of the states $|\tilde{J}=0,M=0\rangle$ and $|\tilde{J}=1,M=0\rangle$ are identical. This magic angle value is independent of the value of the DC electric field strength. No magic angle exists for the states $\tilde{J}=1,|+1\rangle+|-1\rangle$ and $\tilde{J}=1,|+1\rangle-|-1\rangle$.

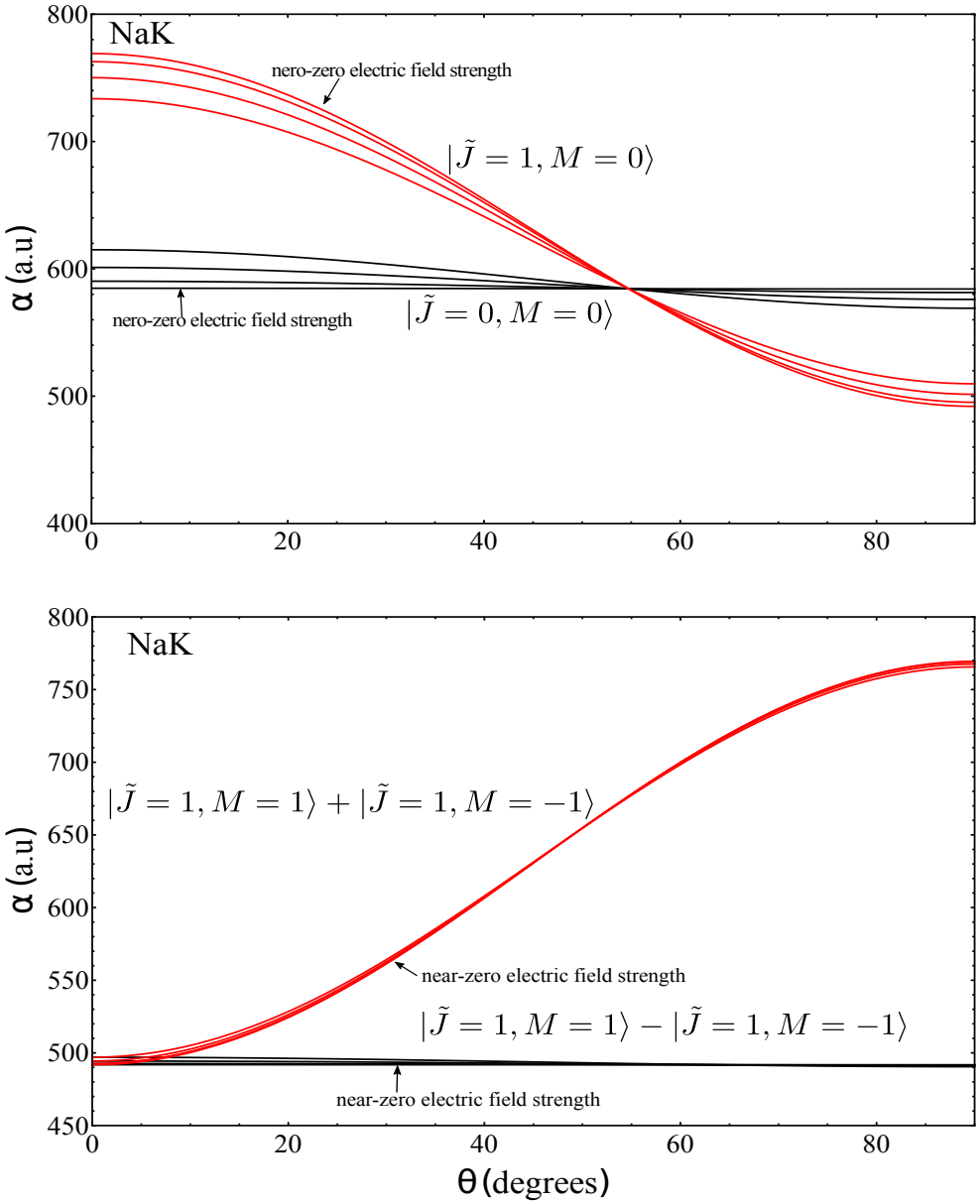

Figure 5.7: We demonstrate here the dynamic polarizability of the rotational states of NaK as a function of the angle θ when the laser field with a wavelength 1064 nm is polarized as $\hat{\epsilon} = \cos\theta\hat{Z} + \sin\theta\hat{X}$. Different curves of each state are corresponding to calculation of the polarizability with different field strength value. At the angle θ_0 which satisfies with $\cos^2\theta_0 = 1/3$, the polarizabilities of the states $|\tilde{J}=0,M=0\rangle$ and $|\tilde{J}=1,M=0\rangle$ are identical. This magic angle value is independent of the static electric field strength value. No magic angle exists for the states $\tilde{J}=1,|+1\rangle+|-1\rangle$ and $\tilde{J}=1,|+1\rangle-|-1\rangle$.

CHAPTER 5. IDENTICAL DYNAMIC POLARIZABILITIES BETWEEN ROTATIONAL STATES OF RBCS AND NAK WHILE APPLYING WITH AC AND DC FIELD SIMULTANEOUSLY

Chapter 6

Realization of identical dipole potential depth of rotational states in various optical lattice geometries

Optical lattices are optical configurations which has a periodic intensity pattern. Due to the interaction between the light and the atoms (see Section 2.1), the optical lattices can trap the atoms at locations which have intensity maximum. The resulting pattern with trapped atoms is analogous to that of the crystal lattice. The simplest one dimensional (1D) optical lattice can be formed by a retroreflected laser beam. A 2D optical lattice can be constructed by two retroreflected beams which are propagating perpendicular to each other. Further, a 3D optical lattice can be realized by adding another retroreflected laser beam which is perpendicular to the 2D lattice laser beams.

In the past few decades, optical lattices has served as ideal environment for strong correlated atomic system in many experiments. In 1998, D. Jaksch and coworkers firstly proposed the idea of loading the ultracold bosons into 3D optical lattice to realize strongly correlated system [71, 72]. In 2002, the quantum phase transition from a superfluid to a Mott-Insulator state has been observed in an experiment by M. Greiner and the coworkers [73] by loading a BEC into a 3D optical lattice. There are still more experiments which operated in optical lattices with either bosonic or fermionic atoms, see for examples of [74–83].

Nowadays, there are arising interests about the investigation of the strongly correlated regime with heteronuclear molecules in optical lattices. Especially, the long-range interactions between polar molecules can provide new opportunities for quantum simulations. In order to achieve the best performance

of the experiments and avoid the detrimental decoherence to the interactions, two internal states of molecules are required to be equally trapped. Various publications have demonstrated ways for the achievement of magic conditions. In this thesis, the magic condition has been accomplished by the magic field strength and magic angle (see Section 5.2 and 5.3).

This chapter is arranged as follows: at first, we introduce the electric field and dipole potential of a Gaussian laser beam. Then, we discuss different dimensional lattices with various geometries. Especially, we introduce here two 2D lattice geometries discussed in the paper [68]: a 2D triangular lattice geometry where the potential minima in the lattice have π polarization and a 2D hexagonal lattice geometry where the polarizations at the potential minima are changing from left-handed circular to right-handed circular alternately.

6.1 1D optical lattice

The electric field of the Gaussian beam which is propagating along the z direction is

$$E(x,y,z,t) = \frac{E_0 e^{-i\phi(z)}}{\sqrt{1+z^2/z_0^2}} e^{ik(x^2+y^2)/2R(z)} e^{-(x^2+y^2)/w^2(z)} e^{-ikz} e^{i\omega t} \tag{6.1}$$

where $w(z)$ is spot size, $R(z)$ is the radius of curvature, and z_0 is Rayleigh range.

The intensity of the Gaussian beam is

$$\begin{aligned} I(x,y,z) =& \frac{c\epsilon_0}{2}|E(x,y,z,t)|^2 \\ =& \frac{2P}{\pi w^2(z)} e^{-2(x^2+y^2)/w^2(z)} \end{aligned} \tag{6.2}$$

where P is the beam power. Therefore, the dipole potential seen by a state with the polarizability $\mathrm{Re}[\alpha(\omega)]$ is

$$V(x,y,z) = V_0 \frac{1}{(1+z^2/z_0^2)} e^{-2(x^2+y^2)/w^2(z)} \tag{6.3}$$

where

$$V_0 = \mathrm{Re}[\alpha(\omega)] \frac{2P}{\pi w_0^2} \tag{6.4}$$

By expanding the potential $V(x,y,z)$ around $z \ll z_0$ and $x^2+y^2 \ll w_0^2$,

we get that

$$V(x,y,z) \approx V_0\left[1 - 2\frac{x^2+y^2}{w_0^2} - \left(\frac{z}{z_0}\right)^2\right] \tag{6.5}$$

The potential in the radial direction is

$$V_r = V_0\left(- 2\frac{x^2+y^2}{w_0^2}\right) \tag{6.6}$$

Therefore the corresponding radial trapping frequency is

$$\omega_r = \sqrt{\frac{4V_0}{mw_0^2}} \tag{6.7}$$

the trapping frequency in axial direction is

$$\omega_z = \sqrt{\frac{2V_0}{mz_0^2}} \tag{6.8}$$

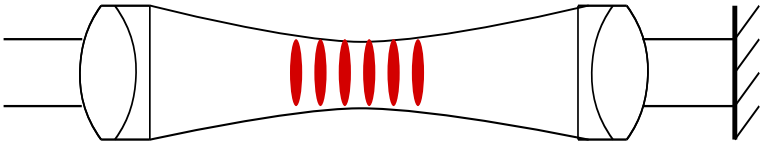

(a) Schematic sketch

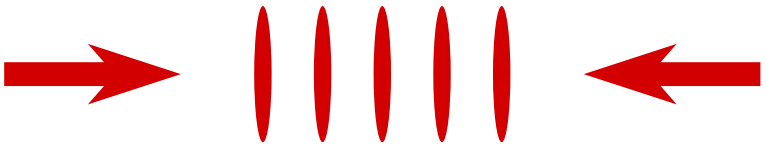

(b) optical lattice configuration

Figure 6.1: 1D optical lattice structure. a) The 1D optical lattice experimental setup by the interference pattern of a retroreflected Gaussian laser beam. b) Periodic pancake-like structure of 1D optical lattice.

If this Gaussian beam retroreflects by a mirror (See Fig. 6.1), the overall

electric field of this 1D optical lattice is

$$\begin{aligned} E_{\text{1D Lattice}}(x,y,z,t) = &\frac{E_0 e^{-i\phi(z)}}{\sqrt{1+z^2/z_0^2}} e^{ik(x^2+y^2)/2R(z)} e^{-(x^2+y^2)/w^2(z)} e^{ikz} e^{-i\omega t} \\ &+ \frac{E_0 e^{-i\phi(z)}}{\sqrt{1+z^2/z_0^2}} e^{ik(x^2+y^2)/2R(z)} e^{-(x^2+y^2)/w^2(z)} e^{-ikz} e^{-i\omega t} \end{aligned} \tag{6.9}$$

and the corresponding intensity is

$$\begin{aligned} I_{\text{1D Lattice}}(x,y,z) &= \frac{c\epsilon_0}{2} |E_{\text{1D Lattice}}(x,y,z,t)|^2 \\ &= \frac{8P}{\pi w^2(z)} e^{-2(x^2+y^2)/w^2(z)} \cos^2(kz) \end{aligned} \tag{6.10}$$

The overall optical potential is

$$V_{\text{1D Lattice}}(r,z) = V_{\text{Lattice}} \frac{1}{(1+z^2/z_0^2)} \exp\left(-2\frac{r^2}{w(z)^2} \right) \cos^2(kz) \tag{6.11}$$

The potential is periodic in the z-direction and has a pancake-like geometry in the other two dimensions. V_{Lattice} is four times as the dipole potential V_0 of a single beam dipole trap ($V_{\text{Lattice}} = 4V_0$) because the counterpropagating beams interfere with each other in a constructive way.

We can expand the potential in Eq.(6.11) in the z and r directions around the center $z = r = 0$. The axial trapping frequency ω_z in the z direction is

$$\omega_z = \sqrt{\frac{2V_{\text{Lattice}}}{m} k^2} \tag{6.12}$$

The trapping frequency ω_r in the r radial direction is

$$\omega_r = \sqrt{\frac{4V_{\text{Lattice}}}{m w_0^2}} \tag{6.13}$$

Given the dependency of the polarizability on the DC field strength in the Chapter 5, we will now illustrate the potentials of two rotational states $|\tilde{J}=0, M=0\rangle$ and $|\tilde{J}=1, M=0\rangle$ of NaK in optical lattices and compare them when the electric field strength is smaller than, equal to, or larger than the "magic field strength" which has been introduced in Section 5.2.

In Figure 6.2, the potentials of the two states are demonstrated in Fig.(a) when the DC electric field strength value is smaller than the magic electric field strength with ε=1kV/cm, in Fig. (b) when the DC electric field strength

value equal to the magic electric field strength at ε=5.2 kV/cm and in Fig. (c) when the DC electric field strength value is larger than the magic electric field strength with ε=12 kV/cm. We see that the potentials of the two rotational states $|\tilde{J} = 0, M = 0\rangle$ and $\tilde{J} = 1, M = 0$ of NaK are identical while applying the "magic field strength" discussed in the Section 5.2. This provides sufficient coherence time for the experiments where polar molecules are trapped in optical lattices.

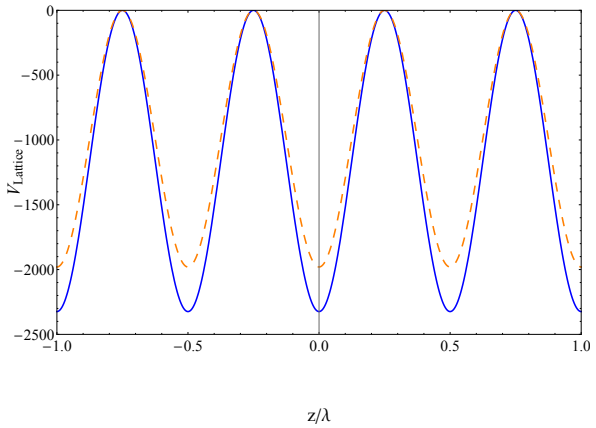

(a) ε=1 kV/cm

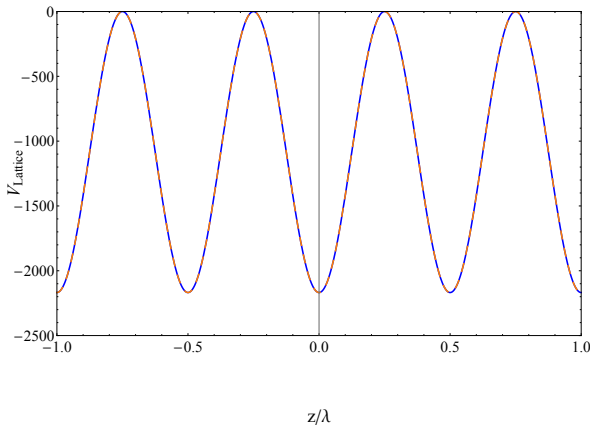

(b) ε=5.2 kV/cm

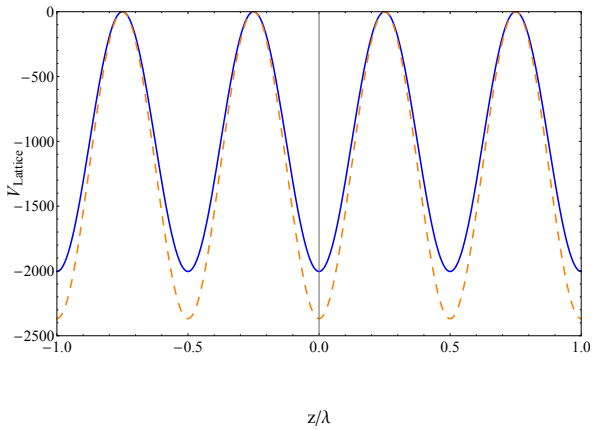

(c) ε=12 kV/cm

Figure 6.2: We demonstrate here the potentials (with a unit of $2P/\pi w_0^2$) in the z axis of a 1D optical lattice. Blue curve is the potential of the state $|\tilde{J} = 0, M = 0\rangle$. Orange dashed curve is the potential of the state $|\tilde{J} = 1, M = 0\rangle$. Fig.(a), Fig.(b) and Fig.(c) compare the two potentials when the external electric field strength is smaller than, equal to, or larger than the magic electric field strength respectively.

6.2 2D lattice configurations

Higher dimensional optical lattices can be created by superimposing additional standing waves from other directions. For example, we can upgrade a 1D optical lattice to a 2D lattice by adding another standing wave. In the following discussion, we first introduce a 2D optical lattice which are constructed by two retroreflected trapping laser beams which are traveling along the y and z directions respectively. Afterwards we introduce another two 2D lattice geometries: triangular geometry and hexagonal geometry.

6.2.1 Two perpendicular propagating laser beams

First, we introduce a case where two retroreflected trapping laser beams are traveling along the y and z directions respectively. Their polarization directions are $\vec{\epsilon_1}$ and $\vec{\epsilon_2}$, and the relative phase is ϕ. Moreover, we consider that the potentials at the center in both y and z directions are the same, which is $V_0^y = V_0^z = V_0$, and the Gaussian beam shapes are the same in both directions.

In order to investigate the periodicity of lattice potential in the propagating direction, we write here the axial component of a 2D lattice potential

$$V_{\text{2D Lattice}}(y,z) = V_{\text{Lattice}}\Big(\cos^2(ky)+\cos^2(kz)+2\vec{\epsilon_1}\cdot\vec{\epsilon_2}\cos(\phi)\cos(ky)\cos(kz)\Big) \tag{6.14}$$

If the polarizations of the two lattice beams are orthogonal to each other $\vec{\epsilon_1}\perp\vec{\epsilon_2}$, the interference term between the two can be eliminated since $\vec{\epsilon_1}\cdot\vec{\epsilon_2} = 0$. The resulting total potential is then simply given by the sum of the two superimposed 1D lattices

$$V_{\text{2D Lattice}}(y,z) = 4V_0\Big(\cos^2(ky) + \cos^2(kz)\Big) \tag{6.15}$$

We can see that in Fig. 6.3, the potential is periodic in both y and z directions, and the 2D optical lattice consists of an array of quasi-one-dimensional tubes.

Again, the "radial" trapping frequencies of a single tube are

$$\omega_z = \omega_y = \sqrt{\frac{2V_{\text{Lattice}}}{m}k^2} \tag{6.16}$$

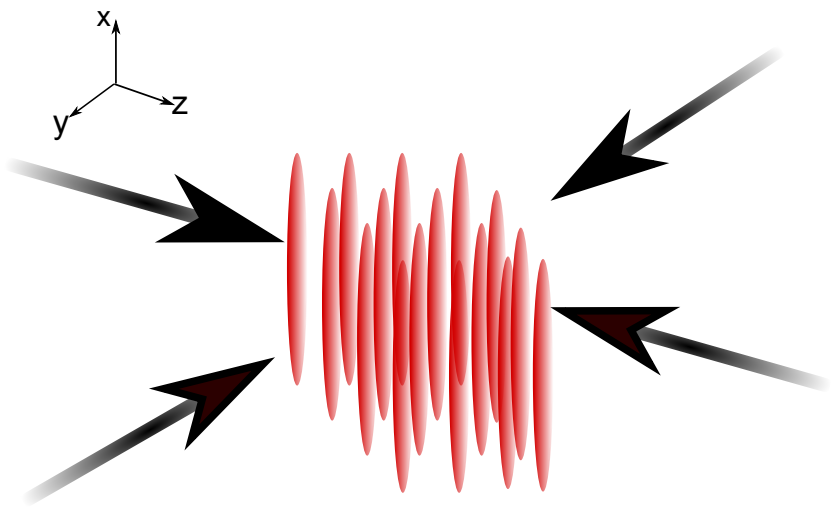

Figure 6.3: A 2D optical lattice which is constructed by two retroreflected trapping laser beams which are traveling along the y and z directions respectively. The polarizations of the two laser beams are perpendicular to each other. The resulting lattice consists of an array of quasi-one-dimensional tubes.

and the "axial" trapping frequency of a single tube is

$$\omega_x = \sqrt{\frac{8V_{\text{Lattice}}}{mw_0^2}} \tag{6.17}$$

Besides the orthogonal polarizations of the two standing waves, the frequencies of the two beams are chosen to be different in order to suppress the residual interference. We can choose the frequency difference on a order of a few ten MHz such that the interference averages out.

When the polarizations of the two lattice beams are not orthogonal to each other, therefore $\vec{\epsilon_1}\cdot\vec{\epsilon_2} \neq 0$. In other words, the interference Eq. (6.3) between the beams is not zero. The change of phase will cause a variation of the lattice geometry, resulting a detrimental effect of heating and decoherence.

In Fig. 6.4, we illustrate that the geometry of the optical lattice changes in terms of the relative phase $\cos(\phi)$. When the phase ϕ changes from 0 to $\pi/2$ and π, we can see that the potential depths of the neighing sites are changing correspondingly.

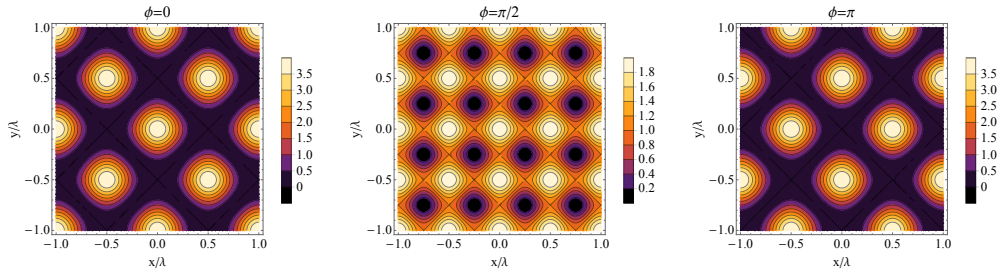

(a) $\phi = 0$ (b) $\phi = \pi/2$ (c) $\phi = \pi$

Figure 6.4: 2D optical lattices which are built by two standing waves which are propagating along y direction and z direction respectively. When the polarizations of the standing waves are arranged as so $\vec{\epsilon_1} \cdot \vec{\epsilon_2} = 1$, the phase difference ϕ leads to a change of the lattice geometry. a) $\phi = 0$. b) $\phi = \pi/2$. c) $\phi = \pi$.

6.2.2 2D triangular lattice geometry and hexagonal lattice geometry

Up until recently, experiments concerning optical lattices have been frequently operated in simple cubic lattices since its requirements can be easily fulfilled [84], comparing with other lattice geometries. However, there is arising experimental and theoretical interest about manipulation in more complex optical lattice geometries. For example, it is proposed [85–87] that loading cold atoms to triangular or hexagonal optical lattices can open up new possibilities for various applications, e.g. superconductivity [68, 88],.

A triangular geometry and a hexagonal geometry can be built by three laser beams. The total field vector is

$$E_{2\mathrm{D}}(\vec{r}, t) = \sum_{i=1}^{3} E_{0i}\vec{\epsilon_i} \cos(\vec{k_i}\vec{r} - \omega t + \phi_i) \tag{6.18}$$

The three laser beams propagate in the $x - y$ plane and intersect with angles of 120° (See Figure 6.5). The corresponding wavevectors are defined as

$$\vec{k_1} = k(0, 1, 0) \tag{6.19a}$$

$$\vec{k_2} = k(-\frac{\sqrt{3}}{2}, -\frac{1}{2}, 0) \tag{6.19b}$$

$$\vec{k_3} = k(\frac{\sqrt{3}}{2}, -\frac{1}{2}, 0) \tag{6.19c}$$

Next we are going to introduce how two different lattice geometries are formed with different polarizations of the three laser beams.

Case a) For a case that all the polarizations are perpendicular to the propagating plane ($x-y$ plane) of the lattice beams. See Figure 6.5a,

$$\vec{\epsilon}_1 = \vec{\epsilon}_2 = \vec{\epsilon}_3 = \hat{z} \tag{6.20}$$

The overall spatial electric field is

$$\vec{E} = E_0\vec{z}e^{iky} + E_0\hat{z}e^{ik(-\frac{\sqrt{3}}{2}x-\frac{1}{2}y)} + E_0\hat{z}e^{ik(\frac{\sqrt{3}}{2}x-\frac{1}{2}y)} \tag{6.21}$$

It is certain that the resulting triangular geometry optical lattice is polarized along the z direction in every potential mimina sites.

Case b) For another case that all the polarizations of the three lattice beams are lying in the $x-y$ plane and they intersect with each other by an angle of 120°,

$$\begin{aligned} \vec{\epsilon}_1 &= \vec{\epsilon}_x \\ \vec{\epsilon}_2 &= -\frac{1}{2}\vec{\epsilon}_x + \frac{\sqrt{3}}{2}\vec{\epsilon}_y \\ \vec{\epsilon}_3 &= -\frac{1}{2}\vec{\epsilon}_x - \frac{\sqrt{3}}{2}\vec{\epsilon}_y \end{aligned} \tag{6.22}$$

The overall spatial electric field is

$$\vec{E} = E_0\vec{\epsilon}_x e^{iky} + E_0(-\frac{1}{2}\vec{\epsilon}_x + \frac{\sqrt{3}}{2}\vec{\epsilon}_y)e^{ik(-\frac{\sqrt{3}}{2}x-\frac{1}{2}y)} + E_0(-\frac{1}{2}\vec{\epsilon}_x - \frac{\sqrt{3}}{2}\vec{\epsilon}_y)e^{ik(\frac{\sqrt{3}}{2}x-\frac{1}{2}y)} \tag{6.23}$$

The potential minima form a hexagonal lattice geometry, as shown in Fig. 6.5b.

Since the polarization vectors relationships are

$$\begin{aligned} \vec{\epsilon}_0 &= \vec{\epsilon}_z \\ \vec{\epsilon}_+ &= -\frac{1}{2}\vec{\epsilon}_x - i\frac{\sqrt{1}}{2}\vec{\epsilon}_y \\ \vec{\epsilon}_- &= \frac{1}{2}\vec{\epsilon}_x - i\frac{\sqrt{1}}{2}\vec{\epsilon}_y \end{aligned} \tag{6.24}$$

The polarizations at the potential minima are circular and they are changing from left-handed to right-handed alternatively.

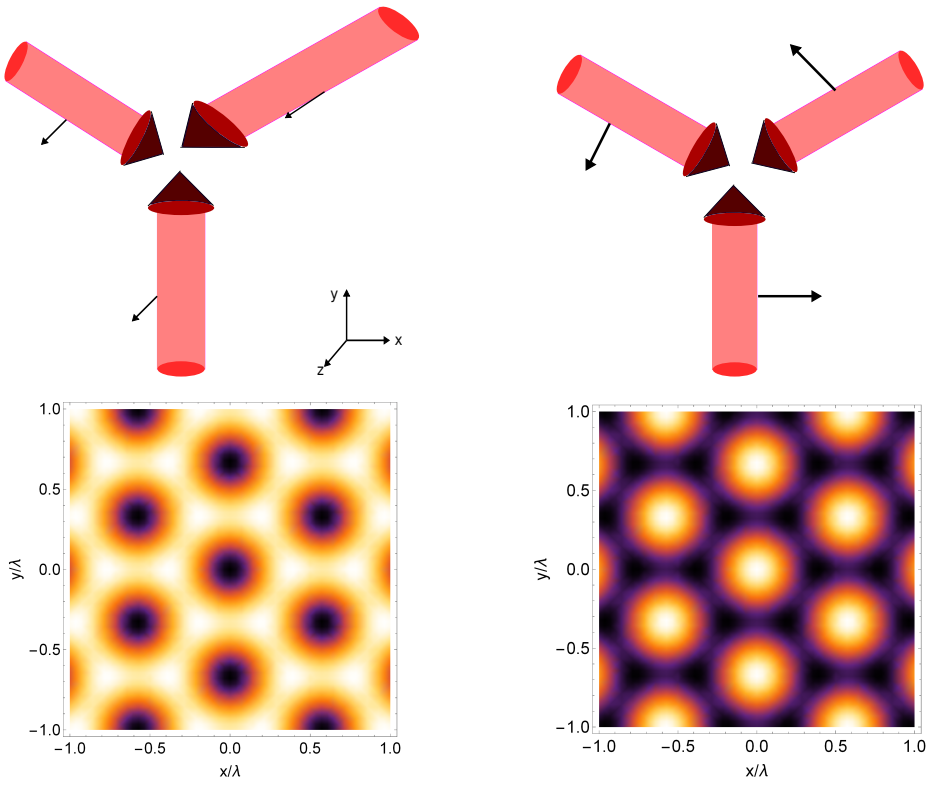

(a) Triangular optical lattice geometry (b) Hexagonal optical lattice geometry

Figure 6.5: Two 2D optical lattice geometries constructed by three laser beams which are propagating in the $x-y$ plane. The intersection angles between the propagating directions are 120°. The potential minina in the figure are the darkest locations. (a) A triangular optical lattice geometry is built when all the polarizations of all laser beams are along z. (b) A hexagonal optical lattice geometry is built when the polarizations are lying in the $x-y$ plane and intersecting with an angle 120°. Moreover, the potential minima are having alternate left-handed circular polarization and right-handed circular polarization.

Using the magic field strength that I have calculated in the Section 5.2, we can also find that in the 2D triangular optical lattice and hexagonal optical lattice constructed in Fig. 6.5, the potentials of the states $|\tilde{J}=0, M=0\rangle$ and $|\tilde{J}=1, M=0\rangle$ of NaK are identical.

6.3 3D optical cubic lattice configuration

A 3D optical lattice can be constructed when an additional standing wave is superimposed perpendicularly to a 2D optical lattice. In Fig. 6.6, the simplest 3D cubic optical lattice is constructed by three retroreflected laser beams which are propagating in the x, y and z directions. Moreover, the polarizations are also chosen to be perpendicular with respect to each other.

Besides the appropriate choice of orthogonal polarizations to eliminate the interference term, the frequencies are also shifted from each other to average out the residual interference.

Similar to the 1D lattice equation (6.11), the intensity and the potential in a 3D optical lattice is

$$\begin{aligned} I_{\text{3D Lattice}} =& \frac{8P}{\pi w^2(z)} e^{-2(x^2+y^2)/w^2(z)} \cos^2(kz) \\ &+ \frac{8P}{\pi w^2(y)} e^{-2(x^2+z^2)/w^2(z)} \cos^2(ky) \\ &+ \frac{8P}{\pi w^2(x)} e^{-2(y^2+z^2)/w^2(z)} \cos^2(kx) \end{aligned} \tag{6.25}$$

and

$$\begin{aligned} V_{\text{3D Lattice}} =& V_{\text{Lattice}} \frac{1}{w^2(z)} e^{-2(x^2+y^2)/w^2(z)} \cos^2(kz) \\ &+ V_{\text{Lattice}} \frac{1}{w^2(y)} e^{-2(x^2+z^2)/w^2(y)} \cos^2(ky) \\ &+ V_{\text{Lattice}} \frac{1}{w^2(x)} e^{-2(y^2+z^2)/w^2(x)} \cos^2(kx) \end{aligned} \tag{6.26}$$

where w_x, w_y, w_z are the x, y, z-dependent waists of the Gaussian laser beams.

Therefore the trapping frequencies in the x, y and z directions are

$$\omega_x = \omega_y = \omega_z = \sqrt{\frac{2V_{\text{Lattice}}}{m} k^2} \tag{6.27}$$

In the Sections 6.1 and 6.2.2, we stated that by applying the "magic field strength" values (2 kV/cm for RbCs and 5.2 kV/cm for NaK), two rotational

states $|\tilde{J}=0, M=0\rangle$ and $|\tilde{J}=1, M=0\rangle$ experience identical potentials. It is easy for us to extend the field strength value to a 3D cubic optical lattice in Fig 6.6 and therefore the lattice can be "state-insensitive".

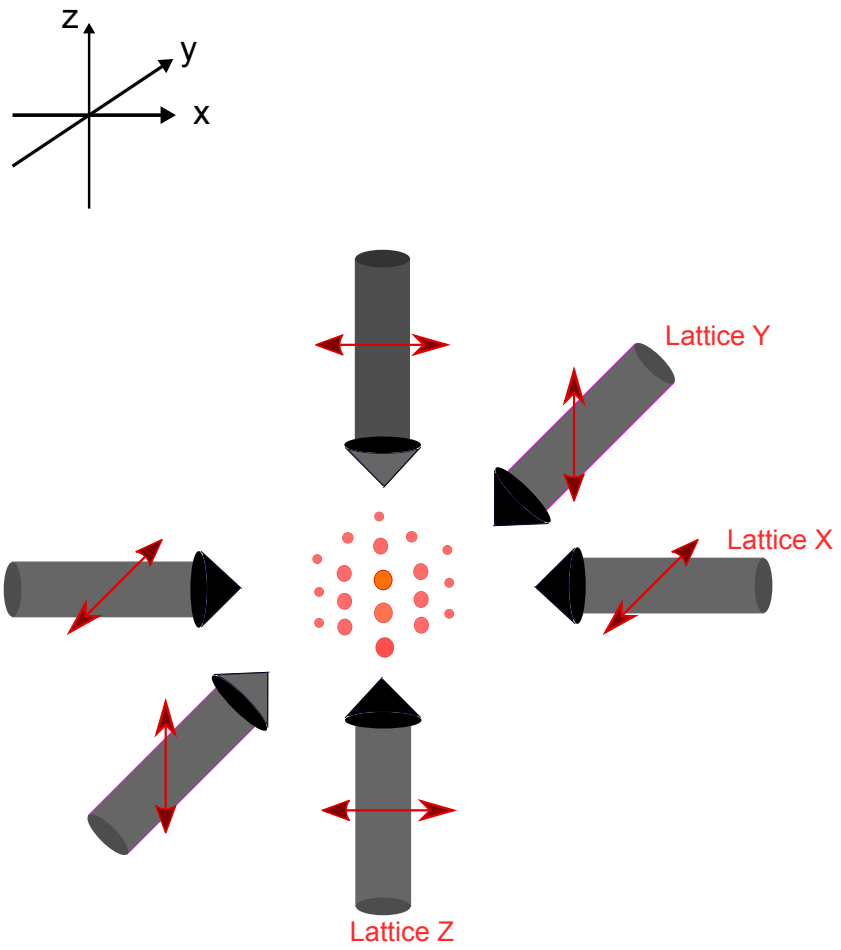

Figure 6.6: The simplest 3D cubic optical lattice configuration. The lattice is constructed with three retroreflected laser beams propagating in the x, y and z directions. The propagating directions are labeled with bold black arrows. The corresponding polarizations of the laser beams are labeled with red arrows. $\hat{\epsilon_x}$ is along the y-direction, $\hat{\epsilon_y}$ is along the z-direction, and $\hat{\epsilon_z}$ is along the x-direction.

Chapter 7

Conclusions

In this thesis, we firstly investigated the dynamic polarizabilities of the two lowest rotational states $\tilde{J} = 0$ and $\tilde{J} = 1$ of the ground state $X^1\Sigma^+$ of RbCs and NaK molecules as a function of the laser frequency. We found that the polarizabilities of the rotational states do not cross in the near infrared laser field. Therefore, there exists no magic frequency.

When we applied a static electric field along the Z direction which mixes rotational states of the diatomic molecules and a laser light with a wavelength of 1064 nm simultaneously, the polarizability depends not only on the static field strength value, it is also a function of the relative orientation between the external static field direction and the polarization direction. We found that the dynamic polarizabilities of the two rotational states $|\tilde{J} = 0, M = 0\rangle$ and $|\tilde{J} = 1, M = 0\rangle$ are identical when the field strength is around 2 kV/cm for RbCs and around 5.2 kV/cm for NaK. The magic field strength value remains the same for any polarization cases of the trapping light. We also found that when the relative angle θ between the external field and polarization direction satisfied the condition of $\cos^2\theta = 1/3$, the dynamic polarizabilities of the states $|\tilde{J} = 0, M = 0\rangle$ and $|\tilde{J} = 1, M = 0\rangle$ match and independent of any external static electric field strength value.

We finished the thesis by applying the magic condition to various optical lattice geometries, so that a pair of rotational states of diatomic molecules can be trapped with identical potentials in optical lattices. The "state-insensitive" lattice environments will bring substantial benefits to quantum simulations and precision measurements.

List of Figures

Bibliography

[1] Keith D Bonin and Vitaly V Kresin. *Electric-dipole polarizabilities of atoms, molecules, and clusters*. World Scientific, 1997.

[2] Masao Takamoto, Feng-Lei Hong, Ryoichi Higashi, and Hidetoshi Katori. An optical lattice clock. *Nature*, 435(7040):321, 2005.

[3] Roger C Brown, Nate B Phillips, K Beloy, William F McGrew, Marco Schioppo, Robert J Fasano, Gianmaria Milani, Xiaogang Zhang, N Hinkley, H Leopardi, et al. Hyperpolarizability and operational magic wavelength in an optical lattice clock. *Physical review letters*, 119(25):253001, 2017.

[4] Jun Ye, HJ Kimble, and Hidetoshi Katori. Quantum state engineering and precision metrology using state-insensitive light traps. *science*, 320(5884):1734–1738, 2008.

[5] VV Flambaum, VA Dzuba, and A Derevianko. Magic frequencies for cesium primary-frequency standard. *Physical review letters*, 101(22):220801, 2008.

[6] Kyle Beloy, Andrei Derevianko, VA Dzuba, and VV Flambaum. Micromagic clock: microwave clock based on atoms in an engineered optical lattice. *Physical review letters*, 102(12):120801, 2009.

[7] N Lundblad, M Schlosser, and JV Porto. Experimental observation of magic-wavelength behavior of rb 87 atoms in an optical lattice. *Physical Review A*, 81(3):031611, 2010.

[8] Brian Neyenhuis, B Yan, SA Moses, JP Covey, A Chotia, A Petrov, S Kotochigova, J Ye, and DS Jin. Anisotropic polarizability of ultracold polar k 40 rb 87 molecules. *Physical review letters*, 109(23):230403, 2012.

[9] Jürgen Stuhler, Axel Griesmaier, Tobias Koch, Marco Fattori, Tilman Pfau, Stefano Giovanazzi, Paolo Pedri, and Luis Santos. Observation of

dipole-dipole interaction in a degenerate quantum gas. *Physical Review Letters*, 95(15):150406, 2005.

[10] PS Jessen and IH Deutsch. Optical lattices. In *Advances in Atomic, Molecular, and Optical Physics*, volume 37, pages 95–138. Elsevier, 1996.

[11] Markus Greiner, Cindy A Regal, and Deborah S Jin. Emergence of a molecular bose–einstein condensate from a fermi gas. *Nature*, 426(6966):537, 2003.

[12] John Doyle, Bretislav Friedrich, RV Krems, and Françoise Masnou-Seeuws. Quo vadis, cold molecules?, 2004.

[13] David DeMille. Quantum computation with trapped polar molecules. *Physical Review Letters*, 88(6):067901, 2002.

[14] Lincoln D Carr, David DeMille, Roman V Krems, and Jun Ye. Cold and ultracold molecules: science, technology and applications. *New Journal of Physics*, 11(5):055049, 2009.

[15] E Urban, Todd A Johnson, T Henage, L Isenhower, DD Yavuz, TG Walker, and M Saffman. Observation of rydberg blockade between two atoms. *Nature Physics*, 5(2):110, 2009.

[16] Svetlana Kotochigova and David DeMille. Electric-field-dependent dynamic polarizability and state-insensitive conditions for optical trapping of diatomic polar molecules. *Physical Review A*, 82(6):063421, 2010.

[17] T Zelevinsky, S Kotochigova, and Jun Ye. Precision test of mass-ratio variations with lattice-confined ultracold molecules. *Physical Review Letters*, 100(4):043201, 2008.

[18] S Kotochigova, T Zelevinsky, and Jun Ye. Prospects for application of ultracold sr 2 molecules in precision measurements. *Physical Review A*, 79(1):012504, 2009.

[19] S Kotochigova and Eite Tiesinga. Controlling polar molecules in optical lattices. *Physical Review A*, 73(4):041405, 2006.

[20] EF O'Brien, VP Gutschick, V McKoy, and JP McTague. Polarizability of interacting atoms: Relation to collision-induced light scattering and dielectric models. *Physical Review A*, 8(2):690, 1973.

[21] Kurt E Oughstun and Natalie A Cartwright. On the lorentz-lorenz formula and the lorentz model of dielectric dispersion. *Optics express*, 11(13):1541–1546, 2003.

[22] Alan Herries Wilson. Perturbation theory in quantum mechanics. *Proc. R. Soc. Lond. A*, 122(790):589–598, 1929.

[23] Jean Dalibard and Claude Cohen-Tannoudji. Laser cooling below the doppler limit by polarization gradients: simple theoretical models. *JOSA B*, 6(11):2023–2045, 1989.

[24] J Dalibard and Claude Cohen-Tannoudji. Dressed-atom approach to atomic motion in laser light: the dipole force revisited. *JOSA B*, 2(11):1707–1720, 1985.

[25] G Wilpers, T Binnewies, C Degenhardt, U Sterr, J Helmcke, and F Riehle. Optical clock with ultracold neutral atoms. *Physical review letters*, 89(23):230801, 2002.

[26] N Poli, F-Y Wang, MG Tarallo, A Alberti, M Prevedelli, and GM Tino. Precision measurement of gravity with cold atoms in an optical lattice and comparison with a classical gravimeter. *Physical review letters*, 106(3):038501, 2011.

[27] JD Miller, RA Cline, and DJ Heinzen. Far-off-resonance optical trapping of atoms. *Physical Review A*, 47(6):R4567, 1993.

[28] Rudolf Grimm, Matthias Weidemüller, and Yurii B Ovchinnikov. Optical dipole traps for neutral atoms. In *Advances in atomic, molecular, and optical physics*, volume 42, pages 95–170. Elsevier, 2000.

[29] Ch Grain, T Nazarova, C Degenhardt, F Vogt, Ch Lisdat, E Tiemann, U Sterr, and F Riehle. Feasibility of narrow-line cooling in optical dipole traps. *The European Physical Journal D*, 42(2):317–324, 2007.

[30] Keir C Neuman and Attila Nagy. Single-molecule force spectroscopy: optical tweezers, magnetic tweezers and atomic force microscopy. *Nature methods*, 5(6):491, 2008.

[31] L Allen, MJ Padgett, and M Babiker. Iv the orbital angular momentum of light. In *Progress in optics*, volume 39, pages 291–372. Elsevier, 1999.

[32] Daniel A Steck. Quantum and atom optics. *Oregon Center for Optics and Department of Physics, University of Oregon*, 47, 2007.

[33] II Sobel'man. Introduction to the theory of atomic spectra, international series of monographs in natural philosophy. vol. 40, 1979.

[34] Nir Davidson, Heun Jin Lee, Charles S Adams, Mark Kasevich, and Steven Chu. Long atomic coherence times in an optical dipole trap. *Physical review letters*, 74(8):1311, 1995.

[35] Max Born and Robert Oppenheimer. On the quantum theory of molecules. In *Quantum Chemistry: Classic Scientific Papers*, pages 1–24. World Scientific, 2000.

[36] Philip M Morse. Diatomic molecules according to the wave mechanics. ii. vibrational levels. *Physical Review*, 34(1):57, 1929.

[37] Richard A Friesner, Robert B Murphy, Michael D Beachy, Murco N Ringnalda, W Thomas Pollard, Barry D Dunietz, and Yixiang Cao. Correlated ab initio electronic structure calculations for large molecules. *The Journal of Physical Chemistry A*, 103(13):1913–1928, 1999.

[38] Jing Kong, Christopher A White, Anna I Krylov, David Sherrill, Ross D Adamson, Thomas R Furlani, Michael S Lee, Aaron M Lee, Steven R Gwaltney, Terry R Adams, et al. Q-chem 2.0: a high-performance ab initio electronic structure program package. *Journal of Computational Chemistry*, 21(16):1532–1548, 2000.

[39] Robert J LeRoy and Richard B Bernstein. Dissociation energy and long-range potential of diatomic molecules from vibrational spacings of higher levels. *The Journal of Chemical Physics*, 52(8):3869–3879, 1970.

[40] Gerhard Herzberg. Molecular spectra and molecular structure. vol. 1: Spectra of diatomic molecules. *New York: Van Nostrand Reinhold, 1950, 2nd ed.*, 1950.

[41] RJ Le Roy. Dparfit 3.3, a computer program for fitting multi-isotopomer diatomic molecule spectra. university of waterloo chemical physics research report cp-660, 2005. see. *The source code and manual for this program may be obtained from the "Computer Programs"link at http://leroy. uwaterloo. ca*, 34.

[42] Robert J Le Roy. Rkr1: a computer program implementing the first-order rkr method for determining diatomic molecule potential energy functions. *Journal of Quantitative Spectroscopy and Radiative Transfer*, 186:158–166, 2017.

[43] Robert J Le Roy. Level: A computer program for solving the radial schrödinger equation for bound and quasibound levels. *Journal of Quantitative Spectroscopy and Radiative Transfer*, 186:167–178, 2017.

[44] Robert J Le Roy and J Van Kranendonk. Anisotropic intermolecular potentials from an analysis of spectra of h2-and d2-inert gas complexes. *The Journal of Chemical Physics*, 61(11):4750–4769, 1974.

[45] Photos G Hajigeorgiou and Robert J Le Roy. A "modified lennard-jones oscillator" model for diatom potential functions. *The Journal of Chemical Physics*, 112(9):3949–3957, 2000.

[46] A Adohi-Krou, W Jastrzebski, P Kowalczyk, AV Stolyarov, and AJ Ross. Investigation of the d 1π state of nak by polarisation labelling spectroscopy. *Journal of Molecular Spectroscopy*, 250(1):27–32, 2008.

[47] Julia Gerschmann, Erik Schwanke, Asen Pashov, Horst Knöckel, Silke Ospelkaus, and Eberhard Tiemann. Laser and fourier-transform spectroscopy of kca. *Physical Review A*, 96(3):032505, 2017.

[48] C Samuelis, Eite Tiesinga, T Laue, M Elbs, H Knöckel, and E Tiemann. Cold atomic collisions studied by molecular spectroscopy. *Physical Review A*, 63(1):012710, 2000.

[49] JL Dunham. The energy levels of a rotating vibrator. *Physical Review*, 41(6):721, 1932.

[50] István Kovács and L Nemes. *Rotational structure in the spectra of diatomic molecules*. Hilger London, 1969.

[51] Klaus-Peter Huber. *Molecular spectra and molecular structure: IV. Constants of diatomic molecules*. Springer Science & Business Media, 2013.

[52] John M Brown and Alan Carrington. *Rotational spectroscopy of diatomic molecules*. Cambridge University Press, 2003.

[53] V Fano and L Fano. Physics of atoms and molecules. 1980.

[54] Brain Judd. *Angular momentum theory for diatomic molecules*. Elsevier, 2012.

[55] DM Brink, GR Satchler, and Michael Danos. Angular momentum. *Physics Today*, 16:80, 1963.

[56] O Docenko, M Tamanis, R Ferber, H Knöckel, and E Tiemann. Singlet and triplet potentials of the ground-state atom pair rb+ cs studied by fourier-transform spectroscopy. *Physical Review A*, 83(5):052519, 2011.

[57] S Kotochigova and Eite Tiesinga. Ab initio relativistic calculation of the rbcs molecule. *The Journal of chemical physics*, 123(17):174304, 2005.

[58] O Docenko, M Tamanis, R Ferber, T Bergeman, S Kotochigova, AV Stolyarov, Andreia de Faria Nogueira, and CE Fellows. Spectroscopic data, spin-orbit functions, and revised analysis of strong perturbative interactions for the a 1 $\sigma+$ and b 3 π states of rbcs. *Physical Review A*, 81(4):042511, 2010.

[59] A Gerdes, M Hobein, H Knöckel, and E Tiemann. Ground state potentials of the nak molecule. *The European Physical Journal D*, 49(1):67–73, 2008.

[60] Heather Harker, Patrick Crozet, Amanda J Ross, Kara Richter, Joshua Jones, Carl Faust, John Huennekens, Andrey V Stolyarov, Houssam Salami, and Thomas Bergeman. Experimental and theoretical studies of the coupled a 1 $\sigma+$ and b π 3 states of nak. *Physical Review A*, 92(1):012506, 2015.

[61] Shunji Kasahara, Masaaki Baba, and Hajime Katô. High resolution laser spectroscopy up to the dissociation limit of the nak b 1π state, and predissociation near the dissociation limit. *The Journal of chemical physics*, 94(12):7713–7720, 1991.

[62] AJ Ross, P Crozet, I Russier-Antoine, A Grochola, P Kowalczyk, W Jastrzebski, and P Kortyka. On the c$1\sigma+$ state of nak. *Journal of Molecular Spectroscopy*, 226(1):95–102, 2004.

[63] M Aymar and O Dulieu. Calculations of transition and permanent dipole moments of heteronuclear alkali dimers nak, narb and nacs. *Molecular Physics*, 105(11-12):1733–1742, 2007.

[64] William Graham Richards, H-P_ Trivedi, and David L Cooper. *Spin-orbit coupling in molecules*. Number 4. Oxford University Press, 1981.

[65] HP Trivedi and WG Richards. A binitio calculation of spin–orbit coupling constant in diatomic molecules. *The Journal of Chemical Physics*, 72(5):3438–3439, 1980.

[66] P Sushkov and VV Flarnbaurn. Parity breaking effects in diatomic molecules. *Zh. Eksp. Teor. Fiz*, 75:1208–1213, 1978.

[67] Paul Adrien Maurice Dirac. On the theory of quantum mechanics. *Proc. R. Soc. Lond. A*, 112(762):661–677, 1926.

[68] C Becker, P Soltan-Panahi, J Kronjäger, S Dörscher, K Bongs, and K Sengstock. Ultracold quantum gases in triangular optical lattices. *New Journal of Physics*, 12(6):065025, 2010.

[69] JG Snijders, EJ Baerends, and P Ros. A perturbation theory approach to relativistic calculations: Ii. molecules. *Molecular Physics*, 38(6):1909–1929, 1979.

[70] Dmitry Budker, Derek F Kimball, Derek Kimball, and David P DeMille. *Atomic physics: an exploration through problems and solutions*. Oxford University Press, USA, 2004.

[71] Dieter Jaksch, Christoph Bruder, Juan Ignacio Cirac, Crispin W Gardiner, and Peter Zoller. Cold bosonic atoms in optical lattices. *Physical Review Letters*, 81(15):3108, 1998.

[72] Matthew PA Fisher, Peter B Weichman, G Grinstein, and Daniel S Fisher. Boson localization and the superfluid-insulator transition. *Physical Review B*, 40(1):546, 1989.

[73] Markus Greiner, Olaf Mandel, Tilman Esslinger, Theodor W Hänsch, and Immanuel Bloch. Quantum phase transition from a superfluid to a mott insulator in a gas of ultracold atoms. *nature*, 415(6867):39, 2002.

[74] C Ospelkaus, S Ospelkaus, L Humbert, P Ernst, K Sengstock, and K Bongs. Ultracold heteronuclear molecules in a 3d optical lattice. *Physical Review Letters*, 97(12):120402, 2006.

[75] Belén Paredes, Artur Widera, Valentin Murg, Olaf Mandel, Simon Fölling, Ignacio Cirac, Gora V Shlyapnikov, Theodor W Hänsch, and Immanuel Bloch. Tonks–girardeau gas of ultracold atoms in an optical lattice. *Nature*, 429(6989):277, 2004.

[76] Toshiya Kinoshita, Trevor Wenger, and David S Weiss. Observation of a one-dimensional tonks-girardeau gas. *Science*, 305(5687):1125–1128, 2004.

[77] Gregor Thalhammer, Klaus Winkler, Florian Lang, Stefan Schmid, Rudolf Grimm, and J Hecker Denschlag. Long-lived feshbach molecules in a three-dimensional optical lattice. *Physical review letters*, 96(5):050402, 2006.

[78] Jit Kee Chin, DE Miller, Y Liu, C Stan, W Setiawan, C Sanner, K Xu, and W Ketterle. Evidence for superfluidity of ultracold fermions in an optical lattice. *Nature*, 443(7114):961, 2006.

[79] Olaf Mandel, Markus Greiner, Artur Widera, Tim Rom, Theodor W Hänsch, and Immanuel Bloch. Coherent transport of neutral atoms in spin-dependent optical lattice potentials. *Physical review letters*, 91(1):010407, 2003.

[80] Tim Rom, Thorsten Best, Olaf Mandel, Artur Widera, Markus Greiner, Theodor W Hänsch, and Immanuel Bloch. State selective production of molecules in optical lattices. *Physical review letters*, 93(7):073002, 2004.

[81] Michael Köhl, Henning Moritz, Thilo Stöferle, Kenneth Günter, and Tilman Esslinger. Fermionic atoms in a three dimensional optical lattice: Observing fermi surfaces, dynamics, and interactions. *Physical review letters*, 94(8):080403, 2005.

[82] Kenneth Günter, Thilo Stöferle, Henning Moritz, Michael Köhl, and Tilman Esslinger. Bose-fermi mixtures in a three-dimensional optical lattice. *Physical review letters*, 96(18):180402, 2006.

[83] Thomas Volz, Niels Syassen, Dominik M Bauer, Eberhard Hansis, Stephan Dürr, and Gerhard Rempe. Preparation of a quantum state with one molecule at each site of an optical lattice. *Nature Physics*, 2(10):692, 2006.

[84] KI Petsas, AB Coates, and G Grynberg. Crystallography of optical lattices. *Physical review A*, 50(6):5173, 1994.

[85] Stefan Wessel and Matthias Troyer. Supersolid hard-core bosons on the triangular lattice. *Physical review letters*, 95(12):127205, 2005.

[86] Congjun Wu, W Vincent Liu, Joel Moore, and Sankar Das Sarma. Quantum stripe ordering in optical lattices. *Physical review letters*, 97(19):190406, 2006.

[87] Ludwig Mathey, S-W Tsai, and AH Castro Neto. Exotic superconducting phases of ultracold atom mixtures on triangular lattices. *Physical Review B*, 75(17):174516, 2007.

[88] Leticia Tarruell, Daniel Greif, Thomas Uehlinger, Gregor Jotzu, and Tilman Esslinger. Creating, moving and merging dirac points with a fermi gas in a tunable honeycomb lattice. *Nature*, 483(7389):302, 2012.